EVALUATION OF CAPILLARY ELECTROPHORESIS AS AN ANALYTICAL TECHNIQUE USING BULK IONIC COMPOSITION OF FLUID INCLUSIONS IN QUARTZ

by

Riana Martin

Thesis presented in partial fulfillment of the requirements for the degree of Master of Natural Sciences at the University of Stellenbosch.

Study Leader: Prof. D.K. Hallbauer

December 2000

DECLARATION:

I, the undersigned, hereby declare that the work contained in this thesis is my own original work and that I have not previously, in its entirety or in part, submitted it at any university for a degree.

Signature:

Date:

ABSTRACT

This study was initialized to introduce capillary electrophoresis (CE) as a useful technique in the analysis of fluid inclusions in quartz. Its advantages are low detection limits for the dissolved ionic content of the fluid, the small amount of sample (1 g or less) for a detailed qualitative and quantitative analysis, and the short time required to obtain results (one run for either cations or anions take approximately 10 minutes).

The study area from which quartz veins were selected is situated within the Neoproterozoic Saldania belt. Syn- and post-tectonic S-, I- and A-type granitoids from the Cape Granite Suite intruded the metamorphosed Malmesbury greywacke and pelites between 550 and 510 Ma. Additional periods of tectonism and metamorphism occurred during Cape Supergroup sedimentation (480 – 400 Ma) as well as Karoo sedimentation and the simultaneous Cape Orogeny (280 –215 Ma).

The quartz-biotite±chlorite veins are hosted by Cape Granite as well as Malmesbury sediments. These barren quartz veins are part of two vein sets, one dipping at an angle between 15 and 50° to the S to SE and striking W, similar to Sn-mineralized quartz veins in the SW-cape, while the other is near-vertical and striking W to NW. Except for their orientation, no differences regarding associated minerals, inclusion characteristics or fluid chemistry indicated a difference in origin.

Four fluid phases within a temperature range of 160 – 390 °C were identified as being largely late-magmatic and released from the underlying Cape Granite plutons, namely an early 370 – 390 °C population, followed by the 310 – 360, 230 – 300 and lastly the 160 – 200 °C populations. Initiation of this fluid system occurred from at least 510 Ma, after final granite intrusion, but the age of the final stage is unknown. Renewed fluid circulation occurred during

a later period of metamorphism, possibly during the Cape Orogeny. These fluids had temperatures between 240 and 360 °C and are of sedimentary origin, most likely released from the Malmesbury metamorphites.

The technique of capillary electrophoresis has been evaluated for its application to bulk fluid inclusion analysis, and the crush-leach fluid extraction procedure of Bottrell, *et al.*, (1988) optimized for CE analysis. Contamination factors were identified and minimized or eliminated, where possible. Bulk fluid inclusion chemistry obtained by CE was therefore proved to provide valuable information regarding the various fluid generations as long as inclusion populations are investigated individually to explain and correlate bulk data.

SAMEVATTING

Die doel van die studie was om te toon dat die tegniek van kapillêre elektroforese bruikbaar is in die analiese van vloeistofinsluitsels in kwarts. Die voordele van hierdie tegniek is lae deteksie limiete vir die opgeloste ioon inhoud van die vloeistof, die klein monstergrootte (< 1g) wat nodig is vir 'n omvattende kwalitatiewe en kwantitatiewe analise, en die kort tydsduur waarin resultate verkry word ('n katioon of anioon analise vir een monster duur 10 minute).

Die studie gebied waar kwarts are gemonster is, is binne die Neoproterosoïese Saldania Gordel geleë. Sin- en laat-tektoniese S-, I- en A-tipe graniete van die Kaapse Graniet Suite het die gemetamorfiseerde Malmesbury grouwakke en peliete tussen 550 en 510 Ma binnegedring. Latere periodes van tektonisme en metamorfose het tydens deponering van die Kaap Supergroep (480 – 400 Ma), en die gelyktydige episodes van Karoo sedimentasie en Kaapse Orogenese (280 – 215 Ma) plaasgevind.

Die gasheer gesteentes vir die kwarts-biotiet±chloriet are is Kaapse Graniet sowel as Malmesbury sedimente. Hierdie ongemineraliseerde are is deel van twee aarstelsels, nl. een met 'n duik hoek tussen 15 en 50° S tot SO en 'n westelike strekking, soortgelyk aan die Sn-gemineraliseerde are in die SW-Kaap, terwyl die ander stel are feitlik vertikaal is en W tot NW strek. Behalwe vir die verskil in oriëntasie was daar geen aanduiding, wat betref 'n verskil in geassosieerde minerale, vloeistofinsluitsel kenmerke of vloeistof chemie, dat hierdie twee aarstelsels van verskillende oorsprong is nie.

Vier vloeistof fases binne 'n temperatuur gebied van 160 – 390 °C en 'n vloeistof saliniteit van 0 – 5.7 gewig % NaCl ekw. is geïdentifiseer, met 'n laat-magmatiese assosiasie en vrygestel deur die onderliggende Kaapse Graniete. Dit behels 'n vroeë 370 – 390 °C

populasie, gevolg deur die 310 – 360, 230 – 300 en laastens die 160 – 200 °C populasies. Inisiasie van hierdie sisteem kon moontlik rondom 510 Ma gelede plaasgevind het, maar die ouderdom van die finale fase is onbekend. Hernude vloeistof sirkulasie het tydens 'n later stadium van metamorfose onstaan, moontlik tydens die Kaapse Orogenese. Hierdie vloeistowwe het temperature tussen 240 en 360 °C en is van sedimentêre oorsprong waar dit moontlik deur metamorfose van die reeds gemetamorfiseerde Malmesbury gesteentes vrygestel is.

Die tegniek van kapillêre elektroforese is vir die toepassing daarvan in die analise van vloeistof insluitsels in kwarts geëvalueer, terwyl die vloeistof vrystellingsmetode van Bottrell en Yardley (1988) vir hierdie tegniek geoptimaliseer is. Kontaminasie faktore is geïdentifiseer en verminder of uitgeskakel waar moontlik. Daar is getoon dat die vloeistof chemie, wat verteenwoordigend is van al die insluitsel populasies in 'n monster, wel bruikbaar is t.o.v. afsonderlike vloeistof generasies, solank elke populasie individueel bestudeer is om die omvattende chemiese data te verduidelik en met 'n enkele populasie te korrelleer.

CONTENTS

1 INTRODUCTION

For the determination of the bulk ionic composition of fluid inclusions in a given mineral, such as quartz, a number of destructive analytical techniques are available, each having some advantages, but at the same time inadequacies, compared to the other. An ideal technique would be one that can determine an extensive range of anionic and cationic species, as well as having low detection limits for these species. It must also be able to perform a large number of analyses in a short period of time, as quick preliminary results are often required, for example, during the early stages of exploration.

The technique of Capillary Electrophoresis, or Capillary Ion Analysis (CIA^{TM}) will be evaluated in this thesis to determine its suitability and effectiveness in fluid inclusion analysis, as previously suggested by Hallbauer (1994).

1.1 Objectives

The objectives of the project would be: a) To optimise the technique itself for inclusion analysis by establishing an effective sample extraction procedure, whereby all contamination factors introduced during sample preparation and crush-leach fluid extraction, are quantitatively delineated and either eliminated if possible or subtracted from the analysis as a constant value. Optimum analytical conditions must also be set to identify the largest amount of ionic species at the lowest level of detection.

b) Determining the applicability of this bulk compositional data in modelling the fluid regime and the P-T-X conditions at the time of fluid entrapment. Since a bulk composition of all the inclusion generations present in a sample is determined, the properties of individual inclusions would have to be investigated by microthermometry to verify the correctness of any conclusions drawn from bulk fluid chemistry.

From the fluid composition and entrapment temperature of the inclusions, as well as the use of O-isotope data, the origin of the quartz veins and their relationship to each other can be evaluated and compared to previous investigations.

1.2 Methodology

For the purpose of this study, mineralized quartz veins as well as barren quartz veins within an area of mineralization (with the possibility of being related to the mineralising period) is considered. Forty four quartz vein samples, hosted by Malmesbury sediments or Cape Granites, were collected from localities in Jonkershoek, Paarl, Sea Point, Simon's Town and Helderberg, as well as from the old Sn mines at Kuiperskraal and Vredehoek, and an old gold digging on the road to Seinheuwel. A sample collected by A.V. Krige in 1921, from the Sn digging on the current farm Zevenwacht, was also analysed. Only the samples from Kuiperskraal and Zevenwacht were mineralized quartz veins. Three quartz vein samples from Kuiperskraal, collected by Bruwer (1997), were also included.

Thirty-two quartz samples were analysed for its ionic composition by CE, and the water content of the inclusions was determined by the Karl Fischer titration. Both were done at the University of Stellenbosch Geology Department.

Oxygen isotope studies on twenty-eight of these samples were done by Dr. C. Harris at the University of Cape Town.

Microthermometry was done at the University of Stellenbosch on eight quartz samples from mineralized as well as unmineralized quartz veins at different localities.

SEM analyses were performed on six quartz samples at the University of Stellenbosch.

2 GEOLOGICAL SETTING

The study area is situated within the Neoproterozoic Saldania belt, which forms the southern continuation of the Pan-African mobile belt extending along the West coast of Southern Africa. The metasedimentary and metavolcanic rocks of the Malmesbury Group are the oldest rocks (950 -600 Ma) of the Saldania belt (Frimmel & Frank, 1998), and has been intruded by the Cape Granite Suite, consisting of a series of Late Precambrian plutons and batholiths, ranging in age between 547 ± 6 Ma and 510 ± 4 Ma (Da Silva *et al.*, 2000; Chemale *et al.*, in press). The Malmesbury Group is divided into three terranes by the NW-trending Colenso and Welington-Piketberg fault zones, namely the south western Tygerberg terrane, the central Swartland terrane, and the north eastern Boland terrane, seen in Figure 2.1 (Hartnady *et al*, 1974). The Malmesbury Group and Cape Granite Suite are unconformably overlain by clastic sediments of the Palaeozoic Cape Supergroup.

2.1 Stratigraphy

2.1.1 Malmesbury Group

In the Tygerberg terrane the thick sequence of rhythmically alternating greywacke, phyllitic shales and siltstone, immature quartzite and thin impure limestone and conglomerate beds of the Tygerberg Formation suggest a turbidite sequence found either in a continent rise / oceanic trench environment, or as submarine fans at the foot of the continental slope in a tectonically active environment (Von Veh, 1983).

The central Swartland terrane, with its sedimentary sequences indicative of a shelf-sea depositional environment, is composed of the Berg River, Klipplaat and Moorreesberg Formations. Chlorite schist, greywacke and impure cherty limestone lenses with quartz schist

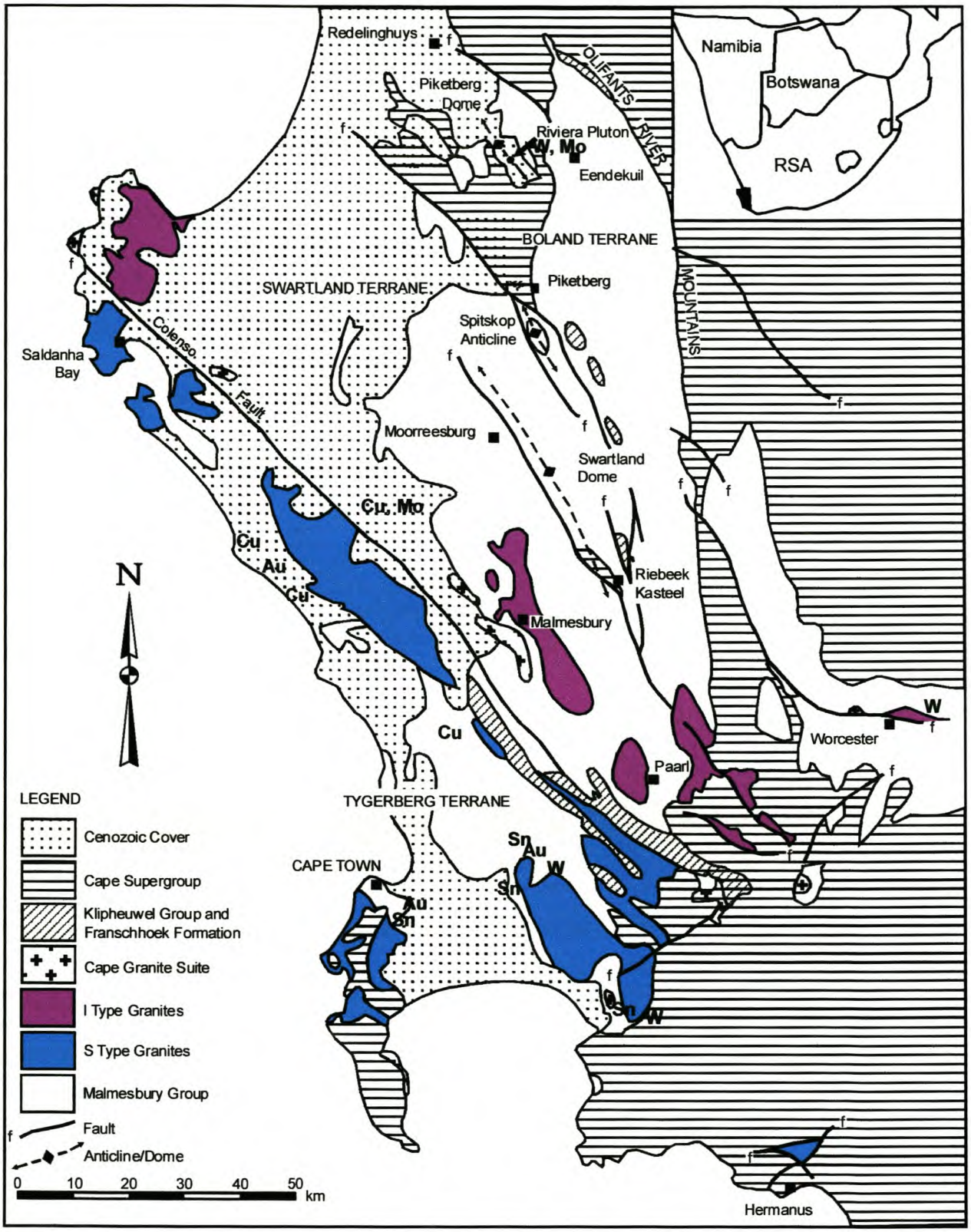

Fig. 2.1. Geological map of the rocks within the Saldania belt, as well as distribution of mineral deposits (from Scheepers, 1995)

towards the top characterises the Berg River Formation, while the overlying Klipplaat Formation consists of quartz-sericite-chlorite-schist with local interbeds of phyllite and limestone. The Moorreesberg Formation, consisting mainly of interlayered greywacke and phyllite, appears to interfinger tectonically with the Klipplaat Formation. The Franschoek Formation, composed of greywacke, conglomeritic bands and dark slates in quartzites, unconformably overlies part of the Swartland terrane, while the metavolcanic Bridgetown Formation follows the Swartland-Boland terrane and consists of complex greenstone bodies, intrusive dykes, dolomite, chert and graphitic schists (Rozendaal *et al.*, 1999).

In the Boland terrane, the Piketberg and Porterville Formations consist predominantly of pelites, fine- to medium-grained greywackes, conglomerates, phyllitic shales, arenitic lenses and limestones, while the Brandwacht Formation comprises greywacke and pelite with interbedded conglomerates and metavolcanic rocks. The sediments found in the Boland terrane reflect a succession that was possibly deposited along a highly irregular, northeastward transgressive coastline (Dunlevey, 1992; Rozendaal, *et al.*, 1999). The volcano-sediments of the Malmesbury Group suggest a depositional basin formed on an evolving continental margin, ocean-bound to the west.

2.1.2 Cape Granite Suite

Granitoid magmatism responsible for the intrusion of the Cape Granite Suite in the Saldania Belt occurred in three major phases (Scheepers & Rozendaal, 1992; Gresse & Scheepers, 1993). The first phase of syn- to post-tectonic, peraluminous, S-type granitoids with a single zircon age of 547 ± 6 Ma (Da Silva *et al.*, 2000), is confined to the Tygerberg terrane. The second phase consists of post-tectonic, metaluminous I-type granitoids that intruded at 539 ± 5 Ma (Da Silva *et al.*, 2000; Armstrong *et al.*, 1998) into the Swartland and Boland terranes. These plutons are related to high-potassium calc-alcaline volcanism, typical of magmatism in

island arcs or active continental margins (Rozendaal *et al.*, 1999). The magmatism was concluded with the intrusion of post-tectonic anorogenic A-type granitoids in the Tygerberg and Swartland terranes at 510 ± 4 Ma (Chemale *et al.*, in press) above a dormant subduction zone (Gresse and Scheepers, 1993; Rozendaal *et al.*, 1999).

2.2 Tectonism and metamorphism

The Neoproterozoic Saldania orogenic cycle started with a rifting phase as a result of the breakup of the supercontinent Rodinia between 780 and 750 Ma. During a period of ocean floor spreading between 700 and 600 Ma the Malmesbury Group, among others, was deposited. A subduction phase between 600 and 545 Ma resulted in low intensity deformation in the Tygerberg and Boland terranes, with subvertical to slightly southwest-vergent folds in the Tygerberg terrane (Gresse and Scheepers, 1993). The Swartland terrane displays more intense deformation.

Plutons of the Cape Granite Suite were emplaced between 550 and 510 Ma in the hinges of anticlines of the Malmesbury Group, resulting in a prominently northwest-elongated arrangement, parallel to the dominant Saldania tectonic grain (Gresse *et al.*, 1992). Chlorite and hornblende in some of the contact aureoles of the granite plutons suggest that temperatures of amphibolite metamorphic grade may have been reached (Rozendaal *et al.*, 1999).

A period of uplift and erosion followed the granite emplacement until the beginning of the Cape Supergroup sedimentation during the Ordovician, lasting from 480 –400 Ma. After another period of uplift and lowering of sea level during the Late Carboniferous, the Karoo sediments were deposited until 215 Ma. The first phase of folding of the Cape Orogeny occurred at 278 ± 2 Ma (Hälbich and Cornell, 1983), with additional tectonic events at 258 ± 2 Ma, 247 ± 3 Ma, 230 ± 3 Ma and 215 ± 5 Ma. Load metamorphism and tectonic regional metamorphism of low greenschist facies were reached at P-T conditions of 1,5 kb and 200 –

300 °C (Hälbich and Cornell, 1983), affecting the Palaeozoic Cape Supergroup and underlying pre-Cape lithotypes.

The Middle to Late Jurassic breakup of Gondwana resulted in the final stage of tectonism within the Cape Fold Belt, causing reactivation of Late Precambrian and Palaeozoic tectonic lineaments. Until present day the rocks in the South Western Cape were subject to erosion.

2.3 Mineralization

The most significant mineralization in the Saldania belt occurs within the Tygerberg and Boland terranes, while the Swartland terrane is relatively barren (Figure 2.1).

In the Tygerberg terrane, mineralization is concentrated along a north-west south-east trending zone, extending from Danger Point near Hermanus to beyond Yzerfontein along the west coast, referred to as the Yzerfontein - Helderberg zone (YHZ) by Scholtz (1946). Cassiterite-wolframite (± Au, Cu, Mo, Fe-sulphides) associations found at Helderberg, Bottelaryberg and Kuilsrivier are hosted by greisenized, S-type granite and display mineralogical and / or alteration features typical of a granite related process of metasomatism by late mineralizing, magmatic, hydrothermal fluids. The mineralizations at Durbanville, Vredehoek and Lion's head would be the exo-granitic equivalents of such a process. The vertical and lateral zonation of Sn-W-Cu-Mo-Au-Zn could be interpreted as the result of evolution of fluids and sequential precipitation as a function of distance from the source (Shcherba,1970; Pirajno & Bentley, 1985). This results in Sn-dominated veins in the centres of the district and base metal sulphide-dominated veins on their peripheries. A felsic magmatic association related to the inner sides of principal arcs is suggested (Rozendaal & Scheepers, 1995).

Copper and gold mineralization towards the northwestern part of the Tygerberg terrane post-dates W-Sn-Mo greisen/vein deposits. Characteristics of the former indicates a porphyry-type

association and is hosted by high-K, calc-alkaline I-type intrusions, which is spatially related to principal arcs above intermediate to steeply dipping subduction zones (Sawkins, 1990).

Subduction related plutonism is suggested as the tectonic setting for the metallization, supported by evidence from the Sn-W back-arc mineralization in the same terrane.

The Cu-Mo-Au mineralization at Alexanderfontein constitutes the last intrusive and mineralising phase of the Cape Granite Suite, emplaced during extensional events at the end of the Saldania orogeny and is spatially and genetically related to post-tectonic A-type leucogranitoids (Scheepers and Cuney, 1992). Figure 2.1 illustrates this distribution of deposits.

Tourmaline nodules, hosted primarily by S-type granites of various phases, occur within the Tygerberg terrane. The nodules are considered to be the result of late-stage volatile-rich (B, F) hydrothermal fluids that post-magmatically replaced their host rock through various metasomatic reactions, reflecting a possible greisen alteration process. These swarms also suggest proximity to the apex of the host granitic plutons and favourable locations for greisen related mineralization, making it useful as a potential regional exploration guide (Rozendaal & Bruwer, 1995).

The Boland terrane hosts the Robertson W-skarn and the Riviera W-Mo-REE skarn. The Riviera deposit is classified as an endo-skarn, hosted by I-type ganitoids, with exo-skarn deposits in the Malmesbury meta-carbonates. The superimposed molybdenite veins and stockworks may have resulted from the later intrusion of an anorogenic A-type granite (Rozendaal and Scheepers, 1995; Rozendaal *et al.*, 1994).

2.4 Plate tectonic setting

Repeated influx of magma and mineralising hydrothermal fluids along the northwest-southeast trending Colenso Fault zone suggests an extensive vertical and lateral crustal weak zone capable of serving as a conduit for lower crustal/ mantel derived magma/ fluids over an

extended period of geological time. The information on the magmatism and metallization points to a continental margin arc and its inner arc plate tectonic environment typical of convergent subduction-related geotectonism. Cessation of subduction produced the inner-arc rift blocks and resultant tectono-stratigraphic terranes, with the sampled areas occupying the inner arc (Rozendaal & Scheepers, 1995).

3 FLUID INCLUSIONS IN MINERAL EXPLORATION

An exploration programme for mineral deposits involves identifying tectonic terranes with which these deposits are associated, namely syn- to late-collision igneous terranes for greisen-related deposits and subduction-related settings for porphyry-style deposits. Fully integrated remote sensing, photogeology and geological reconnaissance mapping are used for this purpose.

Regional and detailed scale exploration makes extensive use of stream sediment, soil and rock sampling with multi-element analyses. Hydrothermal alteration studies are conducted by targeting primary geochemical alteration halos around the deposit, as well as secondary dispersal patterns of chemical elements created during weathering and erosion of the deposit. Elements of the ores are sought, aided by the numerous pathfinders such as W, Sb, Mo, As, Te, Tl, and Hg for Cu, Pb, and/or Zn mineralization, and Cu, Zn, Bi, Mo, Li, F, Cl, Rb, etc. for Sn-W mineralization (Peters, 1978; Pirajno, 1992).

Fluid inclusion studies on quartz veins are incorporated in the exploration process where tectonic terranes favourable for the mineralization sought have been identified and a deposition environment delineated through characteristic alteration haloes. In the case of mineralization not yet found, composition of inclusion fluids may aid in determining if ore-forming processes could have been associated with the alteration event, or, where vein associated mineralization is present, provide information on the ore fluid regime for future exploration.

3.1 Relationship of fluid inclusions to ore fluid

Fluid inclusions are small volumes of fluid which are trapped within crystals by several mechanisms either during crystal growth (i.e., primary inclusions) or by later processes of shearing and rehealing of fractures (secondary and pseudosecondary inclusions). They are

generally representative of the fluids present during crystal growth or in which the crystal was later bathed. Where the host crystals are associated with ore, the primary inclusions are samples of the ore fluid and may therefore reveal much about the conditions of ore transport and deposition (Roedder, 1977).

When relating fluid inclusion type (primary or secondary) to quartz texture, anhedral milky quartz should not be disregarded as host of primary inclusions. This type of quartz may have crystallized from gelatinous, amorphous silica that formed by homogenous nucleation into a colloidal suspension, from a solution very supersaturated with silica. Silica supersaturation at high temperatures may result from a sudden decrease in fluid pressure; possibly from nearly lithostatic to hydrostatic or lower (Fournier, 1985).

3.2 Application of fluid inclusion data in exploration

Fluid inclusions have served as valuable tools for mineral exploration where an empirical relationship can be established between a. fluid inclusion property and the presence of mineralization in a certain area. Because few such studies have been conducted, care should be taken to generalise these relationships to other areas, and fluid inclusions are therefore best used in the restriction of potential targets in areas already selected by strategic exploration (Lattanzi, 1991).

In the search for blind orebodies, fluid inclusions often provide alteration halos surrounding the intrusive ore body and therefore presents a larger exploration target. Temperature of decrepitaion (or homogenization) of the inclusions is the most commonly used parameter for recognising halos, as the new inclusions generally have been formed at higher temperatures toward ore deposition. Other inclusion parameters expected to change on approaching ore deposition include total concentration of salts in the inclusion, the abundance of halite daughter crystals and gas rich inclusions, the ratio of Na to other ions, the sample weight loss on heating,

the sample H_2O content, and the visual estimates of the number of inclusions. The amount of water-leachable Cl, the main anion in fluid inclusions, should also increase toward ore, particularly in typical porphyry copper deposits (Roedder, 1977).

During weathering of ore deposits, resistant gangue minerals such as quartz can be found in the gossan or soil with their original fluid inclusions unchanged, so that fluid inclusions in detrital quartz can also be used to determine their provenance.

Recognition of boiling of the ore fluids, through the presence of vapour-rich and vapour-poor fluid inclusions, also has a significant application in exploration. Since boiling gives a measure of the maximum hydrostatic pressure at the site of ore deposition, it places limits on the depth of cover at the time and have been used to estimate rates of denudation (Voskresenskii *et al.*, 1972).

The most significant impact of fluid inclusions to ore deposit research is the data they have provided on the nature of ore forming fluids; these represent a key basis for constructing quantitative genetic models. By a combination of paragenetic and fluid inclusion studies, the history of fluid evolution can be reconstructed for a given deposit and constraints can be placed on the possible genetic models for the deposit.

Some of the deposit types on which fluid inclusions data provided information includes (Lattanzi, 1991):

1. Porphyry systems (e.g. Roedder, 1971), which, in most cases, show extensive boiling and contain inclusions with highly saline fluids, large amounts of daughter crystals and high homogenization temperatures towards the core;
2. Mississippi-Valley-type deposits (e.g. Roedder, 1976). Fluids associated with these deposits are typically dense, highly saline, moderately warm, commonly containing CH_4 and organic

compounds. The inclusion data seem to suggest an origin based on deep circulating connate brines, with some magmatic component, as suggested by Hall and Friedman (1963).

3. Precious metal epithermal deposits (e.g. Bodnar *et al.,* 1985), where the fluid inclusions contain dilute and low temperature fluids that reflect the involvement of large amounts of meteoric waters, and often evidence of boiling.
4. Quartz-Au veins in metamorphic rocks (e.g. Roedder, 1984b; Ho, 1987) have fluid inclusions with moderate salinity, and the almost ubiquitous presence of CO_2 is a distinctive feature.

3.3 How can data be obtained from fluid inclusions?

Compositional and entrapment data of fluid inclusions can be obtained by various destructive and non-destructive analytical techniques. Non-destructive analysis includes:

- *Visible light microscopy,* where refractive index of the included fluid is a function of its composition (Kalyuzhnyi, 1982);
- *Ultraviolet microscopy,* for the study of fluorescent hydrocarbon inclusions (Burruss *et al.,* 1985);
- *IR absorption spectrometry,* to determine organic molecules and groups in hydrocarbon inclusions (Barres *et al.*, 1987);
- *Microthermometry,* for the determination of general composition, density, total salinity, and temperature and pressure conditions during trapping (Van den Kerkhof, 1990);
- *Laser Raman microprobe,* used in the identification and quantitative analysis of polyatomic gas species such as CH_4, CO_2, N_2, H_2, etc., cations (Dubessy *et al.,* 1982), as well as some solids in single inclusions;
- *Proton microprobe,* which can be used to determine elements of $Z \geq 11$, but it is most suitable for those of $Z \geq 30$ (Horn and Traxel, 1987);

- *Electron microprobe,* largely used to identify daughter minerals in opened inclusions at the freshly broken surface of a sample;
- *Nuclear magnetic resonance,* whereby the amount of water in inclusions could be quantitatively determined (Kalinichenko *et al.,* 1985a,b). This technique was considered as part of this project, but since trial runs produced no data within almost one year after analysis, the *Karl Fischer titration* was decided upon.

Destructive analytical techniques apply largely to bulk analysis, but single inclusions can be opened and analysed by puncturing the inclusion in a vacuum system or using a laser beam to open and release the contents of the inclusion into the system used for analysis. Destructive techniques include:

- For gas analysis: *Gas chromatography* (Andrawes *et al.,* 1984) *and Mass spectrometry* (Guha and Gagnon, 1990).
- For solutes: *Capillary ion analysis* is introduced as another technique in the analysis of the bulk ionic content of fluid inclusions. It is suitable for a very large number of cationic and anionic species and compounds as well as organic acids, with very low detection limits. In combination with the *Karl Fischer titration*, where the bulk water content of the inclusions in a sample is determined, a bulk salinity for the inclusion fluid can be calculated in terms of total dissolved solids. Other techniques include *Atomic absorption spectrometry, Flame-atomic emission spectroscopy, Ion chromatography,* and *Inductively-coupled atomic-emission spectroscopy (ICP-AES)* (Roedder, 1990).

4 LOCAL GEOLOGY OF THE STUDY AREA

4.1 Introduction

Quartz veins from various localities in the Cape Peninsula, Somerset West, Stellenbosch and Paarl were sampled, being hosted by either Malmesbury sediments or granites from the Cape Granite Suite. All veins were unmineralized, with the exception of the sample collected by Krige from the Sn prospect on Zevenwacht, and the samples of Bruwer from Kuiperskraal. Figure 4.1 shows the localities of the samples in relation to the granitoids of the Cape Granite Suite and the mineralization present.

The plutons of the Cape Granite Suite hosting the sampled quartz veins, namely the Cape Peninsula, Kuilsriver-Helderberg and Stellenbosch plutons, are all S-type granites, with the porphyritic types hosting the veins. The Paarl pluton is an I-type, porphyritic granite. Table 4.1 lists the sample localities and the quartz vein and host rock characteristics.

4.2 Sample localities

4.2.1 Cape Peninsula

Three granite varieties have been distinguished in the Cape Peninsula pluton, namely a grey course-grained, porphyritic biotite granite, a fine-grained, non-porphyritic muscovite granite and at Sea Point a hybrid granite of alternating bands of light-coloured granitic and dark-coloured, biotite-rich slaty rock, separating the first two types. Various W- and NW-trending faults cut through the lithologies of the Cape Peninsula. Either granite or Malmesbury hornfels hosts the unmineralized quartz veins sampled at the Sea Point contact and these veins all are vertical, with a northwesterly trend (RM 12 – 17). Quartz veins from the slopes below Lion's Head, as well as those from Vredehoek are also vertical and NW-trending, except one quartz vein from Vredehoek (RM 57), having a low angle dip and intersecting RM 56. Again all are barren. Cassiterite-bearing quartz veins at Vredehoek has been described by Nellmapius

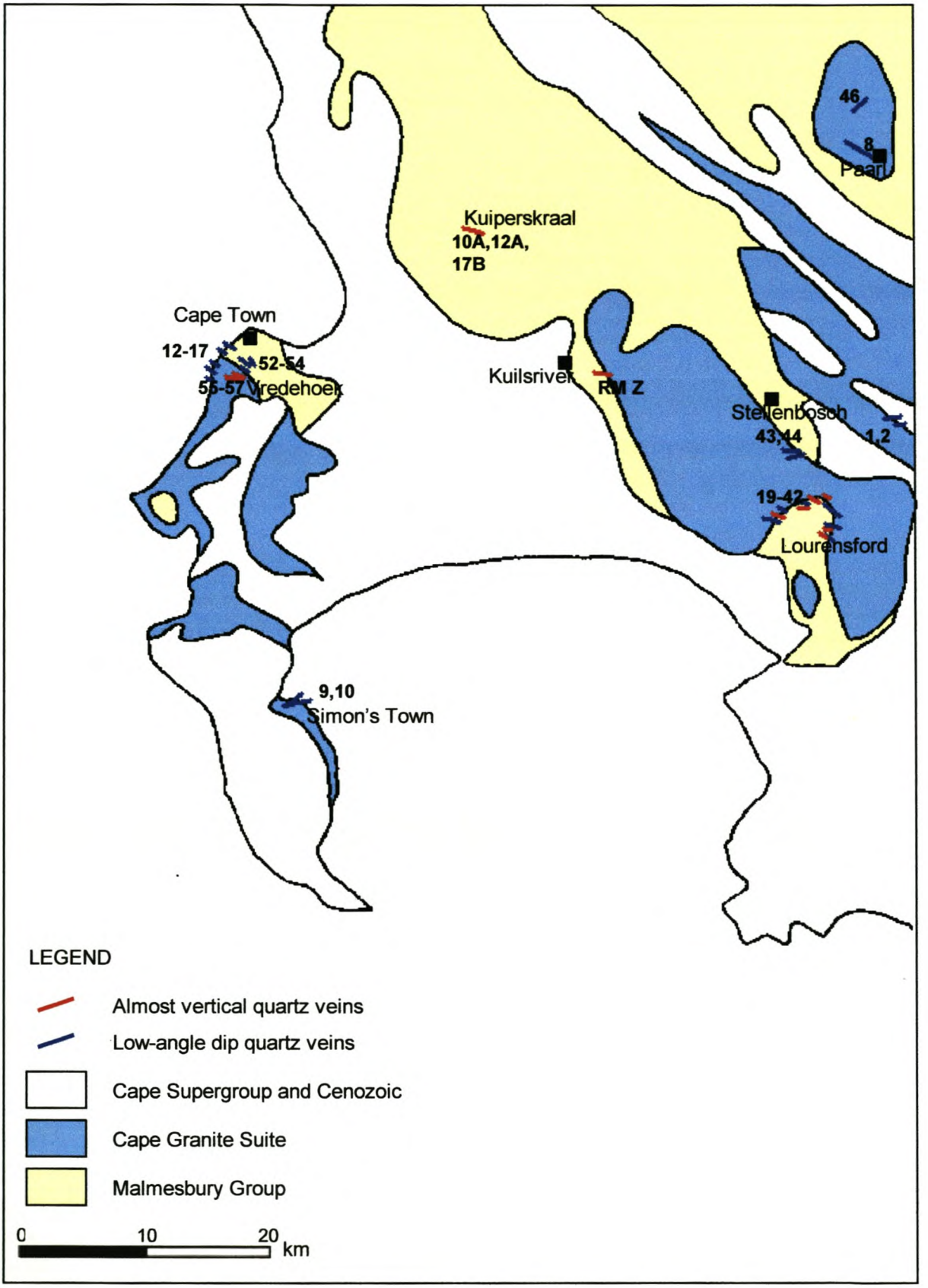

Fig. 4.1. Localities of sampled quartz veins. Compare numbers to those listed in Table 4.1.

(1912). The chief tin-bearing quartz veins, hosted by Malmesbury slates, generally strike in a north-northwesterly direction and are horizontal or have a very small dip. Another series of barren, vertical veinlets cut across this system.

4.2.2 Kuilsriver-Durbanville area

The Kuilsriver tin deposit, on the farm Zevenwacht, is situated within coarse-grained porphyritic granite of the Kuilsriver-Helderberg pluton. A quartz-cassiterite sample collected by Krige in 1921 was used for analysis. According to Wagner (1909) and Krige (1921), the mineralized quartz veins generally strike NNW, with a few striking NNE, and all dipping to the south or east with an angle between 15° and 50°. None of these veins were found to intersect one another.

From the Sn-deposit at Kuiperskraal, three samples, collected by Bruwer (1997), of quartz-cassiterite-arsenopyrite-sphalerite-tourmaline veins were used for analyses. The mineralized quartz veins appear as saddle reefs, striking NNW along the apex of an open anticline and dipping SSE (Bruwer, 1997). It is hosted by greywackes of the Tygerberg Formation that have undergone medium-grade contact metamorphism during granite intrusion as well as earlier regional metamorphism to lower greenschist facies. The metasedimentary rocks have a constant NW-SE strike and dip from SW to NE (Gresse, 1979; De Villiers, 1980; Everett, 1984). Alteration zones associated with the mineralized veins are actinolite, chlorite and carbonate alteration as well as tourmalinization (Bruwer, 1997).

4.2.3 Helderberg – Stellenbosch

Barren quartz veins occur in weathered, medium- to course-grained granite and course-porphyritic biotite granite as well as Malmesbury hornfels on the farm Lourensford on the southern slopes of Stellenbosch Mountain. Two types of quartz veins are present, namely those

Table 4.1. Sample locality and description

Sample no.	Location	Description
RM 1 & 2	Jonkershoek valley	Vertical-dipping q-veins in weathered course porphyritic granite – Stellenbosch pluton.
RM 8	Near Paarl Taal Monument	NW striking, vertical Q-vein > 1m thick in porphyritic granite – Paarl pluton.
RM 9 & 10	Simon's Town	Intersecting q-veins in course porphyritic biotite granite; RM 9 has a westerly trend and RM 10 southwesterly. No angle was evident.
RM 12	Sea Point	Q-vein, vertical with NW strike, in course porphyritic biotite granite – Cape Peninsula pluton.
RM 14 & 15	Sea Point	Parallel q-veins in fine-grained muscovite granite - Cape Peninsula pluton; vertical, NW striking.
RM 16 & 17	Sea Point	Parallel q-veins in Malmesbury hornfels; vertical, NW striking.
RM 21, 23, 25	Lourensford Estate, S. West	Q-veins in weathered course porphyritic, biotite granite of the Stellenbosch pluton. RM 21 & 25 has low angle dips, striking W, and RM 23 is almost vertical, striking W.
RM 28 – 31, 35	Lourensford Estate, S. West	Almost vertical, W-striking q-veins in same granite as above.
RM 32, 33 & 36	Lourensford Estate, S. West	Low-angle dipping, W striking q-veins in fine- to medium-grained porphyritic hybrid granite close to Malmesbury contact.
RM 37a & b	Lourensford Estate, S. West	Parallel, low-angle dipping q-veins in Malmesbury hornfels, striking W.
RM 39 & 42	Lourensford Estate, S. West	Low-angle dipping, blue-grey q-veins in Malmesbury hornfels striking W.
RM 40	Lourensford Estate, S. West	Q-vein in Malmesbury hornfels; almost vertical, W striking.
RM 43 & 44	Farm Alto, south of Stellenbosch	Q-veins in weathered Malmesbury sediments.
RM 46	Nantes Dam – Paarl	Vertical, SW striking smoke-quartz vein in kaolinised porphyritic granite – Paarl pluton.
RM 49	Kuiperskraal Sn-digging	Q-vein with low-angle SE dip in Malmesbury sediments
RM 52	Old Au-digging on slopes below Lion's Head	W striking, almost vertical Q-vein in Malmesbury sediment.
RM 53 & 54	Road section above RM 52	Q veins, same orientation as RM 52, in Malmesbury rock, close to granite contact.
RM 55, 56, 57	Vredehoek - old Sn mine	Q-veins in weathered Malmesbury sediments. RM 55 & 56 are parallel, almost vertical and NW-striking, while RM 57 has a low angle dip, cutting RM 56.
11B, 12B, 17A	Kuiperskraal Sn deposit (Bruwer,'97)	Quartz-cassiterite-arsenopyrite-sphalerite-tourmaline veins in Malmesbury sediments.
RM Z	Kuilsriver (Zevenwacht)	Q-cassiterite vein collected by Krige (1921).

having an almost vertical dip and striking W to NW, and a second type of quartz vein dipping at a low angle to the south or south-east and striking W (Table 4.1). Two veins of blue-grey quartz (RM 39 and 42), having the same orientation as the other sampled veins and hosted by Malmesbury sediment occur on the south-western slopes of Helderberg Mountain.

Two quartz veins (RM 43 and 44) on the farm Alto, between Somerset West and Stellenbosch on the western slopes of Stellenbosch Mountain, are hosted by weathered Malmesbury sediments. The nature of the outcrop is such that no strike or dip is evident.

In the Jonkershoek Valley, between the Stellenbosch and Jonkershoek Mountains, two vertical quartz veins (RM 1 and 2) were found in very weathered, course porphyritic granite of the Stellenbosch pluton.

4.2.4 Paarl

In the porphyritic granite of the Paarl pluton a vertical dipping, NW-striking quartz vein of slightly more than 1 m thick was found some distance from the Taalmonument (RM 8), while a SW-striking vein of smoke quartz was found in kaolinised granite near the Nantes Dam (RM 46).

4.3 Discussion

4.3.1 Correlation between vein systems

The mineralized veins at Kuilsriver correspond in strike with tin-bearing quartz veins on the farm Bonterivier on the northern slopes of Helderberg, as well as on the farms Welbeloond, Hoogekraal and Kuiperskraal northwest of Durbanville, so that they all lie within the same NNW-trending zone (Krige, 1921). The mineralized lodes are either quartz veins or saddle reefs dipping at a low angle to the south or east. The quartz-cassiterite veins of the distant Vredehoek deposit have the same orientation.

Mineralogically the cassiterite-bearing veins in these areas are very similar. At Helderberg, traces of wolframite, löllingite tending to arsenopyrite, chalcopyrite and some pyrite, molybdenite and tourmaline are found with the quartz and cassiterite, while at Kuilsriver quartz, cassiterite, löllingite and arsenopyrite, chalcopyrite, traces of molybdenite, and tourmaline form the vein minerals (Krige, 1921). At Kuiperskraal the mineralized veins consist of quartz, cassiterite, arsenopyrite, sphalerite, pyrite, chalcopyrite and tourmaline (Bruwer, 1997). At Vredehoek, quartz, cassiterite and tourmaline are the most abundant vein-forming minerals, with pyrite, chalcopyrite and arsenopyrite in small quantities and mostly confined to the wall rock (Nellmapius, 1912).

With respect to the proximity of the mineralized veins to the underlying Kuilriver-Helderberg pluton, the lodes at Helderberg occur comparatively deep down in the granite, *i.e.* more than 400m below the eroded surface of the granite. At Kuilsriver they occur approximately 100m below the former roof of the granite dome (Krige, 1921), while at Kuiperskraal they are found in Malmesbury rock about 300m above the level of the granite (Bruwer, 1997). At Vredehoek the veins are also found some distance above the roof of the granite from the Cape Peninsula pluton.

The barren quartz veins that were sampled throughout the study area form part of two apparent vein systems. Veins of the one system dip at a low angle to the SE and generally strike SW to WSW, while those of the other system are close to vertical and strike W to NW. The veins from both systems range in thickness from 5 to 20 cm, with the exception of the one in the Paarl pluton. All occur within either granite or Malmesbury host rock. With respect to the mineralized quartz veins at the various localities mentioned above, these barren veins run almost transversely to the former, but it is unknown if they would intersect. From their difference in orientation, they probably belong to a different fissure system. A study of inclusion characteristics such as formation temperatures and inclusion types present in quartz

from the different systems might reveal which one post-dates the other. Krige (1921) found that none of the barren quartz veins occurring at Kuiperskraal, Kuilsriver and Helderberg, striking either SW or NW, with some dipping vertically, intersected the lodes.

4.3.2 Origin of mineralized and barren quartz veins

Bruwer (1997) has studied the quartz-cassiterite-arsenopyrite-sphalerite-tourmaline veins found at Kuiperskraal in detail and concluded that late-magmatic hydrothermal fluids released from the underlying Kanonkop granite were responsible for this mineralization. The Kanonkop granite is a highly fractionated, peraluminous, tin-enriched leucogranite belonging to the Sa2 granitoid association as defined by Scheepers (1995). During evolution of the magma a metal-enriched, alkali-volatile-rich (B, F) phase developed, which crystallized as late-magmatic fluids, either endo- or exo-granitic. The cassiterite-rich quartz veins were the first to crystallize from this high-temperature fluid. As it cooled, quartz-chlorite-calcite-actinolite followed by quartz-calcite-actinolite veins crystallized. A series of hydrothermal fluid pulses, decreasing in temperature and with continuously evolving composition, were therefore responsible for mineralized and barren quartz veins found in the Kuiperskraal area.

It was suggested by Krige (1921) that the mineralizations at Kuilsriver and Helderberg were related to the underlying granite, but whether their origin could be the Kanonkop granite has not been investigated. The similarities in structure and mineral assemblage certainly suggest the possibility. No detailed work on the barren quartz veins close to these deposits has previously been done to determine if they were related to the period of mineralization or to later regional tectonism.

The Sn mineralization at Vredehoek might be in distal relation to the Kanonkop granite rather than the underlying Cape Peninsula granite, because of the lesser extent of fractionation of the latter required for Sn concentration, as well as the orientation of the mineralized quartz veins

above the granite. They are almost horizontal and it appears that they might never intersect the underlying granite. The horizontal, barren quartz veins might also have their origin in a distant granite to the east, while the vertical, barren quartz veins most likely originates in the underlying granite.

4.4 Conclusion

The two sets of barren quartz vein systems, namely almost horizontal and nearly vertical dipping, might be a late phase related to the Sn mineralization event, and/or were formed during later regional tectonism of the Cape Supergroup sedimentation and Cape Orogeny. A comparison of the characteristics and formation temperatures of inclusions in the quartz of these barren veins as well as with those in the quartz of the mineralized veins might prove to be distinctive of a difference in origin.

5 MICROTHERMOMETRY

5.1 Petrographical study

Quartz from the different veins shows various degrees of whiteness, an indication of the amount of inclusions present. Quartz from samples RM 39, 40 and 42 are blueish-grey, which may result from a larger volume, in comparison with other samples, of a specific type of inclusion.

Deformation textures such as undulose extinction, occur in the quartz of various samples, with its presence or absence not confined to samples from a specific area, host rock or even vein orientation (horizontal or vertical dipping). It is though, notably absent from all quartz veins, almost vertically dipping, sampled along the coast of the Peninsula (RM 11-17). In addition to this extinction, sample RM 25, a vein in granitic host rock, shows folding of the quartz.

Most of the sampled quartz veins have biotite and chlorite filling small cracks between quartz crystals, with the chlorite often an alteration product of the biotite. Few other minerals occur with the quartz in the studied veins. Chlorite needles are found in the quartz of samples RM 12 – an applite vein, RM 26 – pegmatite quartz, RM 48, 49, 52 and 53. Hematite is found within biotite of sample RM 52, possibly as an alteration product, while orthopyroxene is folded with the quartz of sample RM 25 (Photo 1).

5.2 Inclusion characteristics

The inclusions in all the quartz samples studied occur along healed microfractures, forming thin veins or planes of inclusions. All inclusions are secondary, having been trapped at various stages of fluid flow after initial quartz vein formation. Only samples RM 12, 14 and 28 contain possible primary inclusions.

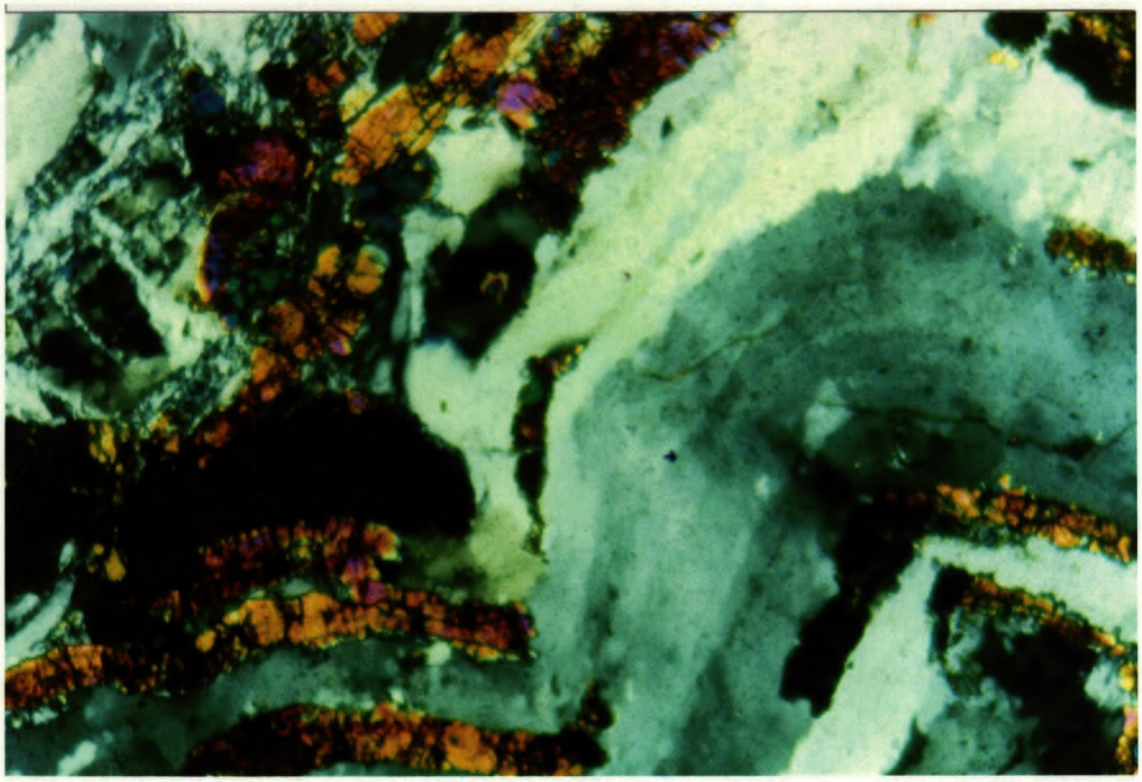

Photo 1. Folding of the quartz and orthopyroxene in sample RM 25, with the inclusions following this texture. 20X Magnification.

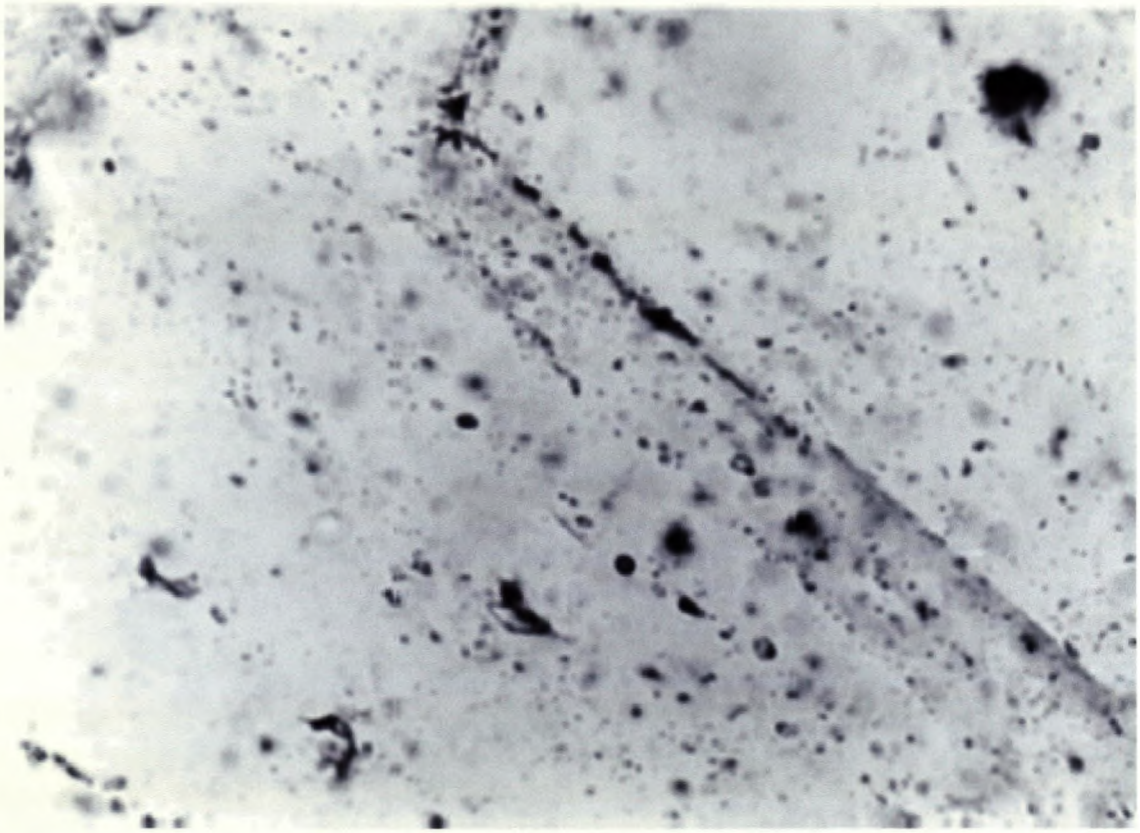

Photo 2. Possible primary inclusions in RM 14, marking growth zones in the quartz. 20X Magnification.

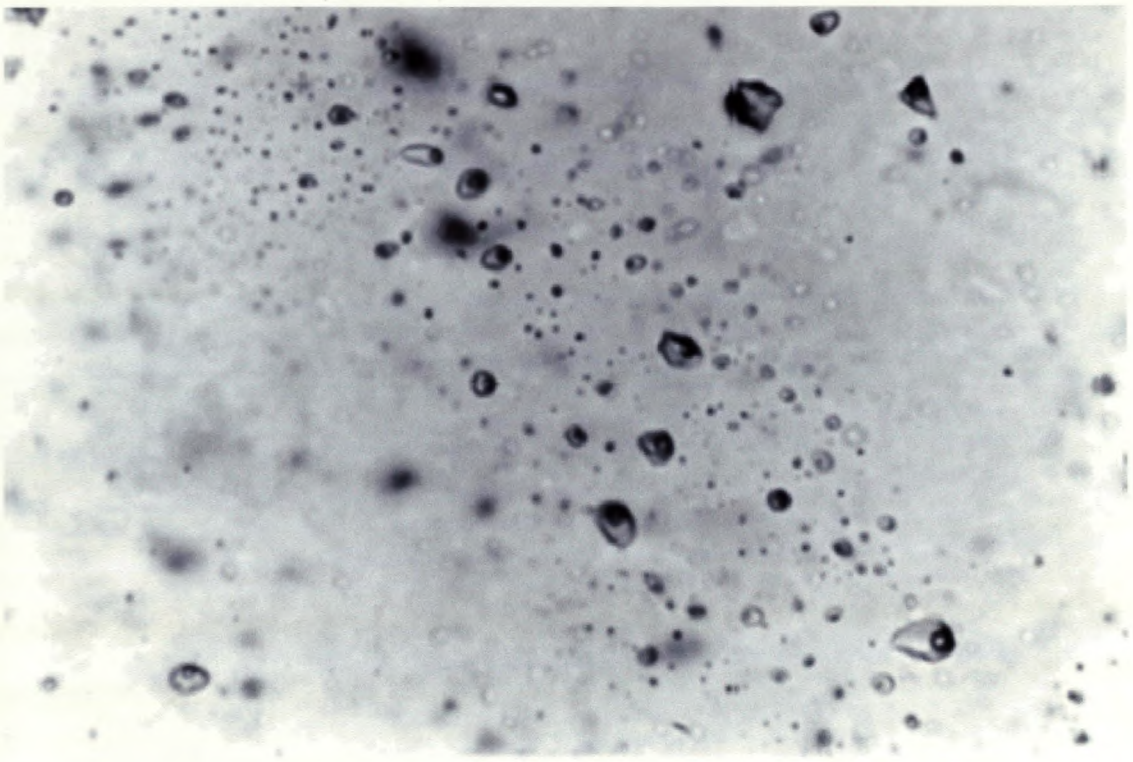

Photo 3. Round to angular inclusions found in the quartz of most samples. 20X Magnification.

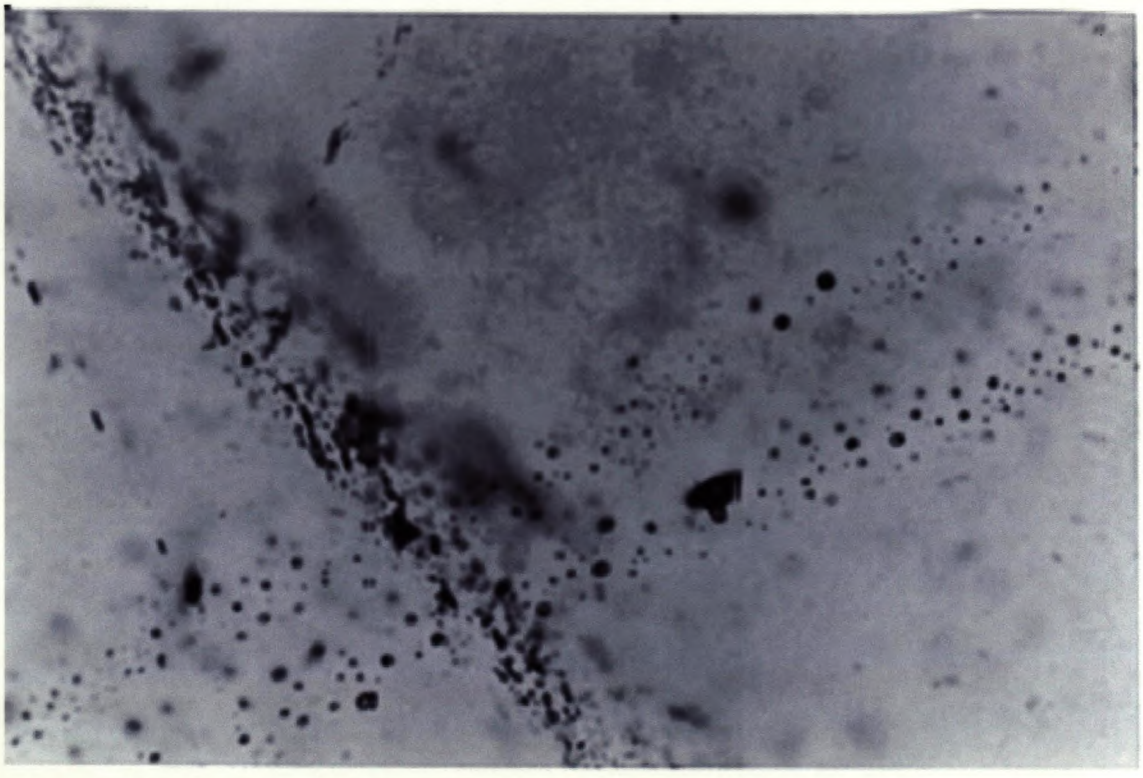

Photo 4. The youngest population of dark, irregular inclusions intersecting a trail of slightly older, small (~ 1μm) round inclusions. 20X Magnification.

Inclusion shapes vary from rounded or slightly angular to very irregular, with sizes between 2 and 10μm for the rounded ones, and up to 15μm for the irregular inclusions (Photo 2).

Two-phase (L+V) inclusions are the most abundant, while some single phase liquid inclusions were also observed (Photo 3). The vapour phase fills between 5 and 40% of the inclusion volume of two-phase inclusions. No three-phase inclusions or inclusions containing daughter crystals were found.

All samples contain at least four different types of inclusions, according to their shape, with planes of irregular inclusions often the most abundant. Veins of a dark, almost black irregular inclusion, seldom having a distinguishable bubble, as well as very thin veins of a small (~ 1μm) round inclusion, are found in all vein quartz samples studied. The dark inclusion might contain gases such as CH_4, N_2 or some sulphur. Both these inclusion types cut across all crystal boundaries, therefore being trapped some time after quartz recrystallization. It appears that the dark, irregular inclusion type is the youngest, obliterating trails of the smaller inclusion (Photo 4). The planes of slightly irregular mixed with larger (8 – 12μm), very irregular inclusions, only occur within individual quartz crystals and is considered the oldest of the inclusion types present, with the exception of the few primary inclusions. The inclusion characteristics of all the samples studied are summarised in Table 5.1.

5.3 Temperature measurements

One or two samples from each area was selected for microthermometry measurements, namely RM 1 from the Stellenbosch pluton; RM 14 and 16a from the Peninsula area; RM 23, 39 and 42 from Lourensford Estate, the last two being blue-grey quartz veins; RM 49 from Kuiperskraal; RM 57 from the Vredehoek tin mine; and RM Z, a quartz-cassiterite sample from Zevenwacht. Horizontal and vertical dipping veins were selected to determine a possible difference in origin for these vein types.

5.3.1 Homogenization temperature

The measured temperatures for the inclusions studied range between 160 and 390 °C. Veins of relatively small (4 – 6μm), round inclusions form the low- temperature population of 160 – 210 °C, found in all samples except RM 42 and 49. Rounded and irregular inclusions homogenising in the range 230 – 300 °C, as well as a higher temperature population of irregular inclusions in the range 310 – 360 °C is present in all the studied samples. Trails of one-phase liquid inclusions homogenise to the vapour phase with temperatures between 240 and 290 °C for samples RM 1 and RM 57, 325 °C in RM 23, and 240 – 370 °C in samples RM 14 and RM 16a. The dark, very irregular inclusions found in all samples analysed, has a temperature range of 240 – 360 °C, homogenising either to the liquid or vapour phase. An even higher temperature population of 370 – 390 °C irregular, one phase liquid inclusions, homogenising to the vapour phase, is present in sample RM 23. The cassiterite of sample RM Z contains the same inclusion populations as the quartz of that sample, namely the dark, irregular type inclusion, homogenising to the vapour phase at around 345 °C, as well as irregular inclusions of the temperature range 270 – 300 °C, homogenising to vapour in the cassiterite and to liquid in the quartz. Because of its small size (~ 1μm), no homogenization temperatures could be obtained for the thin trails of round inclusions found in all samples and which were formed just before the dark, irregular inclusion type of intermediate to high temperature.

None of the inclusion populations indicate trapping from a boiling fluid, where the homogenization pressure was less than the vapour pressure of the fluid. Homogenization temperatures would therefore have to be corrected for the lithostatic and/or hydrostatic pressure at the time of entrapment. As these quartz veins could be related to cassiterite mineralization after the Cape granite emplacement, with an estimated pressure of 1 - 2 kb (Bruwer, 1997), and the Cape Orogeny metamorphism (1.5 – 2 kb) a pressure correction range of 1 – 2 kb would be suitable. Temperature-pressure isochores were used to calculate formation temperatures (Figure

5.1), which is summarised in Table 5.1. After this correction the low temperature, low salinity fluids yield temperatures of 240 – 360 °C, the 200 – 300 °C population is corrected to 320 – 500 °C, while the 340 °C and 370 °C populations could have been trapped from fluids at 460 – 580 °C and > 600 °C.

5.3.2 Salinity

The fluid inclusions from all the samples studied all have final melt temperatures between 0 and –3, representing a salinity range between 0 and 5.7 eq. wt.% NaCl. Only the sample of blue-grey quartz from Lourensford (RM 42) contains inclusions of up to 10 eq. wt.% NaCl. The fluids from which these inclusions were trapped therefor appear to be simple H_2O – NaCl fluids. Temperaure-salinty diagrams indicating the various fluid populations are shown in Figure 5.2, while homogenization temperature and salinity measurements for individual inclusions are contained in Appendix A.

5.4 Discussion

The earliest fluids in the history of the quartz veins are represented by the angular to irregular inclusions that are present as planes or randomly distributed within the quartz, with homegenization temperatures in the range 230 – 360 °C. These temperatures might have been higher at the time of entrapment, as indicated by similar inclusions in one sample having temperatures between 320 and 390 °C. The lower temperatures might have been superimposed by later cooler fluids, such as represented by the veins of late secondary inclusions homogenizing between 160 and 200 °C. Veins of dark, irregular inclusions seem to represent the youngest fluid phase, but they do not have the lowest temperature, as might be expected for consecutive phases in an evolving fluid system. They could therefore represent fluids from a different source, introduced at a late stage during the history of the fracture system.

Table 5.1. Fluid inclusion characteristics and pressure corrected homogenization temperatures.

Sample no. and location	*Inclusion type*	*P, PS, S*	*Size (µm)*	*Main Tm (°C)*	*Main Th (°C)*	*Th range (°C)*	*Pressure corrected Th (°C) for 1-2 kb*	*Salinity (eq. wt.% NaCl)*
RM 1 Jonkershoek	L + V	S	4 – 6	-0.3	170	160 – 300	240 – 310	1.25
					290			
	L + V	S	8 – 12	-0.5	200	180 – 300	280 – 360	1.6
					290			
	L + V - dark	S	8 – 12	+0.3	300	300 – 320		
RM 14 Simon's Town	L + V	S	4-6	-1	160	150-160	240 – 320	
	L + V	P	4 – 12	-0.5	230	220 – 260	350 – 430	1.6
	L + V - dark	S	8 – 12	0	250	240 – 260	340 – 420	
	L	S	± 6	nd	350	340 – 370		
RM 16a Sea Point	L + V	S	4 – 8	-2.5	200	160 – 200	290 – 370	4.92
					270	250 – 270	370 – 465	
	L + V	S	± 6	-0.1	290	270 – 290	390 – 490	0.9
	L + V	S	8 – 12	0	330	300 – 350	420 – 530	
	L/L + V		6 – 10	-1.5	230	200 – 250	320 – 410	3.3
RM 23 Lourensford	L + V	S	6 – 8	-1.0	180	170 – 190	260 – 340	2.46
	L	S	8 – 12	nd	340	320 – 390		
	L - dark	S	8 – 12	nd	270	230 – 280		
RM 39 Lourensford	L + V	S	4 – 8	-	210	200-280		-
		S	4 – 10	-	270			-
		S	6 – 10	-	340	310-350		-
	L + V – dark	S	8 – 12	-	320	310-335		-
RM 42 Lourensford	L + V	S	6 – 10	-4	270	266-280	390 – 500	7.2
	L + V/dark	S	6 – 12	-4	340	320-360	450 - 670	7.2
RM 49 Kuiperskraal	L + V	S	8 – 12	-1.5	300	280-300	390 – 490	3.3
	L + V - dark	S		0	340	310-340	420 – 530	
RM 57 Vredehoek	L + V	S	4 – 10	-2.5	230	200-270	300 – 380	4.92
					250	220-270	350 – 440	
	L + V	S	6 – 10	0	290	280-300	390 – 490	
	L + V - dark	S	8 – 12	-1	270		370 – 460	2.46
				0	340	300 – 380	420 – 530	
RM Z Kuilsriver	L + V	S	4 – 6	-1.5	200	200-230	290 – 370	3.3
			6 – 12	-1.5	280	240-300	390 – 490	
	L + V - dark	S	6 – 12	-3	290	240-340		5.7
				-1.5	340		460 - 580	3.3

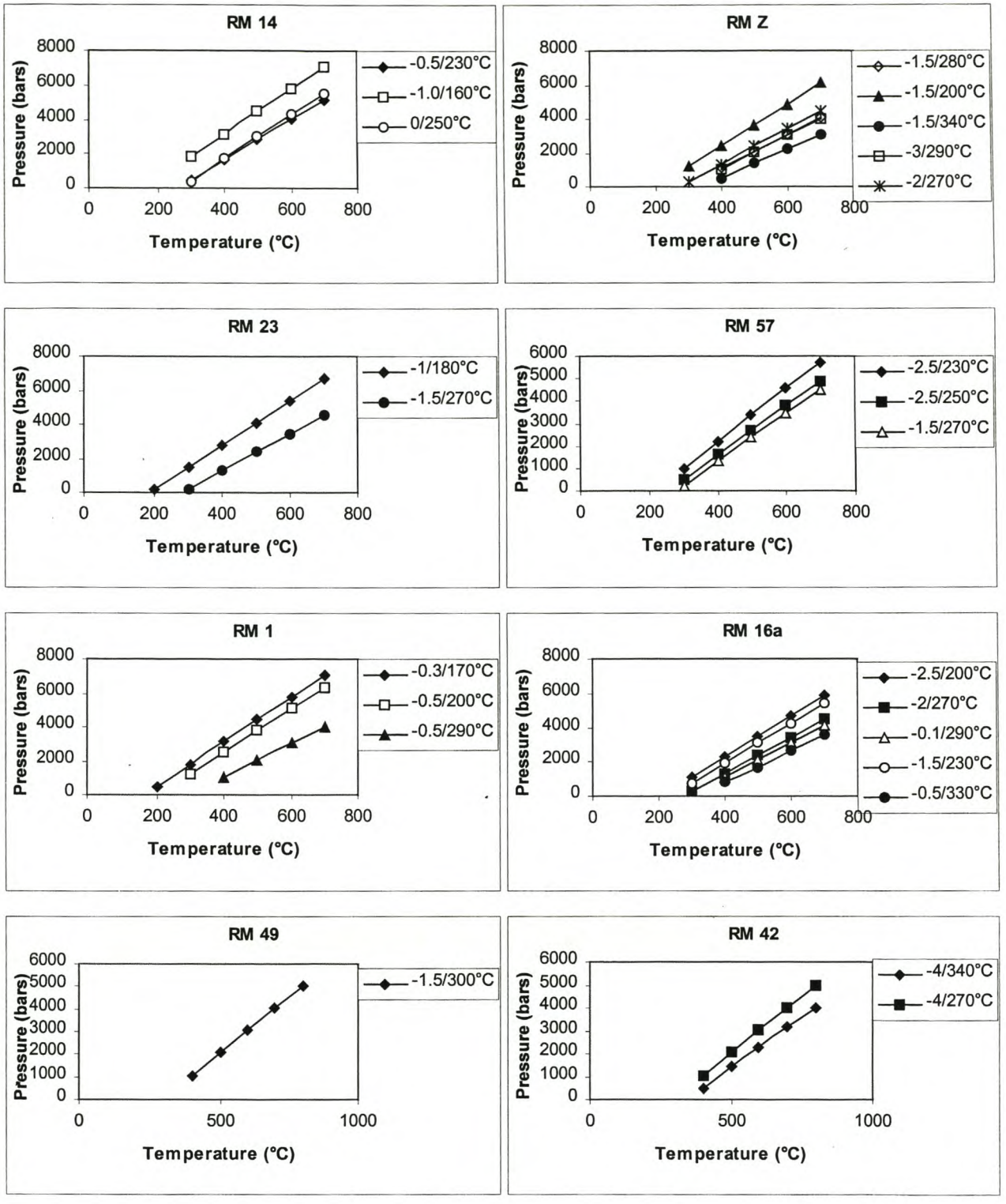

Figure 5.1. Temperature – pressure diagrams to calculate pressure correction.

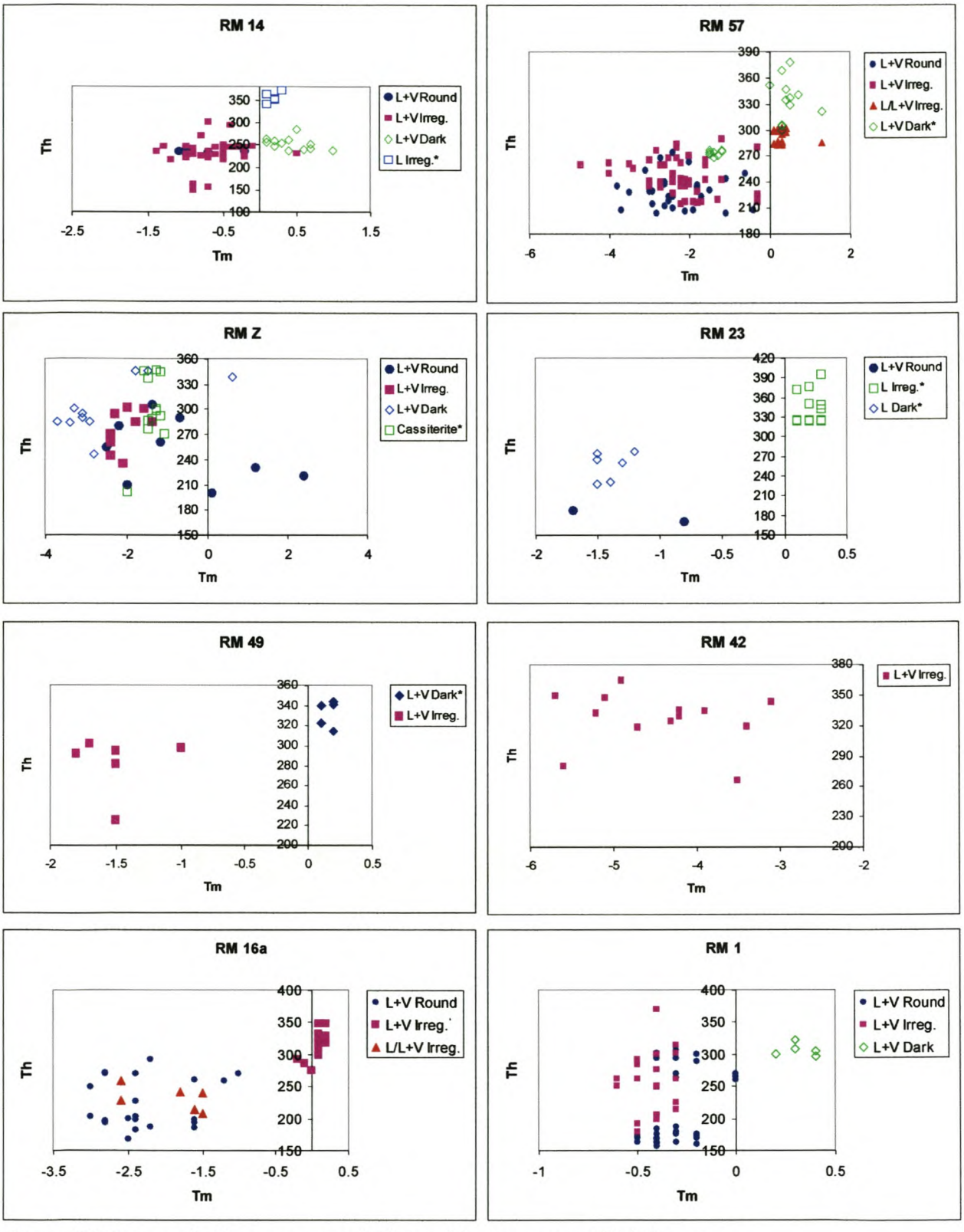

Figure 5.2. Homogenization temperature (Th) vs melting temperature (Tm) diagrams.

5.5 Conclusion

Inclusion temperature and salinity calculations for quartz selected throughout the study area and from apparently different vein systems indicates that they were all formed by and subjected to the same circulating fluid phases.

The very high to very low temperature populations, excluding the veins of dark inclusions, are most likely phases of an evolving fluid system from a single source. The temperature ranges and fluid salinity compare to those found by Bruwer (1997) for fluids in the mineralized and barren quartz veins at the Kuiperskraal Sn-deposit, having a late-magmatic origin. Similar late-magmatic fluids, expelled from the various plutons of the Cape Granites and undergoing cycles of cooling and possible dilution by other circulating fluids, could have resulted in this sequence of inclusions. Renewed fluid circulation at a later stage and with a different gave rise to the veins of higher temperature, dark inclusions.

6 CAPILLARY ELECTROPHORESIS

6.1 Principles of Capillary Electrophoresis

Capillary electophoresis (CE) is a modern analytical technique, which permits rapid and efficient separations of charged components present in small sample volumes. The separation mechanism is based on differences in electrophoretic mobility of the ions, resulting from the individual charge to mass ratio. This separation is achieved within an electrolyte filled fused silica capillary with an internal diameter of ~75μm, connected to storage containers of electrolyte and with an external voltage applied to the electrodes in the containers. Figure 6.1 illustrates the instrumental arrangement.

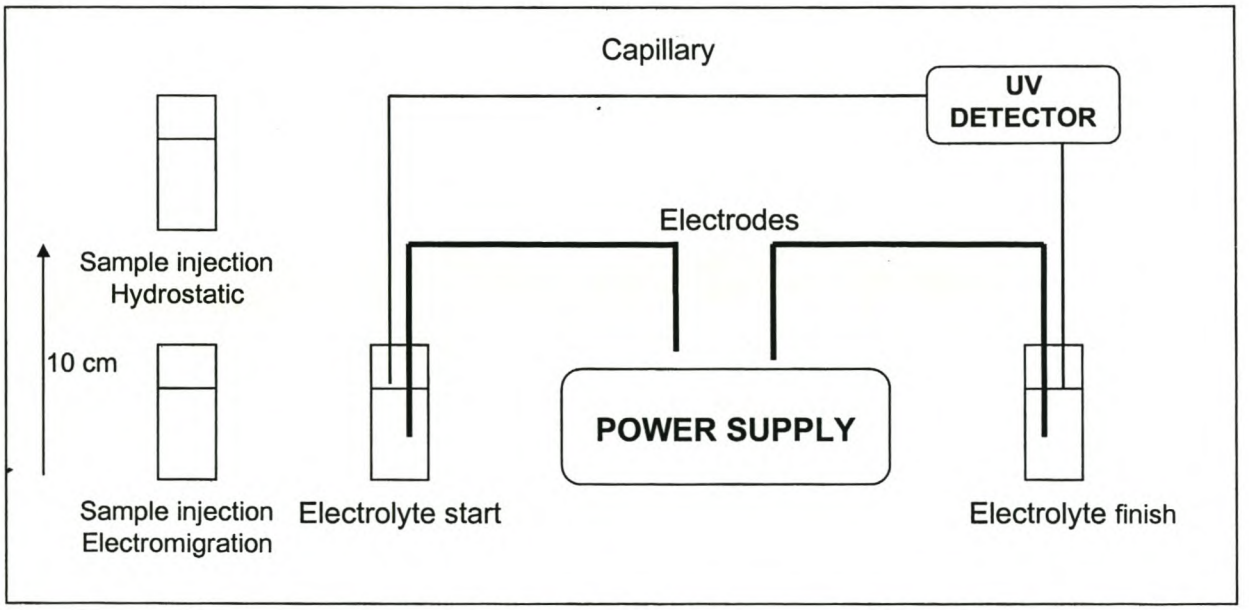

Fig. 6.1 Instrumental arrangement for CE.

6.1.1 Separation dynamics

6.1.1.1 Electrophoretic migration in capillary tubes

When an electric field is applied through narrow capillaries, it induces a flow within the capillary known as ElectroOsmotic Flow (EOF). This is considered the "pump" in CE, with the flow, in general, towards the cathode (-). A detector is therefore placed at this end.

EOF originates from the negative charges on the inner wall of the capillary tubes of fused silica. When a capillary is filled with an electrolyte of pH > 4, acidic silanol groups begin to ionize and form a negatively charged surface. Electrolyte cations (largely hydrated H^+) loosely associate with the silanol groups. In an electric field, these hydrated cations are pulled toward the cathode inducing a bulk flow in that direction (Villafranca, J.J.(ed), 1990; (Jandik, *et al.*, 1991; Li, 1992).

For anion analysis, a negative power supply must be used. This defines the sample side as the cathode and the detection side as the anode. Since one of the separation conditions for CE is for analyte ions to migrate in the same direction as electroosmotic flow (Jandik, *et al.*, 1991), the EOF would therefore have to be reversed to maintain the direction towards the anode and the detector. This can be achieved by adding osmotic flow modifiers (OFM) or quaternary amine surfactants such as tetradecyltrimethylammonium bromide (TTAB) to the electrolyte. OFM coats the capillary surface, yielding a positive surface, as shown in Figure 6.2 (Li, 1992).

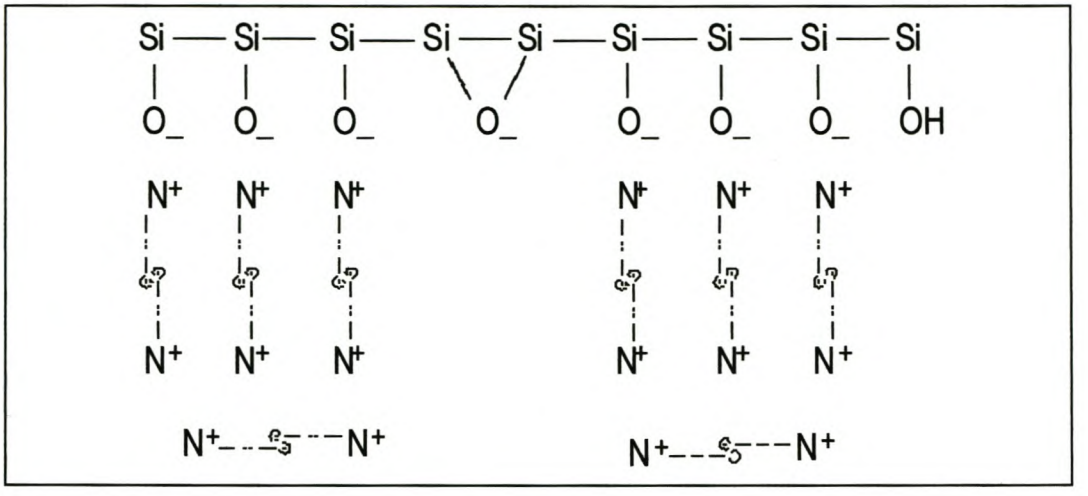

Fig. 6.2. Influence of quaternary amine surfactants on EOF reversal

Sample matrix cations migrate in the opposite direction towards the cathode at the sample side, and do not interfere with anion analysis (Figure 6.3). Sample matrix water and neutral organics pass through the capillary at the same rate as EOF and are observed after the analyte anions, at approximately 10 minutes, and also do not interfere with anion analysis.

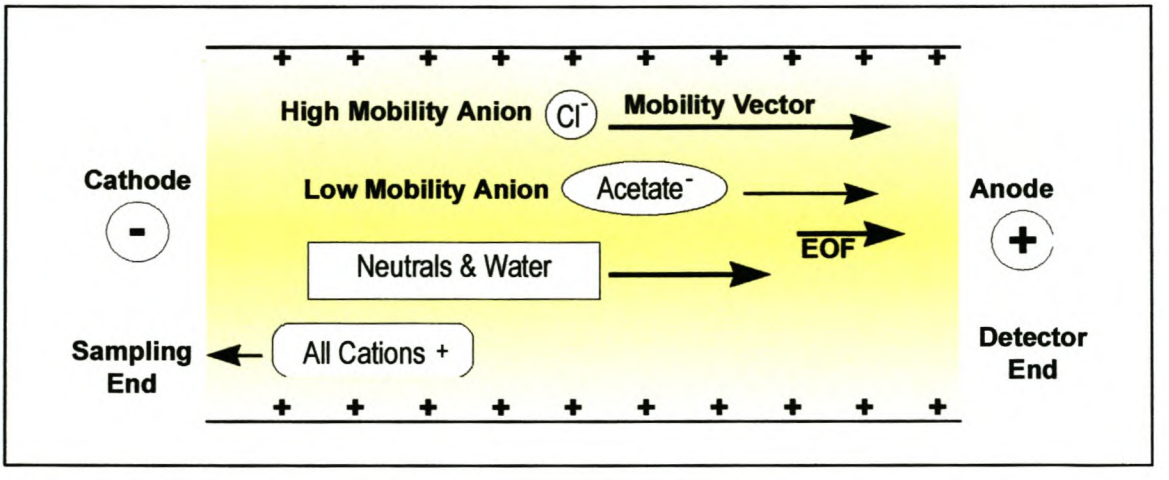

Fig. 6.3. Separation dynamics in CE.

6.1.1.2 Electrolyte system

The choice of electrolyte is of key importance in CE because its composition fundamentally determines the migration behaviour of the analytes. A suitable electrolyte system must ensure the correct electrophoretic behaviour of all individual solutes, the overall stability of the system and satisfactory separation of the analytes (Li, 1992).

Chromate is often chosen as a carrier electrolyte for anion analysis, providing a suitable UV absorbance background in a wide range of wavelengths distant from the absorption maxima of most analyte ions, while at the same time matching the ionic mobility of seven common high mobility inorganic anions: fluoride, carbonate, chloride, nitrite, bromide, nitrate, phosphate, and sulfate. The working electrolyte is made up of 5mM chromate, 0.05 mM OFM (CE-Pak OFM anion BT, WATERS), and 4 per cent 1-Butanol as stabiliser (Benz & Fritz, 1994). A pH of 8.0 is selected to provide best peak separation for the organic acids as well as most of the other anions (Figure 6.4). For the slower anions such as the organic acids, phthalate or 4-hydroxybenzoate could be used, providing good peak symmetry (Jandik, *et al.,* 1991).

The most suitable electrolyte for cations was found to be a solution of 10 mM pyridine (Lee & Lin, 1994), for optimal base level separation of Group I and II elements and transition elements, 25 mM Glycolic acid as a complexing agent, resulting in a pH of about 4.5, and 1mM $^{18}Crown^{6}$ ether to separate the co-migrating cations of K and NH_4. Figure 6.5 illustrates the cation separation sequence.

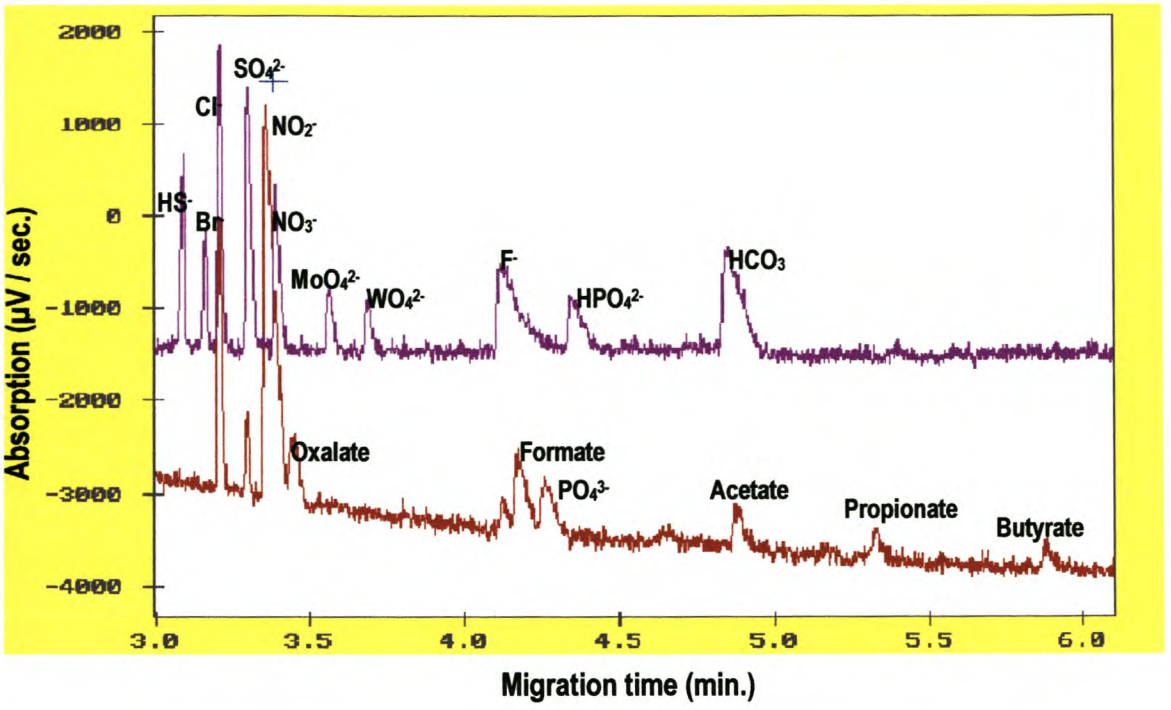

Fig. 6.4. CE electropherogram showing anion separation. The x-axis shows arrival time of the ions at the detector (in minutes), while arbitrary absorbance units (in µV) are on the y-axis.

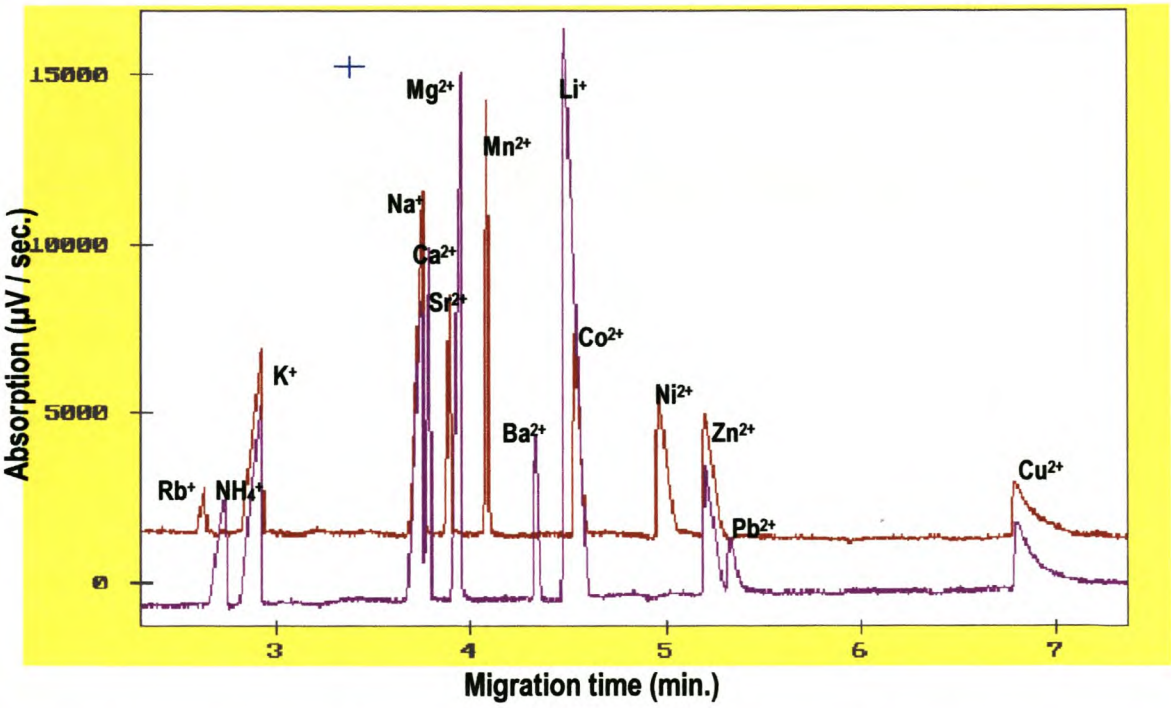

Fig. 6.5. CE electropherogram showing cation separation. Axes are the same as in figure 6.4.

6.1.1.3 Ion mobility

Ions are separated based upon their differences in mobility (μ_{ion}) in the carrier electrolyte when an electric field is applied through the capillary, with mobility being related to the ratio of ion charge to hydrated size in solution. The observed analyte ion mobility (μ_{obs}) is an additive function of ion mobility (μ_{ion}) plus EOF mobility (μ_{EOF}).

Control of EOF is critical for analyte migration time (MT) reproducibility, thereby establishing characteristic arrival times for the different ions, with

$MT = (IL) / (\mu_{obs})(V)$, where

I = Capillary length to detector window

L = Total capillary length

V = Applied voltage

μ_{obs} = Observed ion mobility

It is important that the mobility of the carrier electrolyte ions must be closely matched with that of the analyte ions. If this condition is not met, peak asymmetry will result. When analyte ions have a lower mobility than the electrolyte co-ion, the peaks will tail (e.g. acetate to butyrate in Fig. 6.4); when the analyte mobility is higher, the peaks will front (e.g. NH_4^+ in Fig. 6.5), (Mikkers, Everaerts & Verheggen, 1979).

6.1.2 Sample injection

There are two types of sample injection in CE, namely hydrostatic injection and electromigration. For injection by electromigration, the capillary and electrode is placed in the sample vial and a suitable injection voltage of 1 - 5kV applied to the electrode. Because of the lower conductivity of the sample, a small amount of fluid is moving into the capillary by EOF. However, the ionic species present in the sample migrate into the capillary under their own

electrophoretic mobility, causing a concentration of ionic species in the sample plug subject to individual mobility. Under optimum conditions, an electromigrative sample introduction in CE can be expected to yield an isotachophoretic distribution of ionic concentrations inside the separation capillary. The concentration of the analyte zone in such a isotachophoretic steady state is determined by the Kohlrausch Regulating Function:

$$\frac{c_X}{c_l} = \frac{\mu_X}{\mu_X + \mu_C} \frac{\mu_l + \mu_C}{\mu_X}$$

where c_X and c_l are the concentrations of the analyte anion and leading electrolyte anion in their respective isotachophoretic zones, and μ_X, μ_l and μ_C are the ionic mobility of the analyte anion, leading electrolyte anion and the common counter cation, respectively. When the requirements for carrier electrolytes are met ($\mu_l > \mu_X$), a sample ion is pre-concentrated at a level very near that of the carrier electrolyte ion, which normally lies in the millimolar range. A high enrichment factor can therefore be accomplished for analyte ions present at micro- or nanomolar levels in the original sample, with c_X/c_l normally between 0.2 and 1.0, lowering the detection limits below the ppb range for some elements (Jandik & Jones, 1991; Jandik *et al.* 1991).

In very dilute samples (concentrations in the ppb range and lower), the sample conductivity becomes too low for this pre-concentration to take place. The addition of an anion acting as an isotachophoretic terminating electrolyte, having a lower mobility than any analyte ion of the same polarity, is therefore necessary to permit a sufficient electric charge throughput for ionic transfer from the sample solution into the capillary. Octanesulfonate (at 15-40 µM levels) is a suitable additive for anionic separation since it does not lead to an interfering co-migration with any of the over 50 anionic species analysable by CE (Jandik & Jones, 1991). Figure 6.6 shows four possible stages of such optimised sample introduction by electromigration.

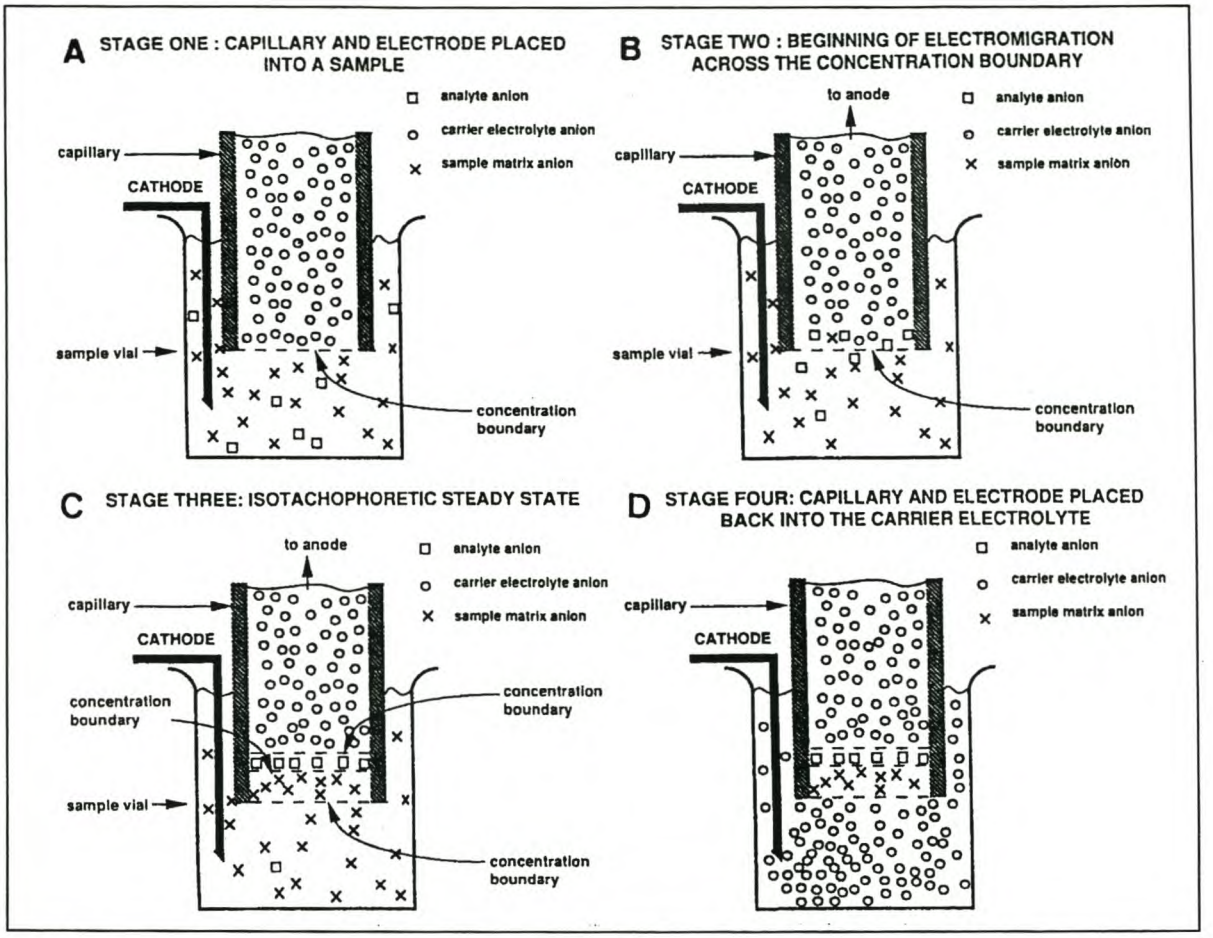

Fig. 6.6. Four stages of sample introduction by electromigration. (From Jandik & Jones, 1991)

Some workers have remarked that bias can occur during injection by electromigration (Huang, *et al.* 1988). This may be the result of differences in mobility of the species in the sample solution, causing a larger effective volume of faster ions than slower ions to be injected. Contrary to electromigration, hydrostatic injection effected by gravity does not discriminate between the ions, and the same effective sample volume of each ion is injected. The capillary and electrode is also placed in sample vial, but raised for a predetermined time (30 seconds) to a height of 10 cm above the electrolyte vessel at the starting site, resulting in a sample volume of about 20 nl to be injected.

6.1.3 Detection in CE

CE uses indirect UV principles to detect all anions and cations. That means that the selection of the carrier electrolyte co-ion must be optimised with respect to both its ionic mobility and UV-absorption properties. The wavelength of the co-ion's UV-absorption maxima must be at least 100 nm greater or less than those of the analyte ions. Unless the electrolyte co-ion generates a UV-absorption background at a wavelength at which analyte absorption does not occur or occurs only minimally, sensitivity is compromised.

Because the analyte displaces the electrolyte charge-for-charge, this requires a UV active electrolyte where the UV active portion of the electrolyte is the same charge as the analyte: a chromate based electrolyte for anion analysis, with detection at 254 nm; and 4 methyl benzyl amine based electrolyte for cation analysis, at a wavelength of 185 or 214 nm. This displacement causes a net decrease in background absorbance, yielding a negative response. Detector polarity is reversed to make the detector signal positive.

UV absorption spectra for the common anions and cations and their electrolytes were recorded at the Chemistry Department, University of Stellenbosch, to evaluate the suitability of the chosen electrolytes as well as the detection wavelength. As can be seen from figure 6.7 and 6.8, the difference in absorbance between electrolyte and analyte ions for both the anions and cations is enough to provide good peak separation. In Figure 6.7a, all the anions have concentrations of 1000 ppm, while the spectrum for the organic anions in 6.7b were recorded for 250 ppm concentrations. In Figure 6.7c, spectra for phosphate and molybdenate were recorded at both 1000 and 100 ppm, with difference in absorbance increasing with a decrease in concentration.

The various anions do not have an absorption maxima at the same wavelength, but it is always lower than that of the anion electrolyte, the latter having a high absorbance over a wide range of wavelengths and always providing good peak separation. For ions at very low concentrations,

concentrations, even with electromigrative injection, its detection can be optimised by varying the detection wavelength.

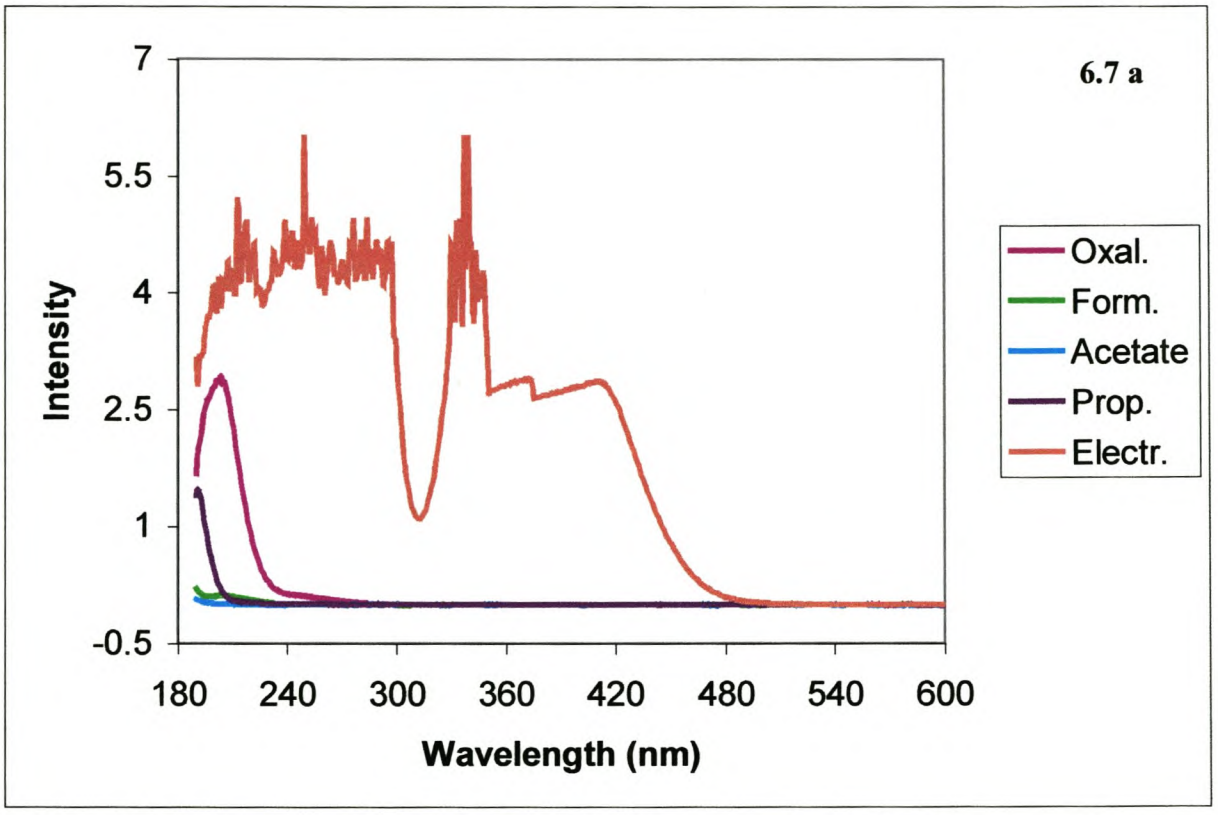

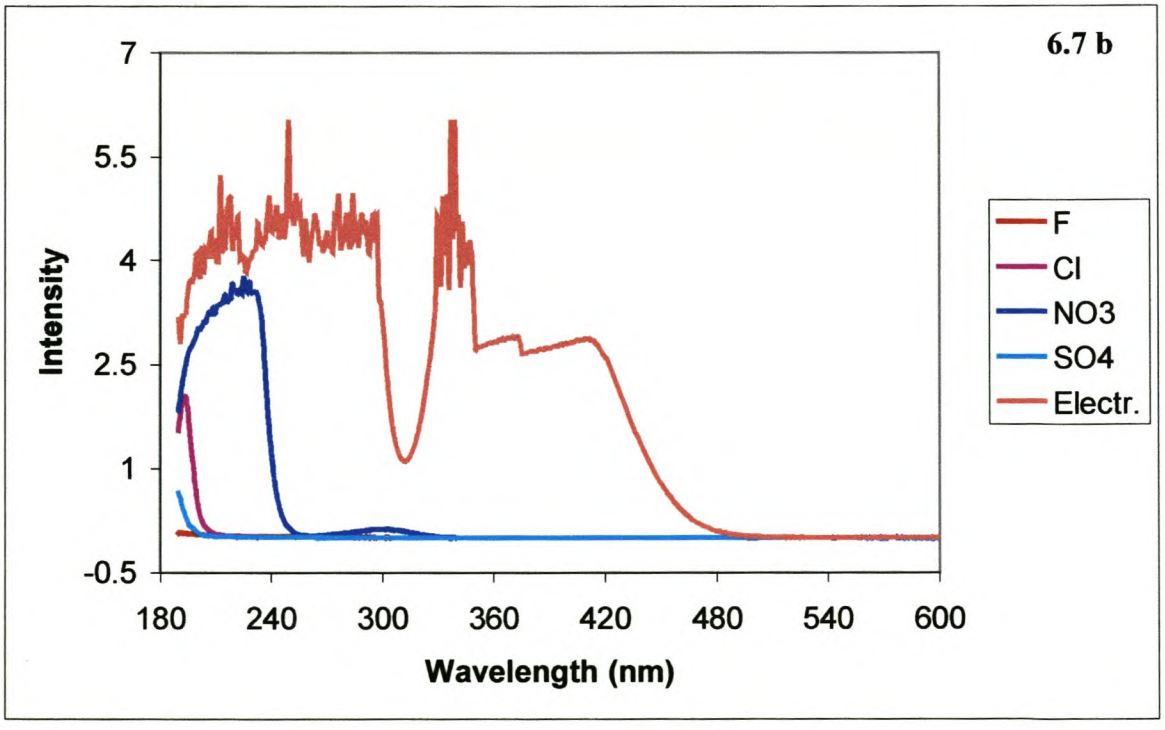

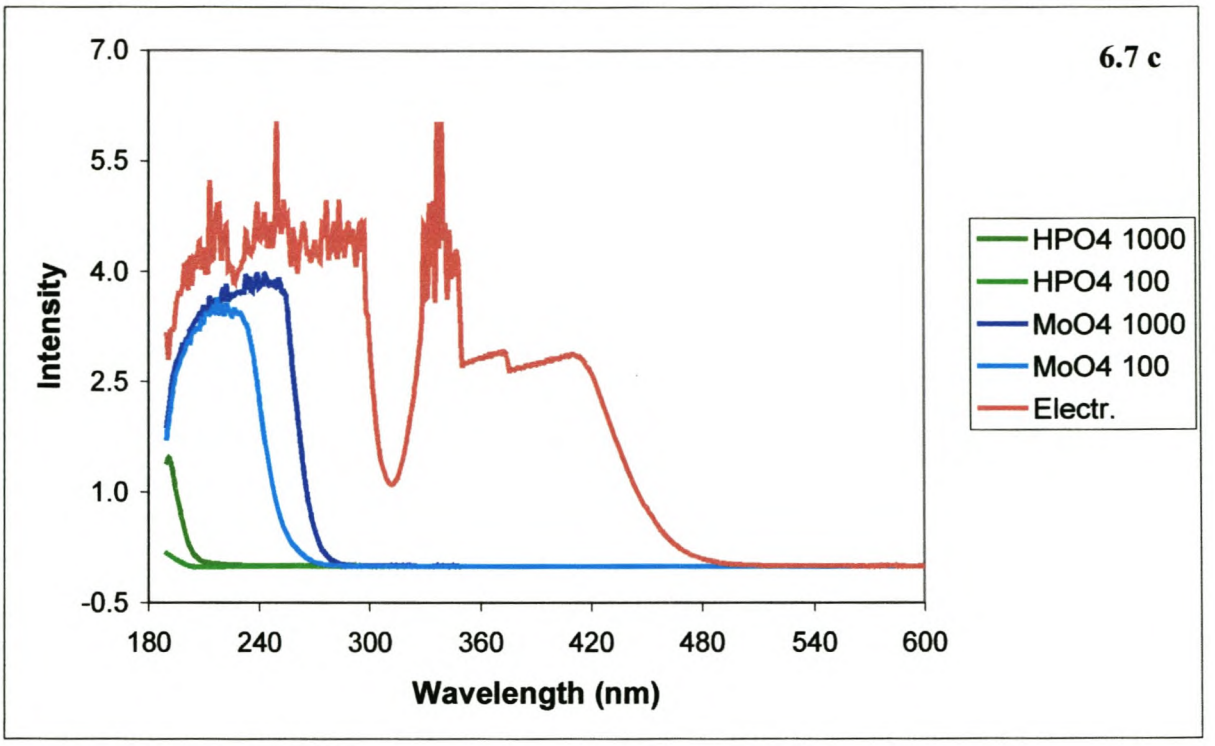

Fig. 6.7 a, b & c. UV absorption spectra for anion species to be detected by CE. Concentrations of anions in (a) is 1000 ppm, in (b) 250 ppm and 100 and 1000 ppm, as indicated, in (c).

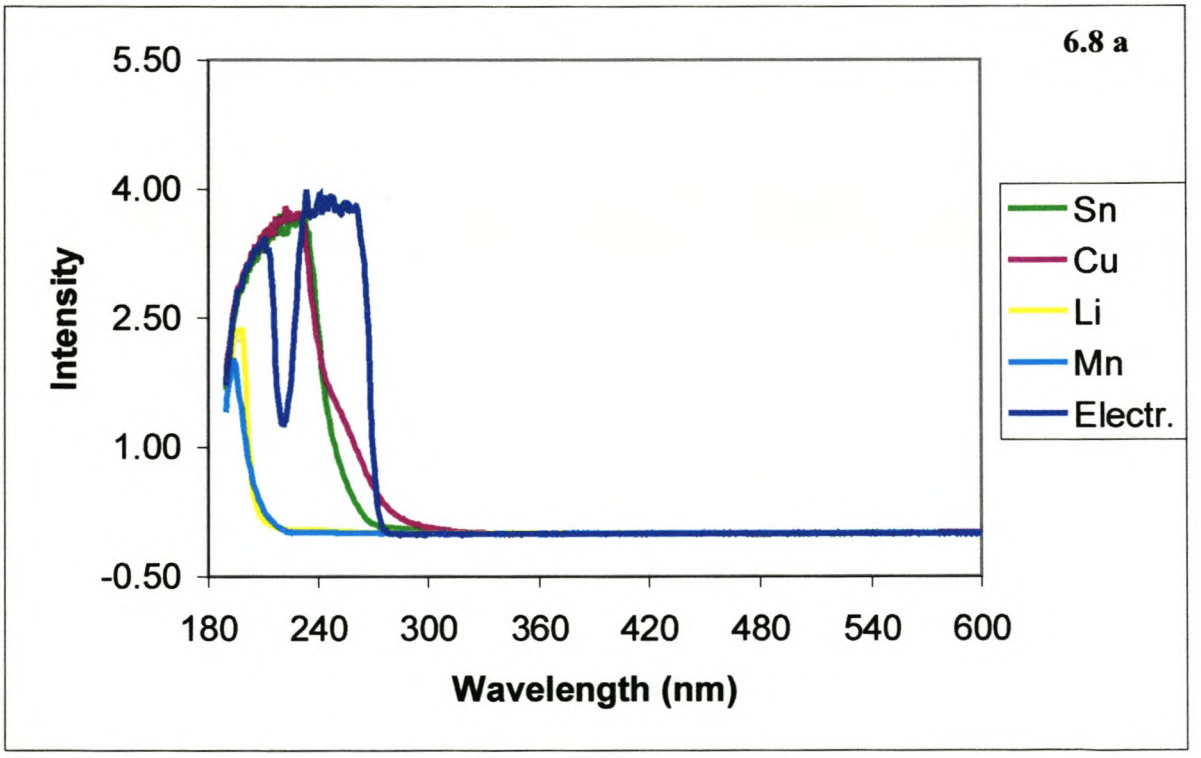

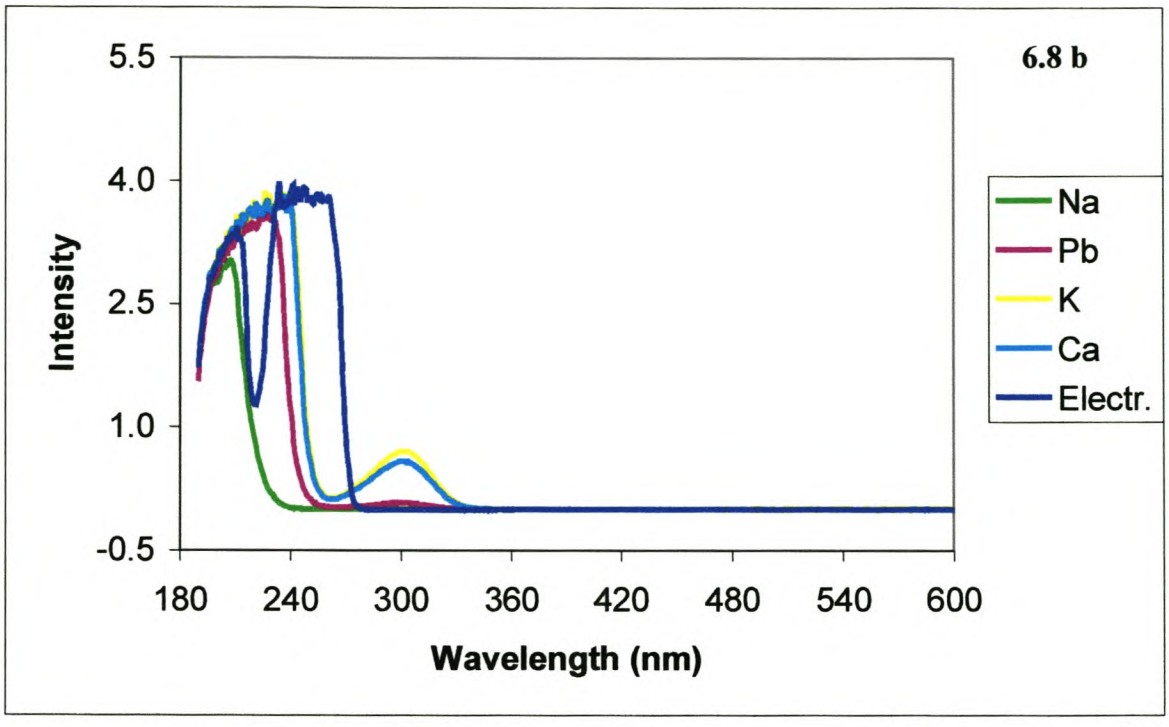

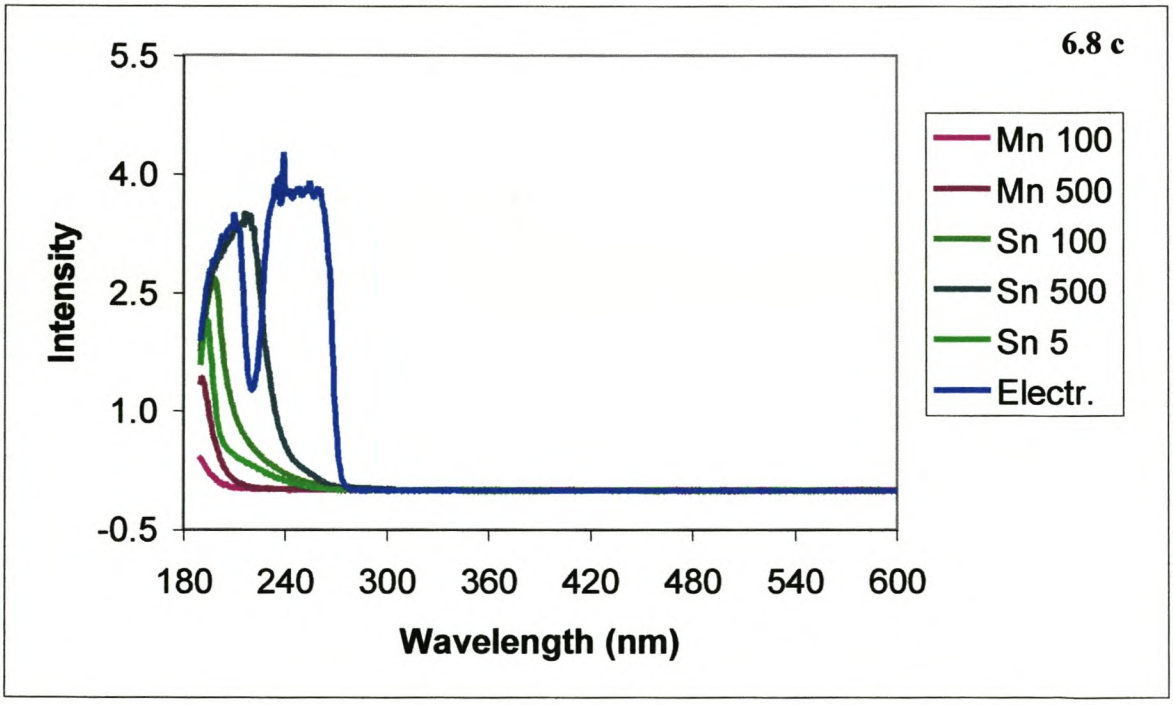

Fig. 6.8. UV absorption spectra for a number of common cations and the electrolyte used for detection with CE. In (a) and (b) all the cations have concentrations of 1000 ppm, while in (c) the legend shows the various concentrations in ppm.

The difference in absorbtivity between the cations and electrolyte at 254 nm wavelength (Figure 6.8 a, b and c) would also result in good peak separation.

6.2 Capillary electrophoresis vs Ion chromatography (IC)

CE offers various advantages over IC. Some of these advantages include fast analysis times, small compact design, and the ability to rapidly convert from anion to cation analysis in minutes rather than hours as by conventional IC. Also, CE uses an open tubular capillary, which allows for minimal sample preparation and is far less expensive than IC columns. Since the separation is performed using electrolytes there is less solvent consumption than by IC (milliliters as compared to liters) (Oehrle, 1996).

When peak capacity of an anion-exchange column is compared to that in CE, within the same time span (Figure 6.9), anion-exchange shows 3 peaks compared to 30 for CE. Column efficiency, measured by the number of theoretical plates, is around 10^3 plates for IC and 10^5 - 10^6 plates for CE, thereby improving detectability considerably (Jones & Jandik, 1991).

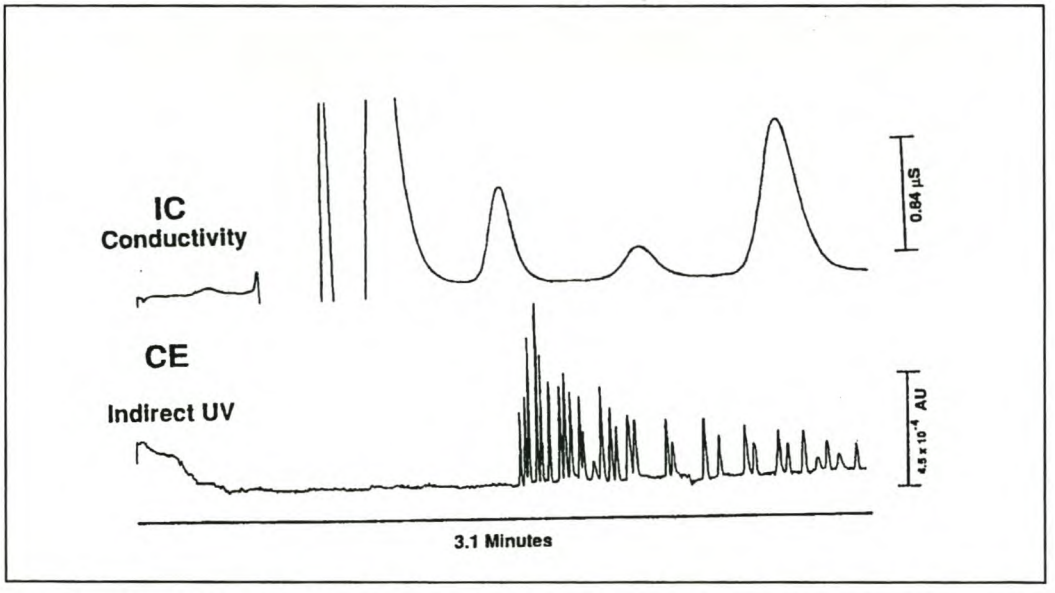

Fig. 6.9. Comparison of the first 3.1 minutes of an IC separation *vs.* a CE separation. In IC (top) only 3 anions, fluoride, carbonate and chloride are separated using a Waters IC-Pak. (From Jones & Jandik, 1991)

6.3 Experimental

6.3.1 Chemical and instrumental parameters

CE analyses were carried out with a WATERS Quanta 4000 instrument. A digital to analogue converter and vendor-provided software assured a smooth sampling of data and their storage on an IBM compatible PC. Sampling of the UV detector was set at 50 Hz intervals.

For the preparation of electrolytes, sample dilution, preparation of standards as well as for cleaning of containers and vials only de-ionised water such as supplied by a Milli-Q system (Millipore, Bedford, MA, USA) was used exclusively. The water blank is routinely checked for contamination and throughout the period of analysis, varied between 5 and 9 ppb K, Na and Ca.

All standards were prepared by diluting 1000 ppm stock solutions containing the individual species. Concentrated standards were made up from their salts and were of analytical grade or better. For hydrostatic injection three standard levels (1, 5 and 10 ppm) and for electromigration four levels of standard (10, 50, 100 and 500 ppb) were used.

All quantitative calculations are based on peak area integration. For standards injected in the hydrostatic mode, linear regression fits were used, while the physical nature of electromigrative injection produces a non-linear fit, of the nature $y = a + b*\ln(x)$.

6.3.2 Crush-leach analysis

6.3.2.1 Principle

Various attempts in establishing an effective crush-leach technique for the extraction of sample fluids from clean mineral fractions have been made and are discussed by Roedder (1990). The principle problems faced involving crush-leach procedures are: 1) Purity of the sample, as small mineral impurities add cations such as Fe, Ca or Mg, creating charge imbalances; 2) Adsorption of cations onto fresh quartz surfaces during crushing; and 3) Multiple inclusion generations, so that analyses reflect the average composition of all inclusions present.

Bottrell *et al.* (1988) made investigations into the behaviour of inclusions and the adsorption and consequent loss of ionic species onto fresh fracture surfaces. In particular, $LaCl_3$ was used in an acidified dilute solution for the extraction of cations, acting as adsorbate to free negative charges on silica surfaces, created during crushing. Banks and Yardley (1992) showed that multi-element analysis obtained from samples less than 100 mg, are in good agreement with results obtained on larger quantities of the same samples. Portions of samples containing a single population of fluid inclusions can therefore be selected for analysis.

6.3.2.2 Procedure

The basic crush-leach method of Bottrell *et al.* (1988), along with modifications by Channer and Spooner (1992), has been followed here, except that $LaCl_3$ was not used in the fluid extraction process. Analyte solutions for CE must have a low conductivity and a pH to near neutral for best results. Tetrabutylammonium Hydroxide (TBA), $C_{16}H_{36}N$-OH, had been suggested and tested (Woitusik & Harrold, 1994) as cation exchange molecule added to low level cationic analytes in concentrations of 50µM in order to meet the *Kohlrausch* condition of a terminating electrolyte. TBA is an acyclic compound with a delocalized charge and known as a strong base.

The quartz fraction to be crushed was thoroughly rinsed, first 4 times with ~20 ml MQ + 50µM TBA water and then 4 times with ~20 ml MQ. If necessary, this process was repeated until analysed blank solutions produced values similar to the TBA-MQ blank value. The washed samples were then left in glass containers at 110 °C for 1 day to dry.

For extraction of the fluids from the inclusions, approximately 1,5 g of sample was weighed and crushed in a corundum mortar with 2,5 ml TBA-MQ water to a less than 50 µm size fraction. This milky fluid was then transferred by syringe to a 0.47 µm membrane filter, along with a further three to four washes of the remaining solids in the mortar, and then vacuum

filtered. After a final wash of the filter, the leachate was transferred to a 10 ml volumetric flask and filled to the mark. From this solution cation analysis was performed immediately, while the rest was stored in washed hard plastic containers for anion analysis. The residence time of the fluid in the containers was less than 1 week.

6.3.3 Contamination Factors

From the moment the sample is crushed until analysis is finished, contamination can occur if care is not taken. Factors of contamination were evaluated and minimised or eliminated where possible.

Purity of MQ and TBA-MQ water

Routine checks on MQ and TBA-MQ water shows the following average results (in ppm):

	MQ	TBA-MQ
K	0.009	0.007
Na	0.006	0.010
Ca	0.005	0.005
Cl	0.001	0.003
SO_4	0.007	0.030

Since these values were relatively uniform within a set of analysis and remained constant throughout the duration of the experiments, representative average MQ peak areas for each element as obtained from CE could be subtracted from peak areas of standards before calibration curves were drawn to correct for the extra cations and anions. TBA-MQ peak areas were subtracted in the same way from sample peak areas.

Sample containers

In order to determine if there was any desorption of ions from the sample container walls, 9 new containers were first washed 4 times with MQ water, then filled with TBA-MQ water and left for 4 days. Conditions were therefore the same as with sample filled containers. After

analysis of this first wash, containers were rinsed and again filled with TBA-MQ water and left for 1 day. Three containers underwent first, second as well as third washes of 7 days, 5 days and a few hours respectively.

Results showed that for the cations NH_4^+, K^+, Na^+, Ca^{2+}, Mg^{2+} and Zn^{2+}, values are generally the same as that of the TBA-MQ blank, namely between 2 and 10 ppb. Figure 6.9 shows the results for NH_4^+ and Ca^{2+}. One or two containers showed increased concentrations above the TBA-MQ average for these two cations, as well as for Na^+ (0.6 ppm) and K^+ (0.1 ppm). The sample containers could therefore be considered a possible source for small amounts of cation contamination.

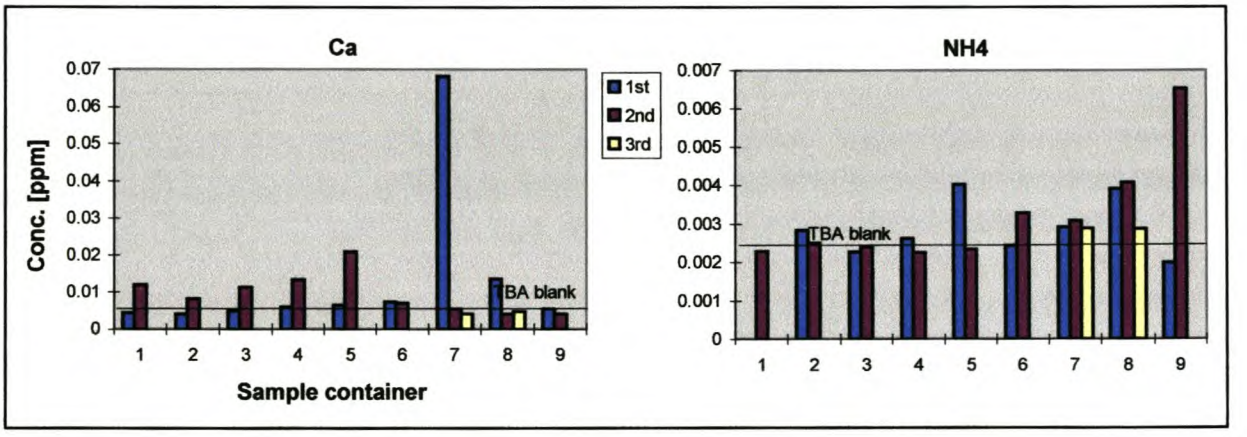

Fig. 6.9. Analysis of the 1st, 2nd and 3rd TBA washes of the sample containers. The 2nd washes often removed more ions than the 1st, with the 3rd washes for most containers below the TBA blank value.

Filter paper

To establish whether crushing in the corundum mortar and filtering through the membrane filter contributes any extra cations, a 10 ml TBA-MQ blank was put through the same process and the filtrate stored in a plastic sample container. A series of 7 analyses were done. Table 6.1 contains the results.

Table 6.1. Results of filter paper blank analysis.

	Concentrations [ppm]							TBA filter	TBA-MQ
	1	2	3	4	5	6	7	Avg.	Avg.
NH4	0.326	0.133			1.130	0.026	0.024	0.328	0.002
K	1.608	1.545			1.947	0.081	0.061	1.048	0.007
Na	22.934	24.072	18.307	22.242	6.267	0.633	0.660	13.588	0.011
Ca	3.267	3.384	3.759	2.645	8.118	0.245	0.114	3.076	0.005
Sr							0.007		
Mg	0.007		0.006	0.007	0.008	0.008	0.007	0.007	
Mn	0.003			0.002		0.002		0.002	
Zn		0.005			0.006			0.005	

There is a considerable variation in the concentrations of the major cations from analysis 1 to 7. It is therefore impossible to say which would be the true amount of contamination and even more inaccurate to simply subtract an average value for each element from the sample analyses in order to correct for any contamination. It can be said that even the lowest values still are of a factor between 10 and 100 times more than that of the average TBA-MQ concentrations and the filtering process do contribute largely as a contamination factor. Very large cation excess in a sample analysis might though, be a result of this factor.

When considering all the above factors of possible contamination, the one that is always present in relatively constant amounts is that of the TBA-MQ blank and it is therefore safe to correct for this factor by subtracting it from the sample analyses, for both cations and anions. The other factors should simply be used to explain any discrepancies such as cation or anion imbalances.

6.3.4 Efficiency of TBA sample washes

Three samples, RM8, 23 and 50, were selected to establish if 4 washes with TBA-MQ water was sufficient to remove any cations adsorbed onto the quartz surfaces before the final crushing and leaching procedure. As can be seen from Table 6.2, the higher values for the 5th TBA wash indicates that even more cations were removed during this wash, with the final MQ wash

reflecting this by values lower than MQ1, particularly in the case of Ca^{2+}. When the MQ2 values are compared to the cation values of the actual sample analysis, however, and expressed as a % error, the values are still quite high, indicating that the washing procedure does not remove enough adsorbed cations. The possibility of contamination by filtration should not be ruled out and could contribute to this large error.

Table 6.2. Results of TBA sample washes.

	Concentrations [ppm] after 4 TBA washes								
	RM 8			**RM 17**			**RM 23**		
	MQ1	*5th TBA*	*MQ2*	*MQ1*	*5th TBA*	*MQ2*	*MQ1*	*5th TBA*	*MQ2*
NH4	0.11	0.20	0.04	0.14	0.15	0.65		0.12	0.07
K	0.10		0.41	0.10		0.22	0.10		0.10
Na		77.24	0.68		1.27	13.81		62.67	0.61
Ca	2.55	4.20	0.22	21.43	2.07	0.23	1.36	5.86	0.24
Mg	0.08	0.08	0.06	0.07	0.08	0.06	0.05	0.05	0.05
Mn	0.11	0.10		0.10	0.10	0.11		0.10	0.10
	Error margin resulting from insufficient washing (%)								
NH4			3.13			42.10			9.73
K			15.14			8.41			10.77
Na			5.07			100.63			5.19
Ca			2.43			7.93			11.34
Mg			14.58			6.81			20.72
Mn						55.24			195.45

6.3.5 Consistency and Reproducibility of analysis

Analyses were done to determine whether several crushes of the same sample yields similar results, thereby determining the if each sample portion is representative of all the inclusion fluids present in a specific quartz vein. Sample RM 8 (Paarl) and RM 44 (Alto) were used for this purpose. The separate portions of each sample were crushed and leached in the same way as for all the other sample analyses. Cation analysis however, is only available for sample RM 44.

Figure 6.10a shows that for the anions Cl^-, NO_3^- and HCO_3^- of both samples RM 8 and RM 44, very little variation occurs between separate crushes in one period of analysis (8.1 - 5 & 4.1 - 5), but between different analytical runs there is a large variation in HCO_3^- concentration. This

inconsistency is also true for the cations. In Figure 6.10b the large drop in concentration for the October analysis might result from loss of inclusion fluid, possibly due to leaking, during the time between sample crushing into smaller fractions and extraction of fluid for analysis. The major cations in Figure 6.10c, with the exception of NH_4^+, do not show such extreme variations. Sample selection therefore seems fairly representative, but can be improved. It is also clear that samples should not be left too long before being analysed to ensure accurate results.

6.10 (a)

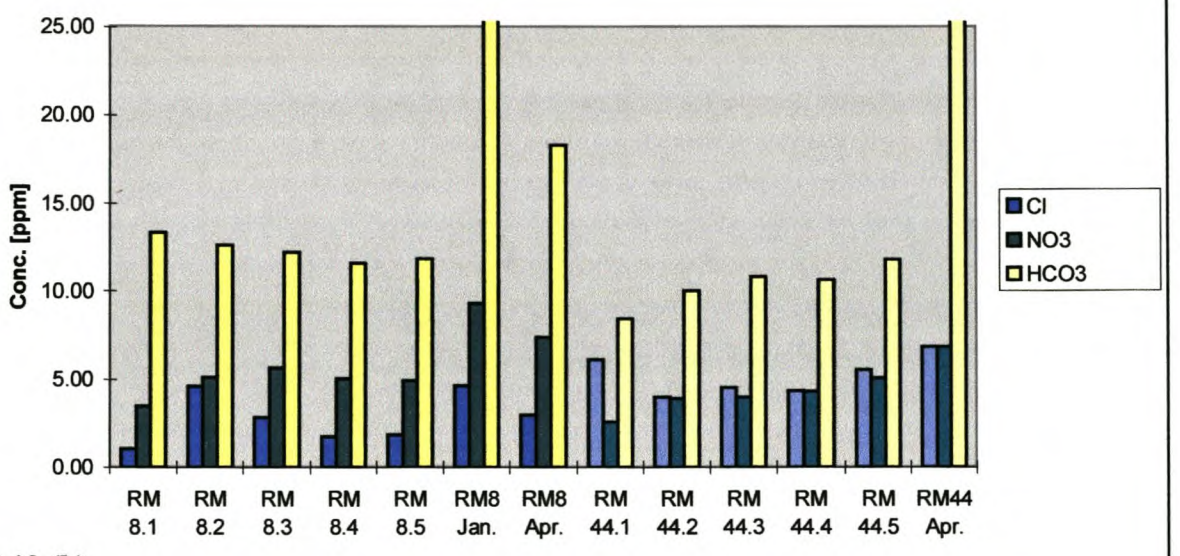

6.10 (b)

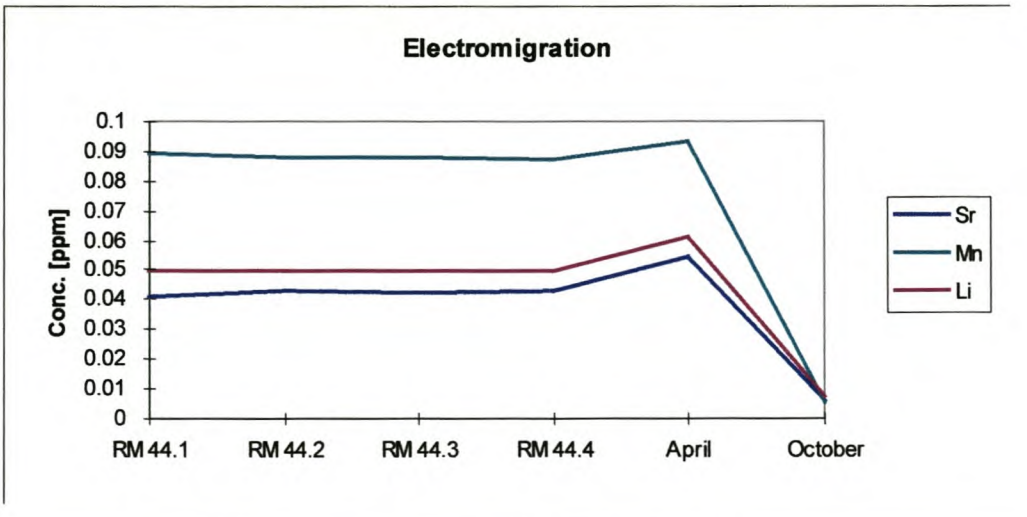

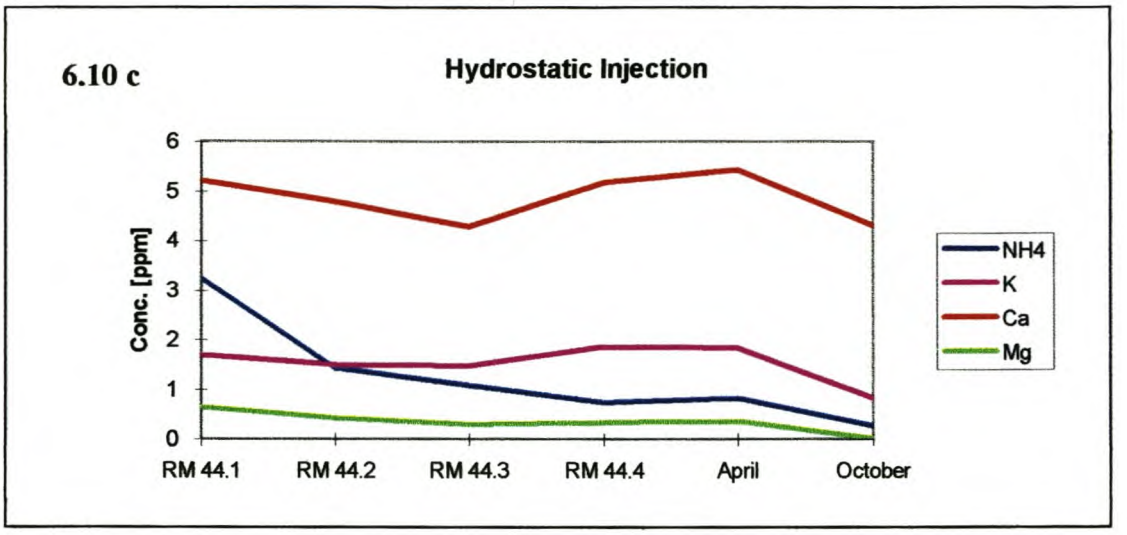

Fig. 6.10c. Several crushes of the same sample showed that values for both anions (a) and cations (b) and (c) are not very reproducible over long periods of time.

6.4 Data processing

Data obtained during CE were stored and processed using an APEX Chromatography software program. Absorption peaks were identified by aligning end member peaks which always has fixed positions, such as Na^+ and Zn^{2+}, and Cl^- and HCO_3^- to the same peaks in the calibration standard. Appendix B contains electropherograms of all the samples analysed. Peak areas were then calculated and for data acquired by hydrostatic injection, ionic concentrations were determined using linear regression calibration curves, while electromigration analysis required regression using the equation $y = a + b*\ln x$. Corrections were also made for dilution using a factor determined by the water content of the sample as determined by Karl Fischer titration.

6.5 Charge balancing

Concentrations calculated for each ion were converted to milli-equivalents and charge balances calculated for cations and anions. Most samples show cation excesses of between 1 and 10%, the highest imbalance being 20%. Samples RM 16a & b, 17 and 21, as well as all the October re-run analyses, show abnormally large anion excesses of between 50 and 80%, with the same samples in the initial analysis having an imbalance, some positive and some negative, of

between 0 and 5%. HCO_3^- is mostly responsible for this imbalance, with high concentrations of Cl^- and F^- also contributing in samples RM 16-21.

7 KARL FISCHER TITRATION

7.1 Principle and reaction mechanism

The Karl Fischer titration is introduced in this study for the determination of the water content of the inclusion fluids, thereby rendering data acquired by CE as qualitative and making it possible to calculate fluid salinity in terms of total dissolved solids.

In Karl Fischer's original formulation of the titration reaction (Fischer, 1935), the determination of the water content is based on the oxidation of sulphur dioxide by iodine in the presence of water:

$$I_2 + SO_2 + 2H_2O \Leftrightarrow 2HI + H_2SO_4 \qquad (7.1)$$

He used a solution of iodine and sulphur dioxide in a non-aqueous, water-free solvent - methanol proved to be particularly suitable. In order to shift equilibrium quantitatively to the right, the resultant sulphuric acid and hydrogen iodide must be neutralized. Of the many bases examined by Karl Fischer, pyridine proved to be the most suitable.

Smith, Bryant and Mitchell (1939) discovered that methanol function not only as a solvent, but is directly involved in the reaction. In their formulation, pyridine was also involved.

Verhoef and Barendrecht (1977,1978) showed that 1) pyridine does not play a role within the reaction mechanism, provided the pH of the solution is kept constant. Pyridine only serves as a buffer; and 2) the rate of the Karl Fischer titration is dependent on the pH of the medium in which the reaction is taking place. They discovered that between pH 5.5 and 8 the reaction rate remains constant, while increasing at pH lower than 5 and higher than 8.5. An explanation for this dependence of reaction rate on pH is that it is not sulphur dioxide itself, but a basic sulphite anion (methyl sulphite, resulting from SO_2 and methanol), which is being oxidized by iodine under the influence of water:

$$2CH_3OH + SO_2 \Leftrightarrow CH_3OH_2^+ + CH_3OSO_2^- \quad (7.2)$$

The solvation of the sulphur dioxide by the solvent is the first step during the Karl Fisher titration (reaction 7.2, with methanol as the solvent). If primary alcohols, such as methanol, is used, it results in a $H_2O:I_2$ mole ratio of 1:1.

Oxidation of the methyl sulphite anion $CH_3OSO_2^-$ represents the second step in the mechanism of the Karl Fischer reaction, although not yet fully understood.

In summary, the currently accepted reaction occurring during titration of a sample containing water by Karl Fischer solution in a methanolic medium is:

$$I_2 + SO_2 + 3B + CH_3OH + H_2O \Leftrightarrow 2BH^+I^- + BH^+CH_3SO_4^-,$$

where B represents pyridine or other bases suitable for neutralizing the resultant acids and fixing the pH at a definite value.

7.2 Practical Aspects: pH and solvent dependency

Only in the pH range between 5.5 and 8 does the Karl Fischer titration proceed at a maximum rate. The sample solvent should, therefore, possess a sufficiently large buffer capacity. Karl Fischer solution pyridine-free (solvent) is recommended.

Investigations by Eberius (1958) show that during Karl Fischer titration with approximately 25% methanol in the titration solvent, water and iodine react in the same mole ratio $H_2O:I_2$ as in pure methanol. For this reason, methanol should always be present in the titration solvent, at least in this minimum required amount. If this is not the case, different stoichiometric ratios for the conversion of water and iodine, i.e. different titres of Karl Fischer solution, may be observed (Wieland, 1987).

7.3 Crush-leach Analysis

7.3.1 Method

It is important that the volume of inclusions opened for Karl Fischer titration is in correlation with that for CE. This can be achieved by using a similar crush-leach procedure.

A sample amount similar to that used during CE (~1,5g) is crushed in a corundum mortar with an accurately measured volume of methanol (the same used as a solvent during titration), to the same grade as for CE, with the water being released in the methanol. This would ensure that the volume of inclusions opened be similar to that for CE. From this solution a specific volume (200µl in this study) is extracted and titrated with Karl Fischer solution. Corrections would have to be made for methanol evaporating during crushing, as well as methanol blanks taken to correct for the small amount of water present in the methanol.

7.3.2 Analytical Procedure

Before analysis was started the titration chamber was conditioned by adding ~10ml methanol and titrating it with Karl Fischer (K.F.) solution until no water remained. The solution was left like this for one day.

7.3.2.1 Determination of titre

The titre expresses the volume of Karl Fischer solution used to titrate a given amount of water, with the Karl Fischer reagent in these experiments using 1 ml of Karl Fischer solution per 5 mg H_2O. The determination of a titre is therefore necessary to calibrate the instrument and is obtained by titrating 50µl of water to endpoint as follows:

$$\text{Titre } t = \frac{(\text{sample size}) \cdot \text{factor}}{\text{ml of K.F. solution}} \qquad (7.3)$$

where, if sample size is in: g - factor = 1000

µl - factor = density of H_2O [g/ml] ~1

Three titres are normally determined each time and an average taken. A satisfactory value ranges between 5.0 and 5.1.

7.3.2.2. Calculating methanol evaporation

During crushing of the sample in the mortar, a significant portion of the methanol will evaporate, influencing the percentage of the water determined in the methanol. In order to determine the final true volume of methanol containing the released H_2O from the fluid inclusions for analysis, blank "crushes" were produced under the same conditions as for sample crushes. A volume of 50µl H_2O were added to 2ml of methanol in the mortar and mixed in the same way as in the sample crushing procedure, for 2 minutes, then sucked up by syringe and stored in a closed glass container. Six blank "crushes" were produced, with 2 to 4 analyses of 200µl from each separate "crush". Values are contained in Table 7.1.

The volume water determined during the titration (expressed as wt%) is calculated as follows:

$$\textbf{Water content (wt\%)} = \frac{\text{(K.F. volume (ml) - blank)} \cdot \text{titre} \cdot \text{factor}}{\text{(sample size (ml))} \cdot \text{divisor}} \qquad (7.4)$$

Factor and divisor are used for the conversion of the result to different units, in this case being 0,1 and 0.7914 g/ml (density of methanol) respectively.

The volume methanol that now contains the 50µl H_2O was calculated by rewriting the relationship

$$\text{Wt\% } H_2O = \frac{\text{Volume } H_2O}{\text{Volume solution (meth.) x meth. density}} \text{ x } 100$$

Table 7.1. Calculation of the true volume methanol in the mortar that would contain the released water after crushing of the quartz.

Analysis	K.F. Vol.	wt% H_2O	Corrected wt% H_2O
1.1	1.26	3.78	3.82
1.2	1.33	3.99	4.03
1.3	1.32	3.96	4.00
1.4	1.32	3.96	4.00
2.1	1.29	3.88	3.92
2.2	1.3	3.89	3.93
3.1	1.35	4.05	4.09
3.2	1.38	4.15	4.19
4.1	1.18	3.59	3.63
4.2	1.22	3.74	3.78
5.1	1.2	3.66	3.70
5.2	1.23	3.75	3.79
5.3	1.23	3.75	3.79
5.4	1.22	3.74	3.78
6.1	1.18	3.61	3.65
6.2	1.22	3.74	3.78
6.3	1.2	3.66	3.70
Average		**3.82**	**3.86**

Blank = 0,07 for 1.1 - 3.2
0,045 for 4.1 - 6.3

Titre = 5,033

True volume methanol

$$= \frac{H_2O \text{ added (ml)}}{(\text{avg wt\% } H_2O * \text{methanol density (g/ml)})}$$

$$= 0{,}05/(3{,}82\% * 0.7914) - 0.05$$

$$= 1{,}604 \text{ ml} \qquad \text{Eq. (7.5)}$$

7.3.2.3. Sample Analysis

Samples were crushed in the same way as described for the methanol evaporation tests. A portion of quartz similar to that for CE, was weighed, put in the mortar, and 2ml of methanol added. The mortar was covered with a perspex shield, with an opening in the middle for the pestle, to prevent any quartz pieces flying out. The sample was crushed for 2 minutes, sufficient to powder the quartz to a ±10μm fraction. The fluid was then sucked up by syringe and pressed through a 0,45μm filter into a small glass container, and closed. A volume of 200μl fluid was then extracted and added to the conditioned Karl Fischer titration chamber. The time duration for one analysis, from crushing of the quartz until endpoint titration, was no more than 3 minutes.

The results are contained in Table 7.2. When looking at the consumption of Karl Fischer solution, there is for all but three samples an increase between the first and third analysis of a

sample. It does not imply a larger volume of water, but a larger percentage of water per 200µl of sample analysed, resulting from a small amount of methanol evaporation during sample extraction, which is then picked up in the following analysis. The first analysis would therefore be the more accurate and is used in the calculations. An average was used for samples RM25, 36, and 56 to compensate for the small discrepancy. For samples RM 2 and RM 14 no second and third Karl Fischer volumes are given because of a too long extraction time, causing excessive methanol evaporation and inaccurate results.

The calibrated volume of water determined in the methanol was calculated first by determining the wt% H_2O in the methanol (eq. 7.4) and converting it to a volume, then correcting for the true amount of methanol present after evaporation during crushing (eq. 7.5):

Volume H_2O (µl) =

$$\frac{(\text{K.F. volume} - 0{,}045)*5{,}0474*0{,}1}{(0{,}2*0{,}7914)} * \frac{(1.604*0{,}7914*1000)}{100}$$

where blank = 0,045

titre = 5,0474

true volume methanol = 1,604ml

The volume of water determined for each sample was converted to the equivalents for the amount of sample analysed with CE, which will then be used with the data on ionic composition and concentrations determined by CE to calculate the bulk salinity of the fluid from the inclusions.

Table 7.2. Calibrated volume of water present in each sample. Two sets of data are available for some samples, hence (a) and (b, October analysis).

Sample	Sample Weight	K.F. Volume 1st	2nd	3rd	Average	Calibr. Vol. H_2O in meth. [µl]	H_2O equivalent of CE sample weight [µl]
RM 1	1.49788	0.35	0.37	0.39		12.35	12.73
RM 2	1.50044	0.42				15.18	15.64
RM 8	1.50027	0.35	0.35	0.37		12.35	12.65
RM 8	1.50027	0.35	0.35	0.37		12.35	12.72
RM 14	0.74514	0.13				3.44	7.15
RM 15	1.50131	0.38	0.39	0.42		13.56	14.13
RM 16a	1.50078	0.28	0.29	0.30		9.51	9.70
RM 16b	1.50015	0.28	0.31	0.31		9.51	10.00
RM 17	1.49997	0.36	0.37	0.36		12.75	13.07
RM 21	1.49971	0.24	0.25	0.28		7.89	8.22
RM 23	1.4995	0.52	0.53	0.54		19.23	19.82
RM 23	1.4995	0.52	0.53	0.54		19.23	19.82
RM 25	1.49984	0.30	0.29	0.32	0.30	10.32	10.63
RM 32	1.4997	0.24	0.26	0.27		7.89	8.22
RM 36	1.50047	0.21	0.20	0.22	0.21	6.68	6.99
RM 37b	1.50082	0.21	0.24	0.24		6.68	6.75
RM 39	1.49963	0.23	0.24	0.24		7.49	7.80
RM 40	1.49935	0.23	0.25	0.25		7.49	7.72
RM 42	1.50048	0.27	0.28	0.27		9.11	9.49
RM 43	1.4324	0.23	0.25	0.27		7.49	8.09
RM 44	1.5003	0.32	0.34	0.34		11.13	11.39
RM 48 a	1.50006	0.27	0.29	0.30		9.11	9.49
b							8.27
RM 49 a	1.50003	0.37	0.41	0.41		13.16	13.58
b							11.74
RM 50	1.4998	0.26	0.29	0.28		8.70	9.03
RM 50b	1.5	0.44	0.47	0.45		15.99	16.49
RM 53	0.98822	0.18	0.21	0.23		5.46	8.57
RM 54	0.82299	0.17	0.18	0.18		5.06	9.53
RM 55 a	1.29523	0.22	0.24	0.25		7.08	8.47
b							8.73
RM 56 a	1.42804	0.31	0.30	0.32	0.31	10.73	11.63
b							11.18
RM 57 a	0.91005	0.24	0.27	0.25		7.89	13.44
b							12.84

8 O-ISOTOPE DATA

8.1 Introduction

Isotopic compositions of igneous, metamorphic and sedimentary rocks often, but not always, display systematic variations that provide insight into the origin of such rocks. Systematic differences in the $\delta^{18}O$ values of cogenetic minerals may be interpreted in terms of the temperature at which they equilibrated their oxygen with a common reservoir, with differences in $\delta^{18}O$ decreasing with increasing temperature or grade of metamorphism (Faure, 1977). The general range of O-isotope values found in nature can be seen in Figure 8.1.

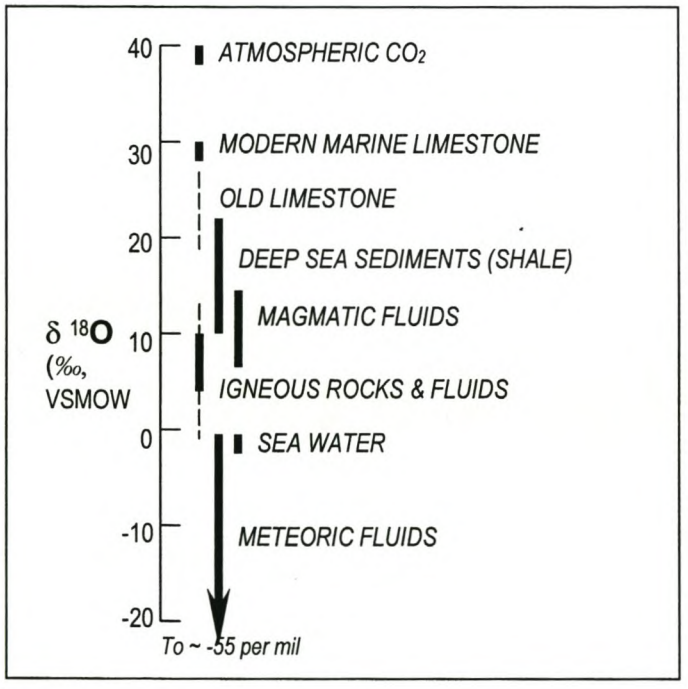

Fig. 8.1. The distribution of $\delta^{18}O$ values for common earth reservoirs Important in hydrothermal systems. (From Campbell & Larson, 1998)

8.2 Analytical method

O-isotope analyses of the vein quartz were done by Dr. Chris Harris at the UCT Department of Geological Sciences. Oxygen isotope data were obtained by conventional methods using ClF_3 as the fluorinating reagent and reported in the familiar δ notation where $\delta^{18}O = (R_{sample}/R_{standard} - 1) \times 1000$ and $R = {}^{18}O/{}^{16}O$. The data have been calibrated to the SMOW scale using an in-house standard MQ (Murchison Line quartz). Two aliquots of MQ were analysed with each batch of eight samples.

8.3 Results and discussion

Oxygen isotope data for all the vein quartz samples analyzed are contained in Table 8.1. From Figure 8.2 it is evident that Malmesbury hosted quartz veins have higher $\delta\ ^{18}O$ values (between 12.5 and 16.3‰) than those within a granitic host (8.7 to 14.6‰). With the exception of a few samples, most granite hosted quartz veins have $\delta\ ^{18}O$ values that falls within the range of isotopic composition of magmatic fluids - $\delta\ ^{18}O = 7 - 13‰$ - (Taylor, 1968).

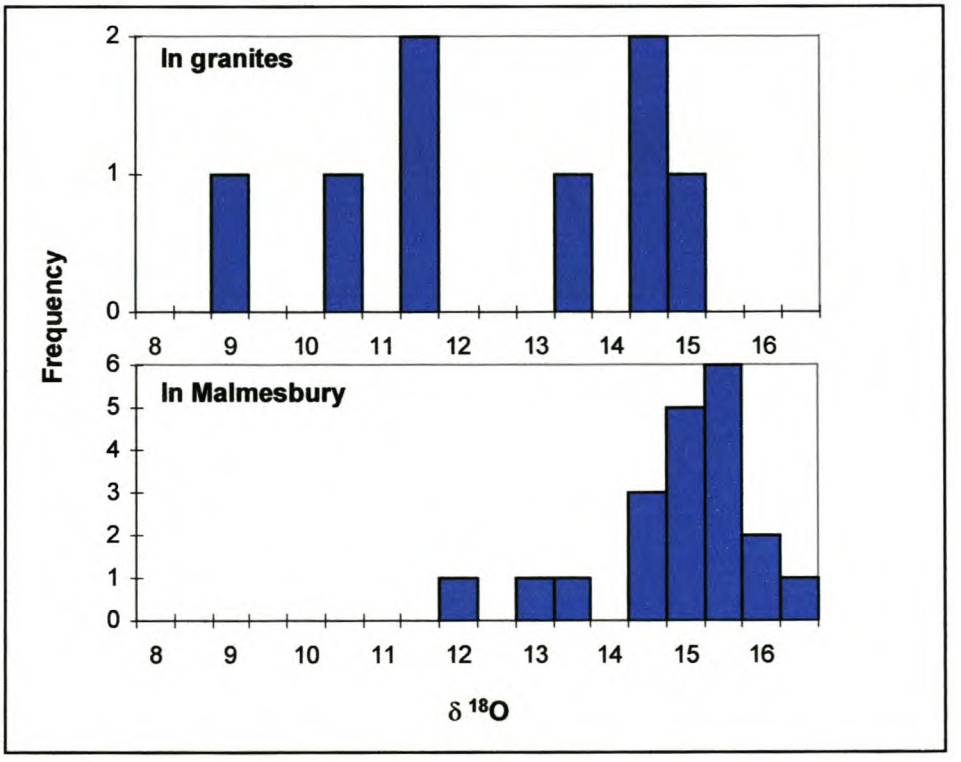

Fig. 8.2 Histogram of O-isotope frequency.

Harris *et al.* (1997) studied the O-isotope geochemistry of quartz from the Cape Granite Suite and Malmesbury Group sediments. They have shown that the whole rock $\delta^{18}O$ values of the Malmesbury group metasediments (range 8.1 - 18.3‰) are higher than that of the Cape granites (range 6.4 - 11.4‰) (Figure 8.3), with the S-type granites having higher $\delta^{18}O$ values (10.61‰) than the I-types (7.75‰). Granite hosted vein quartz samples from Lourensford Estate show a very close distribution of $\delta^{18}O$ values around 10.5‰, close to the isotopic composition of S-type granites. The higher $\delta^{18}O$ value of Malmesbury hosted as opposed to granite hosted quartz veins might be the result of contamination by Malmesbury host rocks.

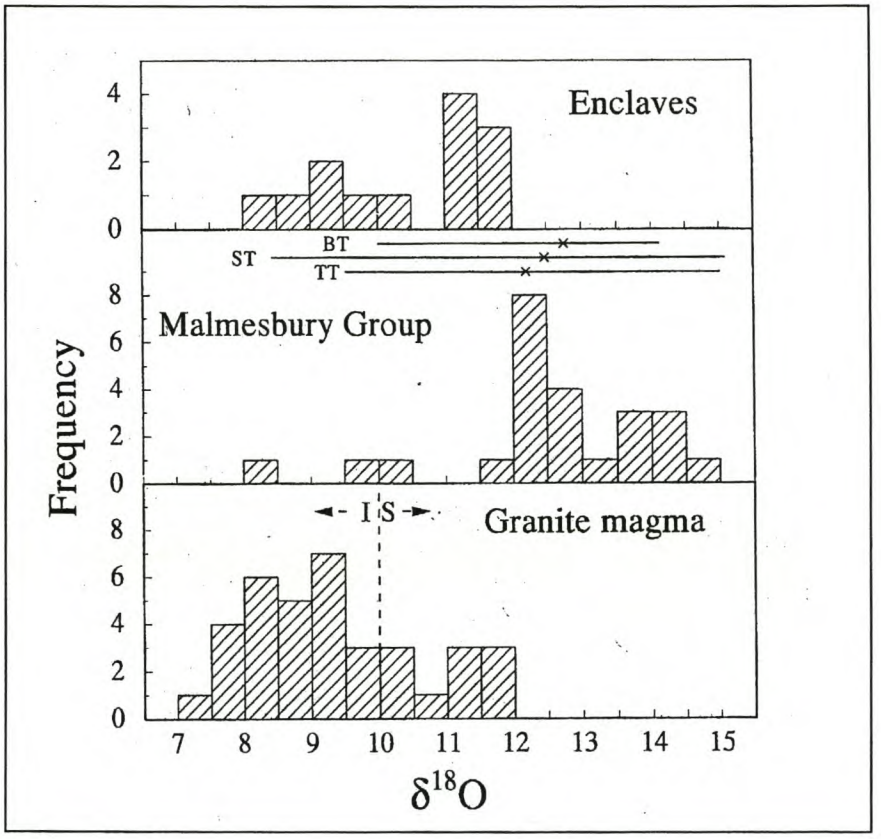

Fig. 8.3. Histogram of $\delta^{18}O$ values of granite magmas and Malmesbury Group rocks (from Harris *et al.*, 1997).

Table 8.1. O-isotope values (per mil $\delta\ ^{18}O$) of quartz from sampled veins.

O-isotope values			
Q-veins in granite		Q-veins in Malm.	
RM 1	13.5	15.2	RM 16a
RM2.1	14.1	15	RM 16b
RM 8	8.7	15.3	RM 17
RM 14	14.6	13.4	RM 32
RM 15	14.3	14.1	RM 36
RM 21	11.1	14.5	RM 37b
RM 23	10.4	15.1	RM 39
RM 25	11	14.8	RM 40
		15.6	RM 42
		12.5	RM 43
		16.3	RM 44
		15.7	RM 48
		14.9	RM 49
		14.5	RM 50
		11.6	RM 50b
		15.2	RM 53
		14.3	RM 54
		14.9	RM 55
		14.4	RM 56
		15	RM 57

8.4 Conclusion

The O-isotope composition of granite hosted quartz veins suggest a possible magmatic origin for the fluid/fluids responsible for original vein formation. The higher $\delta\ ^{18}O$ value of Malmesbury hosted veins most likely resulted from contamination of this magmatic fluid by Malmesbury wall rocks. Bruwer (1997), in her study of the Kuiperskraal Sn-Zn-As deposit, has suggested that various late- to post-magmatic fluids, following the intrusion of the Cape Granites, were responsible for this mineralization. As has been shown from microthermometry work, the entrapment temperatures of the various fluid phases in quartz from the current study compares to those found by Bruwer for mineralized and unmineralized quartz veins. It is therefore possible that the quartz veins in these two studies are part of the same fluid system, originating as magmatic fluids after the intrusion of the Cape Granites, with the characteristics of various periods of fluid reactivation superimposed on the original veining episode.

9 FLUID INCLUSION CHEMISTRY

9.1 Ionic composition of inclusion fluids

CE provided a bulk ionic composition for all the inclusion populations in each sample analysed. Major element cation chemistry consists of $Na^+ > Ca^{2+} \geq K^+ \geq NH_4^+$, with Na^+ concentrations between 2000 and 7000 ppm, and less than 1000 ppm for the other. Sr^{2+}, Li^+, Mn^{2+} and Zn^{2+} are present in concentrations less than 50 ppm. The major anions are Cl^- and HCO_3^-, (1000 - 9000 ppm), acetate (500 - 1000 ppm), NO_3^- > propionate ≥ SO_4^{2+} > F^-, (100 - 1000 ppm), with formate and oxalate less than 100 ppm. Table 9.1 contains the fluid chemistry CE data for all the samples. Figures 9.1, 9.2 and 9.3 illustrate the concentration patterns of the major cations and anions throughout the sample series. With the exception of a few samples, these ions follow relatively similar enrichment patterns, without any distinctive difference in chemistry between the low-angle an almost vertical dipping vein sets. RM Z show low concentrations compared to the other samples, because not enough sample was available to determine the fluid volume and hence the usually large correction factor was not applied. The close association between Na^+ and Cl^- (Fig. 9.1) in most samples indicates it to be the dominant salt species. The organic acids as well as NO_3^- are also very closely associated and present in all samples (Fig. 9.3), indicating an organic component in one (or more) of the inclusion populations.

The cations and anions all show positive correlations (Figure 9.4), indicating that the fluid source(s) remained relatively stable in composition and that the fluid itself was not involved in any significant exchange reactions until entrapment and later recrystallization processes.

No REE could be detected by CE, to provide information on possible sources for the fluid populations. The value of REE in such a bulk analysis is, however, only limited to the extent that it identifies one source (or more) which produced any one of the inclusion generations.

More parameters such as age relationships and formation temperatures of the inclusion populations should therefor be known for inclusion chemistry to be most useful.

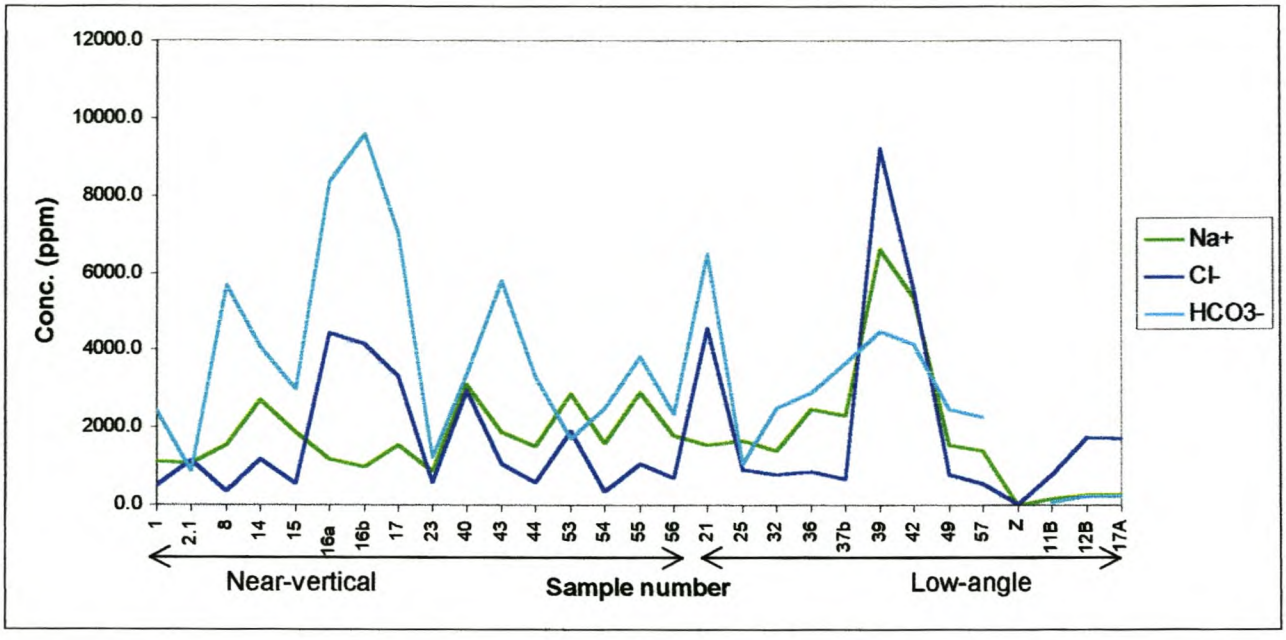

Fig. 9.1. Na^+, Cl^- and HCO_3^- concentrations, determined by CE, in the inclusion fluid of the sampled quartz veins.

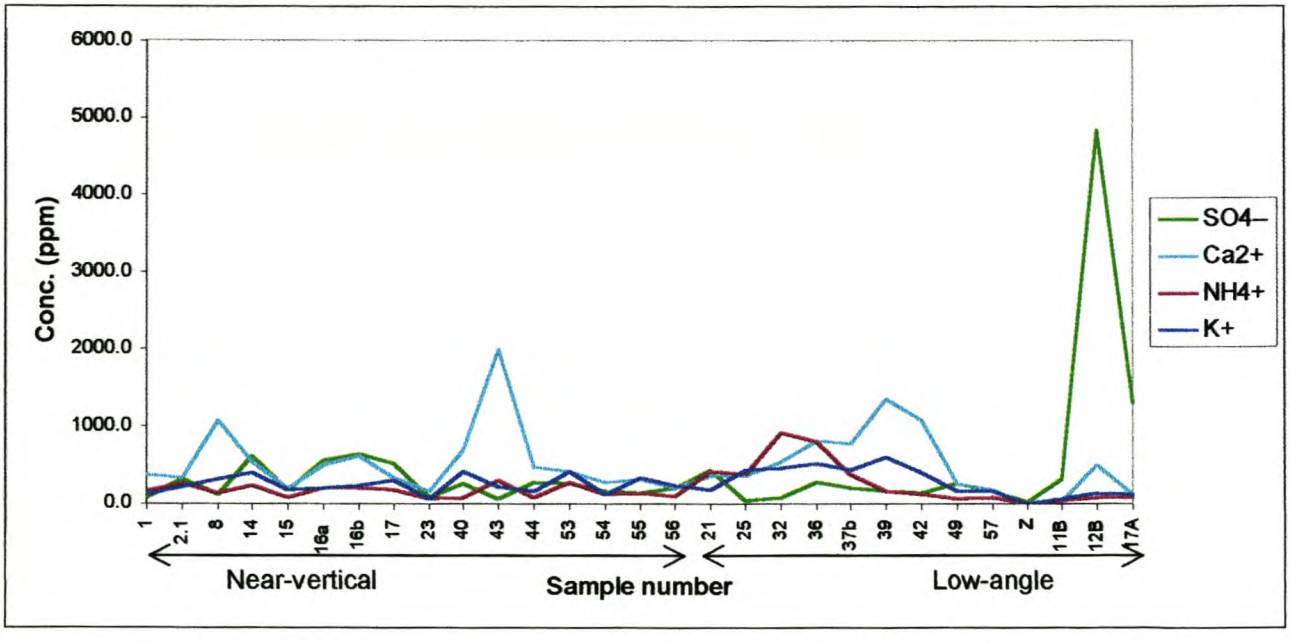

Fig. 9.2. SO_4^{2-}, Ca^{2+}, NH_4^+ and K^+ concentrations, determined by CE, in the inclusion fluid of the sampled quartz veins.

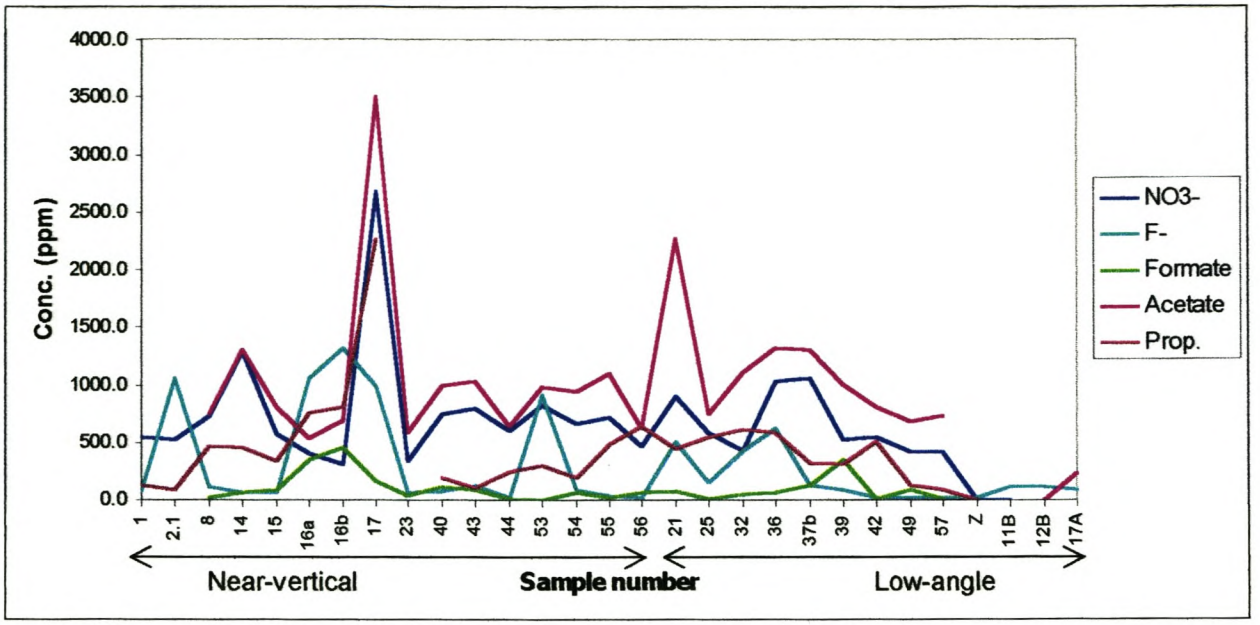

Fig. 9.3. NO_3^-, F^-, formate, acetate and propionate concentrations, determined by CE, in the inclusion fluid of the sampled quartz veins.

Table 9.1. Bulk CE compositional data for inclusion fluids in vein quartz. Values are in ppm. Concentrations are corrected for dilution of the volume inclusion fluid (determined by Karl Fischer titration) in the leach medium used for CE, so that concentrations are that of the bulk inclusion fluid. Only for sample RM Z is concentration given as per 1g sample weight.

Quartz veins having a near-vertical dip																
Cations																
	RM 1	**RM2.1**	**RM 8**	**RM 14**	**RM 15**	**RM 16a**	**RM 16b**	**RM 17**	**RM 23**	**RM 40**	**RM 43**	**RM 44**	**RM 53**	**RM 54**	**RM 55**	**RM 56**
NH_4^+	151.5	268.8	142.9	247.4	72.7	193.3	208.6	177.4	51.7	75.7	292.3	73.0	270.6	122.5	145.3	98.8
K^+	118.4	225.8	319.6	400.3	189.2	207.0	240.7	298.4	67.2	411.0	217.9	161.1	413.2	123.5	333.6	230.9
Na^+	1137.9	1079.2	1583.5	2735.0	1888.1	1203.4	984.2	1575.5	882.5	3113.9	1875.0	1544.4	2890.4	1607.0	2911.5	1803.4
Ca^{2+}	382.9	341.7	1081.0	543.1	204.5	499.8	615.7	334.7	162.1	696.0	1997.6	477.0	428.9	282.7	324.6	207.7
Sr^{2+}	4.9	3.2	4.9		3.4	6.2	6.2	4.7	2.4	6.7	8.2	4.8			5.7	
Mg^{2+}	35.4	52.3	45.9	60.3	20.0	92.8	178.3	98.7	18.6	47.9	143.9	31.8	76.0	33.9	36.2	21.7
Mn^{2+}	22.4	5.6				29.6	29.5	22.3	4.1	11.9	37.1	8.2	9.4	8.4	9.6	7.2
Li^+	9.0		6.0	10.4	6.3	8.6	7.8	6.8	3.0	8.2	9.3	5.3	8.4	7.4	9.6	6.8
Zn^{2+}	10.9	10.0			9.3			10.1		20.1	16.7	12.0	16.7		17.0	11.4
Anions																
	RM 1	**RM2.1**	**RM 8**	**RM 14**	**RM 15**	**RM 16a**	**RM 16b**	**RM 17**	**RM 23**	**RM 40**	**RM 43**	**RM 44**	**RM 53**	**RM 54**	**RM 55**	**RM 56**
Cl^-	517.6	1157.3	366.6	1195.0	562.2	4460.5	4174.4	3323.7	591.7	2969.4	1071.8	602.2	1914.7	365.2	1067.6	739.0
SO_4^{2-}	75.9	320.1	116.3	616.8	183.7	556.0	634.9	513.3	89.1	268.8	62.3	289.8	268.8	159.2	145.8	195.6
NO_3^-	546.3	516.6	737.3	1290.1	579.5	405.6	310.4	2677.6	340.6	738.9	797.5	602.6	828.3	664.1	719.2	473.4
Oxalate	7.9	5.3	7.7	14.4	6.7	8.4	8.5	7.5	4.7	11.0	11.2	8.5	10.2	10.0	10.9	8.2
F^-	80.7	1062.6	115.5	63.2	69.6	1054.5	1316.4	999.4	66.6	84.4	124.8	30.4	920.0	94.7	43.4	26.9
Formate	34.5		30.2	61.6	90.0	357.4	453.2	166.0	43.0	122.2	89.7	14.6	0.0	71.1	21.8	70.1
HPO_4^-																
HCO_3^-	2440.1	882.3	5683.0	4100.6	3000.2	8380.3	9585.9	7042.1	1252.4	3395.6	5827.3	3321.3	1712.1	2543.7	3839.3	2374.3
Acetate	721.7		742.7	1301.3	814.5	535.5	695.5	3507.3	592.2	991.2	1038.4	634.0	985.5	937.7	1091.8	626.9
Prop.	133.3	91.2	472.7	451.9	342.9	752.5	811.4	2262.4		196.3	104.2	254.7	303.0	199.2	484.8	641.4

Table 9.1 (Continued)

Quartz veins having a low-angle dip													
Cations													
	RM 21	**RM 25**	**RM 32**	**RM 36**	**RM 37b**	**RM 39**	**RM 42**	**RM 49**	**RM 57**	**RM Z**	**11B**	**12B**	**17A**
$NH4^+$	415.1	371.5	910.4	800.9	375.9	166.4	120.5	67.7	87.1	3.07	43.02	81.95	71.94
K^+	186.7	438.7	456.1	511.7	438.7	599.7	403.3	160.4	165.4	3.27	54.06	147.79	114.30
Na^+	1571.4	1684.4	1417.6	2504.7	2318.1	6623.0	5365.8	1560.8	1410.0	7.93	172.05	269.15	293.56
Ca^{2+}	367.8	356.0	542.3	822.4	773.3	1363.6	1073.9	255.0	184.9	2.81	39.41	495.13	122.46
Sr^{2+}	32.7	5.7			9.1	6.7	5.5	3.7		0.04	1.16	1.54	1.46
Mg^{2+}	80.2	67.8	75.6	149.3	74.3	103.8	93.0	16.8	15.5	0.53	27.47	144.88	37.01
Mn^{2+}	34.5	27.1			43.4	12.7	10.0	6.2				19.19	0.38
Ba^{2+}										0.05		74.91	2.33
Li^+	8.9				11.1	9.3	7.3	4.8	5.7	0.13	3.08	8.03	6.47
Zn^{2+}						18.4	13.5	9.7		0.42			
Cu^{2+}													
										0.06			
Anions													
	RM 21	**RM 25**	**RM 32**	**RM 36**	**RM 37b**	**RM 39**	**RM 42**	**RM 49**	**RM 57**	**RM Z**	**11B**	**12B**	**17A**
Br^-										0.25			
Cl^-	4562.9	914.3	813.7	884.0	688.4	9234.0	5591.6	793.5	548.5	28.46	783.02	1753.74	1744.68
SO_4^{2-}	436.0	38.1	83.8	288.8	204.8	158.7	133.2	253.0	151.0	17.75	310.67	4830.07	1296.78
NO_3^-	903.1	582.4	437.4	1032.2	1061.1	526.5	548.9	421.2	416.1	3.63	1.84		
Oxalate	11.0	8.6	11.2	14.4	13.8		8.8	6.9	7.1				
F^-	507.1	159.9	434.8	628.7	126.6	96.4	28.3	20.5	25.4	27.82	120.93	117.00	86.21
Formate	82.6	16.1	55.0	62.8	124.6	348.1	17.8	92.3	12.4				133.93
HPO_4^-												8.50	11.78
HCO_3^-	6496.3	1099.5	2530.2	2941.4	3686.0	4482.8	4169.4	2475.4	2304.8		92.11	225.81	224.94
Acetate	2269.5	741.4	1111.7	1321.5	1304.5	1012.1	809.6	676.5	735.8			4.16	235.91
Prop.	445.7	544.6	611.4	594.1	329.2	315.3	511.9	130.9	94.1	0.06			3.56

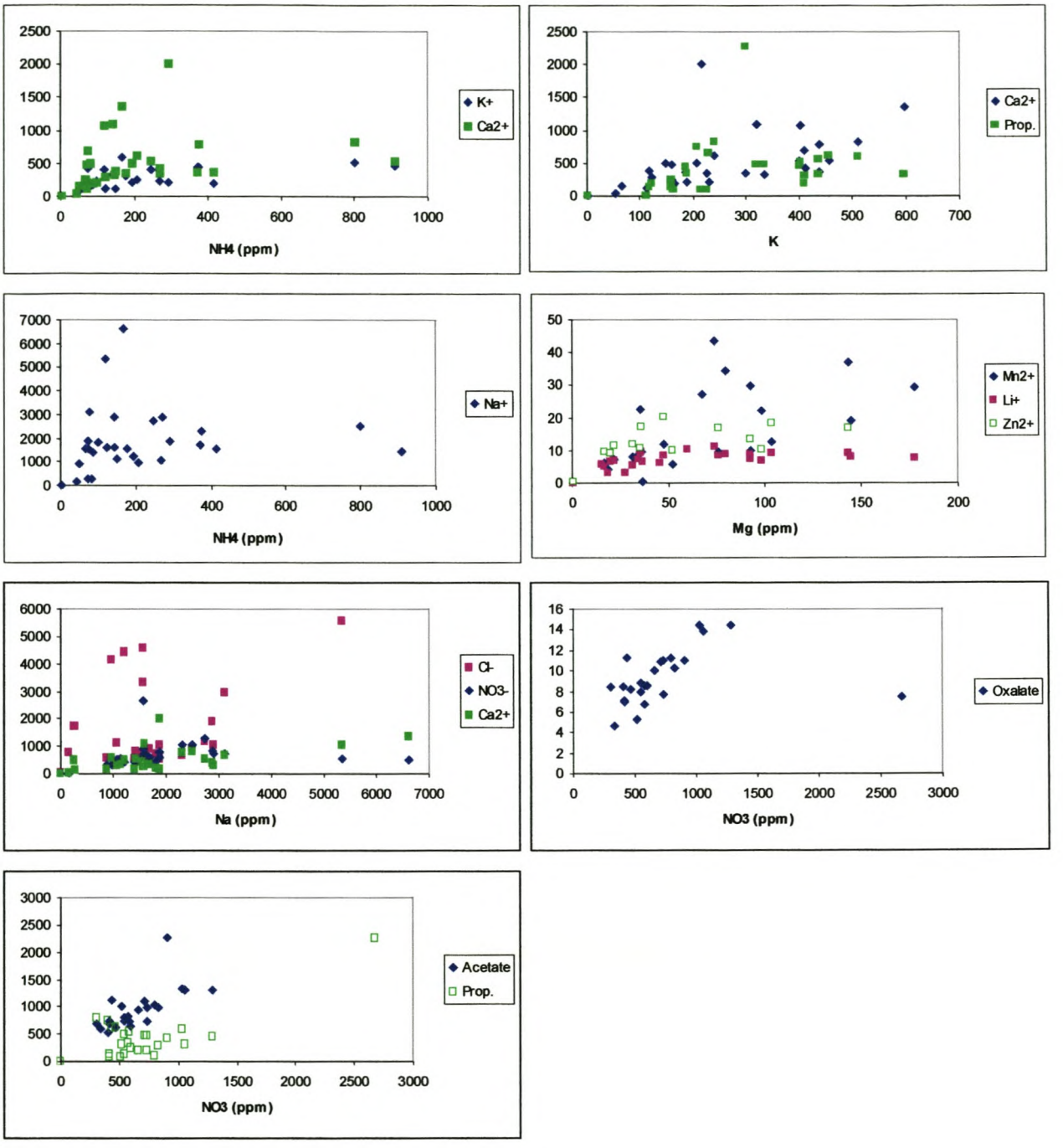

Fig. 9.4. Correlation diagrams from CE data.

9.2 Fluid salinity

Compositional data obtained by CE can be combined with H_2O content determinations from the Karl Fischer titration to calculate fluid inclusion volumes (as sample wt %) and describe fluid salinity in terms of the dissolved ion content. From Table 9.2 and Figure 9.5 it can be seen that bulk fluid salinity range on average between 0.3 and 1.3 wt % TDS, with the volume of fluid inclusions per sample between 0.5 and 0.8 sample wt %. The high salinity values in samples RM 16a & b, 17, 21, 39 and 42 could result from the presence of a large amount of higher salinity inclusions. This was in fact confirmed by microthermometry measurements for samples RM 16a, 39 and 42 and is likely to be true for the others as well. Again no distinct variation in salinity between the two quartz vein sets is evident.

The salinity range calculated from CE data is, however, much lower than measured by microthermometry. The bulk nature of CE analysis and a fluid content determination that is just slightly out might result in such differences.

Corrections for true water content as well as salinity calculations are described in Appendix B.

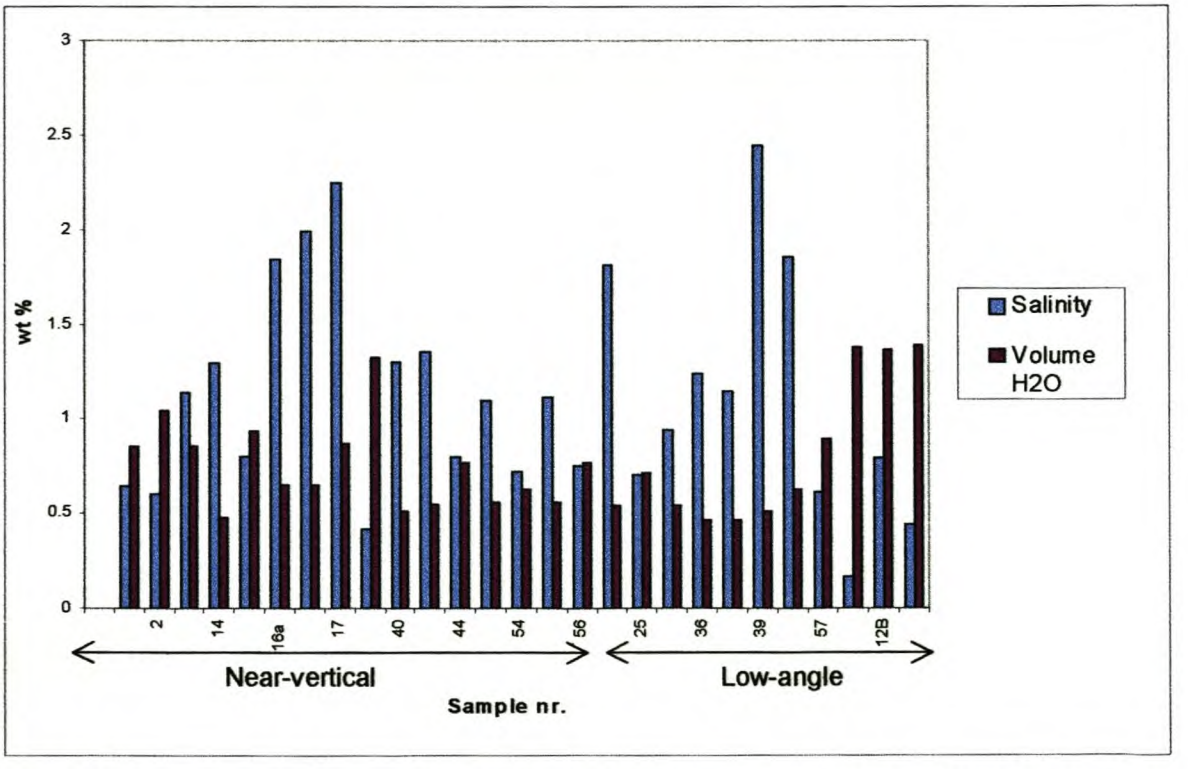

Fig. 9.5. Water content of inclusions determined by Karl Fischer titration, combined with CIA data to calculate bulk fluid salinity.

Table 9.2. Bulk fluid salinity and inclusion volume of quartz samples analysed.

	Near-vertical Q-veins										
	RM 1	**RM 2**	**RM 8**	**RM14**	**RM15**	**RM16 a**	**RM16 b**	**RM17**	**RM23**	**RM40**	**RM43**
Salinity (wt % TDS)	0.64	0.60	1.13	1.29	0.80	1.84	1.99	2.25	0.42	1.30	1.35
wt% H_2O per samp.	0.85	1.04	0.85	0.48	0.93	0.65	0.65	0.87	1.32	0.51	0.55
	RM44	**RM53**	**RM54**	**RM55**	**RM56**						
Salinity (wt % TDS)	0.80	1.09	0.72	1.11	0.75						
wt% H_2O per samp.	0.77	0.56	0.63	0.56	0.77						
	Low-angle Q-veins										
	RM21	**RM25**	**RM32**	**RM36**	**RM37 b**	**RM39**	**RM42**	**RM57**	**11B**	**12B**	**17A**
Salinity (wt % TDS)	1.81	0.70	0.94	1.24	1.15	2.45	1.86	0.61	0.16	0.79	0.44
wt% H_2O per samp.	0.54	0.71	0.54	0.46	0.46	0.51	0.63	0.89	1.38	1.36	1.39

9.3 Geothermometry

White (1965) and Ellis (1970) have shown that the atomic ratio Na/K, above about 180°C, is a very useful geothermometer, which is presumably controlled by mineral equilibria related to feldspar alteration. A study by Henley *et al.* (1984) of mineral alteration equilibria suggests that calcic minerals (plagioclase, epidote, calcite) also play an important role in controlling fluid chemistry. The empirical Na-K-Ca thermometer derived by Fournier and Truesdell (1973) is based on equilibria involving these mineral phases, and is calibrated to give more acceptable temperatures over the temperature range 100° - 300°C.

At low temperatures - where calcite solubility is relatively high - the P_{CO2} of the solution may markedly affect the results. Also, although the solubility of magnesium silicates is very low at high temperatures, high magnesium contents at low temperatures affect the geothermometer and an empirical correction must be applied. Uncertainty exists on the use of this Mg-correction and it was not applied.

Table 9.2 lists the last temperature of water-rock interaction derived for all the samples with the use of the Na-K-Ca geothermometer. This temperature is calculated from bulk fluid composition and therefore reflects the average temperature of formation of all the inclusion

populations or that of the dominant inclusion type. A range of 180 – 220 °C was calculated for most samples.

When temperatures obtained by microthermometry is compared to that calculated by the geothermometer (Figure 9.6), the latter is in the range of the lowest temperature population. Only for RM 14 can this be explained by the dominance of the low temperature population. In RM 42, for example, high temperature inclusions ranging between 270 and 340 °C are present, while the geothermometer calculated a temperature of only 190 °C.

It can therefore be concluded that applying the above Na-K-Ca geothermometer to a mixture of various inclusion generations is not representative of any of the individual populations, but more importantly, this geothermometer does not appear to be suitable to fluid inclusions as it renders inaccurate results.

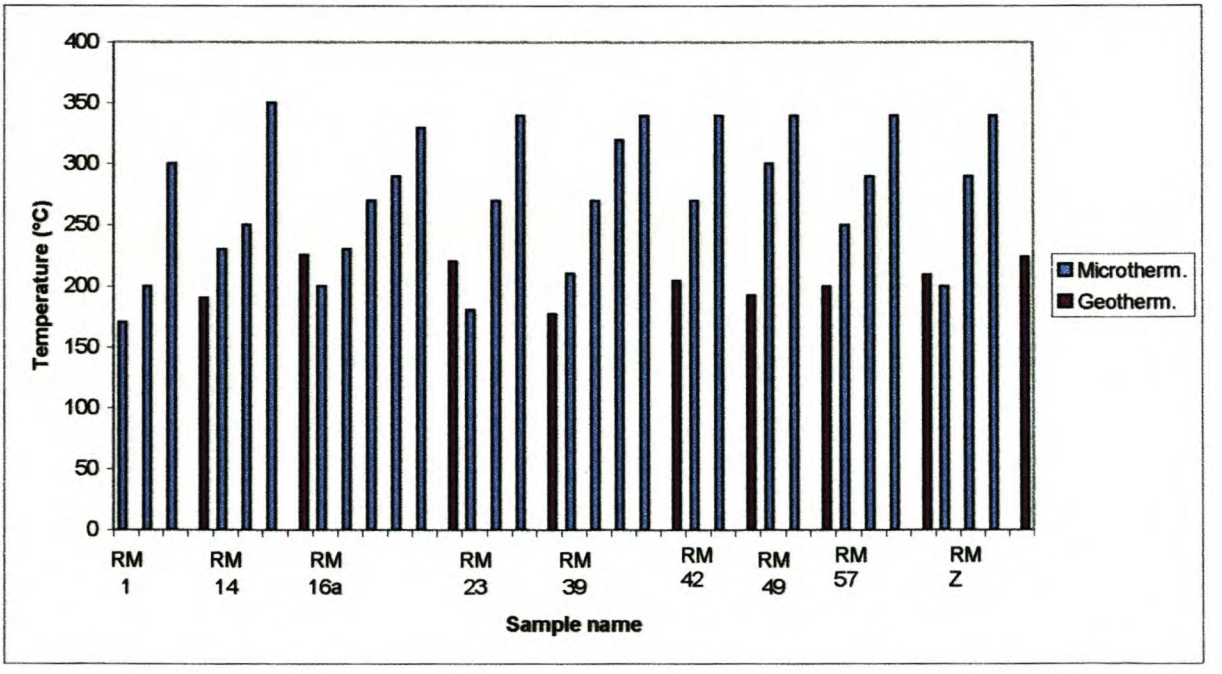

Fig. 9.6. Comparison between fluid inclusion temperatures obtained by microthermometry and those calculated from bulk fluid composition.

9.4 Thermodynamic principles

9.4.1 pH calculations

Direct measurement of pH on the leach fluid would provide inaccurate results of the actual inclusion fluid, as this fluid do not contain gasses under high pressure, have been diluted several hundred times and has been in contact with the host mineral and possible impurities that may affect the pH. Calculations made on ion pairs such as HS^- / SO_4^{2-} or NH_4^+ / NO_3^- would provide more satisfactory results, although there is little assurance that the high temperature equilibrium is reflected (Roedder, 1969).

Henley *et al.* (1984) have shown that simple alteration phase equilibria can be assumed to control or buffer pH and fluid composition in many hydrothermal studies, for example the pH controlling reactions

$$1.5\ KAlSi_3O_8 + H^+ = 0.5\ KAl_3Si_3O_{10}(OH)_2 + 3\ SiO_2 + K^+ \qquad (1)$$

$$3\ NaAlSi_3O_8 + K^+ + 2\ H^+ = KAl_3Si_3O_{10}(OH)_2 + 6\ SiO_2 + 3\ Na^+ \qquad (2)$$

From equilibrium constant data for these reactions, a theoretical estimate of pH_t as a function of salinity (approximated as $m_{Na^+} + m_{K^+}$) can be made. By using Truesdell's Na-K geothermometer in reverse and determining log m_{K^+} as a function of ($m_{Na^+} + m_{K^+}$) and temperature, then using equilibrium constant values calculated from thermodynamic data, pH_t can be calculated directly from the Kmica-Kspar equilibrium constant.

Although this estimation of pH should theoretically be more accurate, as it takes all the pH-dependent species into account, it makes use of an empirically calculated geothermometer that has been shown to yield inaccurate results.

If inclusion temperatures obtained by microthermometry are used though, along with fluid salinity values from CE (expressed as $m_{Na^+} + m_{K^+}$), a diagram such as Figure 9.7 can be constructed for samples RM 1, 14, 16a, 23, 39, 42, 49, 57 and RM Z. By establishing a set of

equations for salinity in the range 0.01 – 0.3 ($m_{Na^+} + m_{K^+}$), covering the range of sample fluid salinity, a pH range for the inclusions in each sample can be calculated and plotted. The dependence of solution pH on temperature, decreasing for fluids trapped at higher temperatures, is evident from this diagram, with the 300 – 340 °C population in all samples having the lowest pH. It can also be noted that the neutral pH for water at higher temperature (around 250 °C) is 5.6, so that most of these fluids will be classified as alkaline.

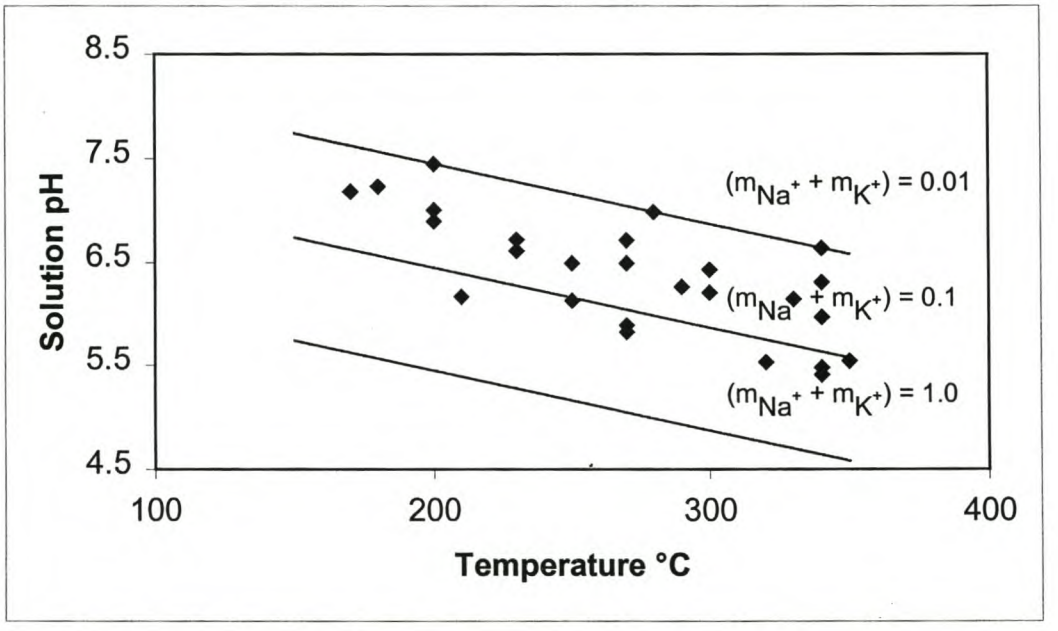

Fig. 9.7. Solution pH calculated as a function of temperature and salinity.

By determining the oxidation state of the formation environment from redox ion pairs in solution, a rough estimate can be made of the pH of the samples not analysed by microthermometry, where reducing conditions would have an acid pH and oxidising conditions tend to be more alkaline. The NH_4^+ / NO_3^- ratio was selected in this study since other ion pairs were not detected simultaneously by CE. With the exception of sample RM 32, this ratio is <<1 and therefore suggests oxidising and alkaline conditions.

9.4.2 Log f_{O_2} - pH predominance diagrams

Fluid inclusion analyses to determine the ionic species present in solution are performed at 25 °C and 1 atm. pressure, while entrapment of the fluids took place at higher temperature and pressure, yielding different equilibrium conditions and, hence, different species in solution. It is therefore necessary to establish which species of a given ion will dominate under specific conditions of formation, using thermodynamic principles to calculate dominant regions of stability for these species.

When redox reactions are involved in chemical processes, stability relationships can be depicted using pε - pH or log f_{O_2} – pH diagrams. The parameter pε is a variable that defines the state of the redox couple. Unfortunately, the stoichiometries of many redox couples are difficult to define, especially in high-temperature fluids or those containing decomposing organic matter (which may be a source of electrons). In these cases the oxygen fugacity may be a more reliable variable. These diagrams are very similar, with the species boundaries in the one diagram analogous to those in the other, and the interpretation is identical (Fletcher, 1993).

Basic thermodynamic principles are followed in calculating these diagrams. By definition, pH = -log a_{H^+} and $a_{O_2} = f_{O_2}/f_{O_2}^{\ 0}$, and if we choose our standard state for O_2(g) to be the ideal gas at temperature and 1 bar, then $f_{O_2}^{\ 0}$ = 1 bar and $a_{O_2} = f_{O_2}$. SUPCRT92 (Johnson *et al.*, 1992) has been used to calculate the standard partial molal Gibbs free energies of all the reactions required to draw the diagrams from the apparent standard partial molal Gibbs free energies of formation, based on the following relationship:

$\Delta G°_R = \sum G°_{fc}(\text{products}) - \sum G°_f(\text{reactants})$

Equilibrium constants for the reactions were also calculated from SUPCRT92 Gibbs free energies of formation from the equation

$$\text{Log K} = \frac{\Delta G°}{2.303*RT}$$

The two systems that will be used for these stability diagrams are that of sulphur and nitrogen, with log fO_2 – pH diagrams produced at 25°C and saturated water vapour pressure (SWVP), being analytical conditions whereby the ionic species were detected.

The aqueous sulphur species we wish to plot are H_2S^0, HS^-, HSO_4^-, and SO_4^{2-}. Thermodynamic data for the species S^{2-} are highly uncertain, but it appears that this species is not predominant under any geologically relevant conditions (Seward and Barnes, 1997). It can be shown via thermodynamic calculations (cf. Barnes and Kullerud, 1961), that other sulphur species, such as thiosulphate ($S_2O_3^{2-}$), sulphite (SO_3^{2-}), tetrathionate ($S_4O_6^{2-}$) and polysulphide (S_x^{2-}), although present, are also never predominant under reasonable geological conditions. Thermodynamic data required are given in Table 9.3.

Table 9.3. Apparent standard molal Gibbs free energies (in kcal / mole) from SUPCRT92 for aqueous sulphur species (25°C, SWVP).

Species	$\Delta_f G°$
HS^-	2.86
SO_4^{2-}	-177.93
$O_2(g)$	0.00
H_2S^0	-6.67
HSO_4^-	-180.63

The following set of reactions describes the equilibrium solution chemistry of sulphur, while Table 9.4 lists the log K values of the various reactions at different temperatures and pressures.

$$H_2S^0 = HS^- + H^+ \quad \text{- (1)}$$

$$HSO_4^- = SO_4^{2-} + H^+ \quad \text{- (2)}$$

$$H_2S^0 + 2O_2(g) = HSO_4^- + H^+ \quad \text{- (3)}$$

$$H_2S^0 + 2O_2(g) = SO_4^{2-} + 2H^+ \quad \text{- (4)}$$

$$HS^- + 2O_2(g) = SO_4^{2-} + H^+ \quad \text{- (5)}$$

Table 9.4. Equilibrium constant log values for above reactions of the various sulphur species at analytical conditions of 25 °C and 1 bar pressure, as well as at the approximate calculated temperature of formation and various pressures.

	25 °C / 1 bar	200 °C / 1 bar	200 °C / 500 bar	200 °C / 2500 bar	200 °C / 5000 bar
$\log K_1$	-6.99	-6.68	-6.53	-6.11	-5.74
$\log K_2$	1.98	-4.47	-4.28	-3.82	-3.53
$\log K_3$	127.55	71.4	77.64	79.20	80.88
$\log K_4$	125.57	66.69	73.36	75.38	77.35
$\log K_5$	132.56	73.6	79.90	81.49	83.09

The equilibrium constants for the above reactions at 25 °C and 1 bar can be written as follows:

$$\log K_1 = \log \frac{a_{HS^-}}{a_{H_2S^0}} + \log a_{H^+} = -6.99$$

$$\log K_2 = \log \frac{a_{SO_4^{2-}}}{a_{HSO_4^-}} + \log a_{H^+} = -1.98$$

$$\log K_3 = \log \frac{a_{HSO_4^-}}{a_{H_2S^0}} + \log a_{H^+} - 2\log f_{O_2} = 133.308$$

$$\log K_4 = \log \frac{a_{SO_4^{2-}}}{a_{H_2S^0}} + 2\log a_{H^+} - 2\log f_{O_2} = 131.329$$

$$\log K_5 = \log \frac{a_{SO_4^{2-}}}{a_{HS^-}} + \log a_{H^+} - 2\log f_{O_2} = 138.317$$

The boundaries we wish to calculate are called predominance or isoactivity boundaries because they separate the region of $\log f_{O_2}$ – pH space where each ionic species has the highest activity. At the boundary itself the activities of the two species are equal, so that the term of above equations containing these equal activities reduces to zero, and, with $\log a_{H^+}$ = -pH, above equations simplify to:

H_2S^0 – HS^- boundary: pH = 6.99

HSO_4^- - SO_4^{2-} boundary: pH = 1.98

H_2S^0 – HSO_4^- boundary: $\log f_{O_2}$ = -0.5pH – 66.65

H_2S^0 – SO_4^{2-} boundary: $\log f_{O_2}$ = -pH – 65.66

HS^- – SO_4^{2-} boundary: $\log f_{O_2}$ = -0.5pH – 69.16

These predominance regions are shown in Figure 9.8. Note that none of the boundaries calculated depend on the actual total activity or concentration of sulphur in solution.

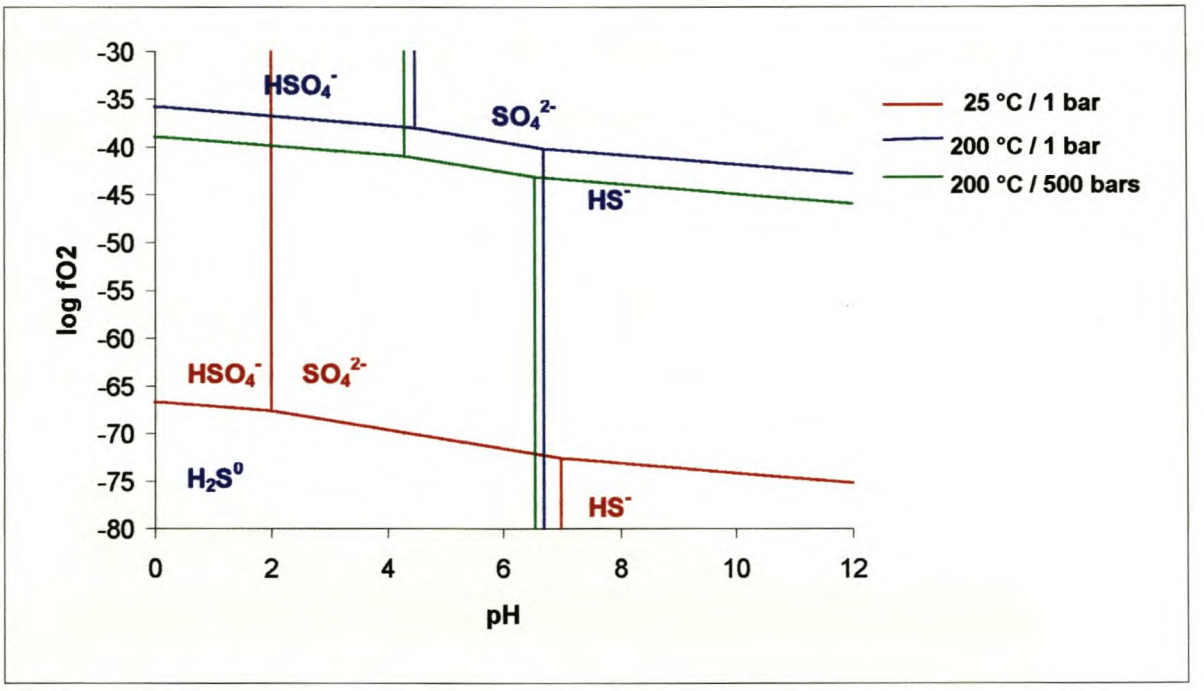

Fig. 9.8. Log f_{O_2} – pH diagram for the sulphur system at various temperatures and pressures.

These predominance boundaries between aqueous species merely separate regions of the diagram where one of the species is predominant over the rest. For example, in the SO_4^{2-} field, the other species are still present, but at much lower activities or concentrations than SO_4^{2-}. Also, SO_4^{2-} does not completely disappear when crossing the boundaries that enclose its field of predominance, but only decreases in concentration with distance from its predominance field. It can be seen that at 25 °C and 1 bar pressure H_2S^0 and HS^- will only be present under strongly reducing conditions, leaving SO_4^{2-} as the dominant species and indeed the ion detected

by CE. The pH calculated for the inclusion fluids range between 5.4 and 7.4, explaining the absence of HSO_4^- at these equilibrium conditions.

At the conditions of formation of these trapped fluids, calculated at around 200 °C and pressure between 1 and 2kb, other sulphur species may however be present. From Figure 9.8, at 200 °C and 1 and 500 bar pressure the H_2S^0 and HS^- predominance fields stretch over a larger oxygen fugacity range, increasing the possibility of their presence. The boundary between these two phases fall in the pH range calculated for the fluids, so that both phases, if any, would be likely to co-exist. From the oxidising conditions inferred by NH_4^+ / NO_3^- ratio, it is probably more likely that SO_4^{2-} would still be the dominant phase at higher temperature. Figure 9.9 shows that with increasing pressure above 500 bar and constant temperature there is very little shift in the positions of the boundaries between species, so that the equilibrium conditions remain relatively constant.

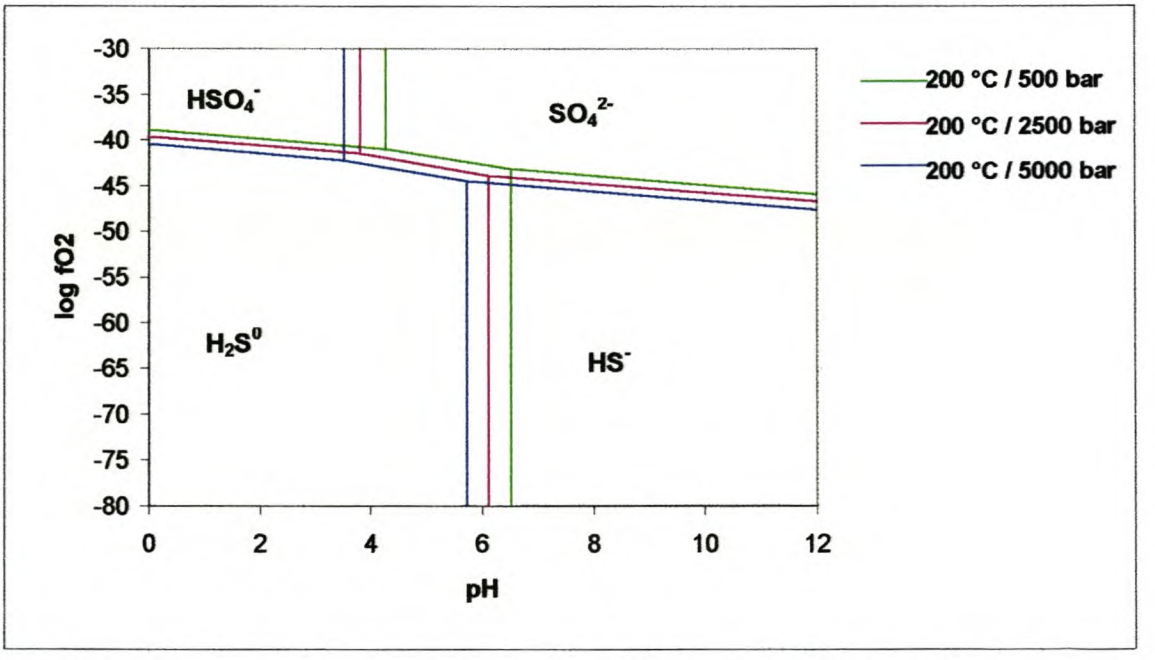

Fig. 9.9. Predominance boundaries for the sulphur system at 200 °C and 500, 2500 and 5000 bar pressures.

The nitrogen system can similarly be used for log f_{O_2} – pH diagrams, with the equilibrium reactions as follows. Table 9.5 contains the log K values for these reactions.

$NH_3^0 + H^+ = NH_4^+$ - (1)

$N_2^0 + 3H_2O(l) = 2NH_3^0 + 1.5O_2(g)$ - (2)

$N_2^0 + 3H_2O(l) + 2H^+ = 2NH_4^+ + 1.5O_2(g)$ - (3)

$NO_3^- + 2H^+ + H_2O(l) = NH_4^+ + 2O_2(g)$ - (4)

Table 9.5. Equilibrium constant log values for above reactions at analytical conditions of 25 °C and 1 bar pressure, as well as at the approximate calculated temperature of formation and various pressures.

	25 °C / 1 bar	200 °C / 500 bar	200 °C / 2500 bar	200 °C / 5000 bar
log K_1	9.24	5.84	6.00	6.16
log K_2	-116.46	-71.81	-71.95	-72.17
log K_3	-97.98	-60.124	-59.96	-59.84
log K_4	-52.86	-29.28	-30.08	-30.91

Substituting pH and log K in the same way as for the sulphur system, the above reactions give the equations of the boundary lines between the different nitrogen species as follows:

$NH_3^0 - NH_4^+$ boundary: $pH = -\log K_1$

To plot the $N_2^0 - NH_3^0$ boundary, a value of 0.001 is assigned to the total activity of dissolved nitrogen, to give $\log f_{O_2} = 2/3(\log K_2 + 3)$

$N_2 - NH_4^+$ boundary: $\log f_{O_2} = 2/3(\log K_3 + 3) - 4/3pH$

NO_3^- - NH_4^+ boundary: $\log f_{O_2} = ½\log K_4 - pH$

These boundaries are plot in Figure 9.10.

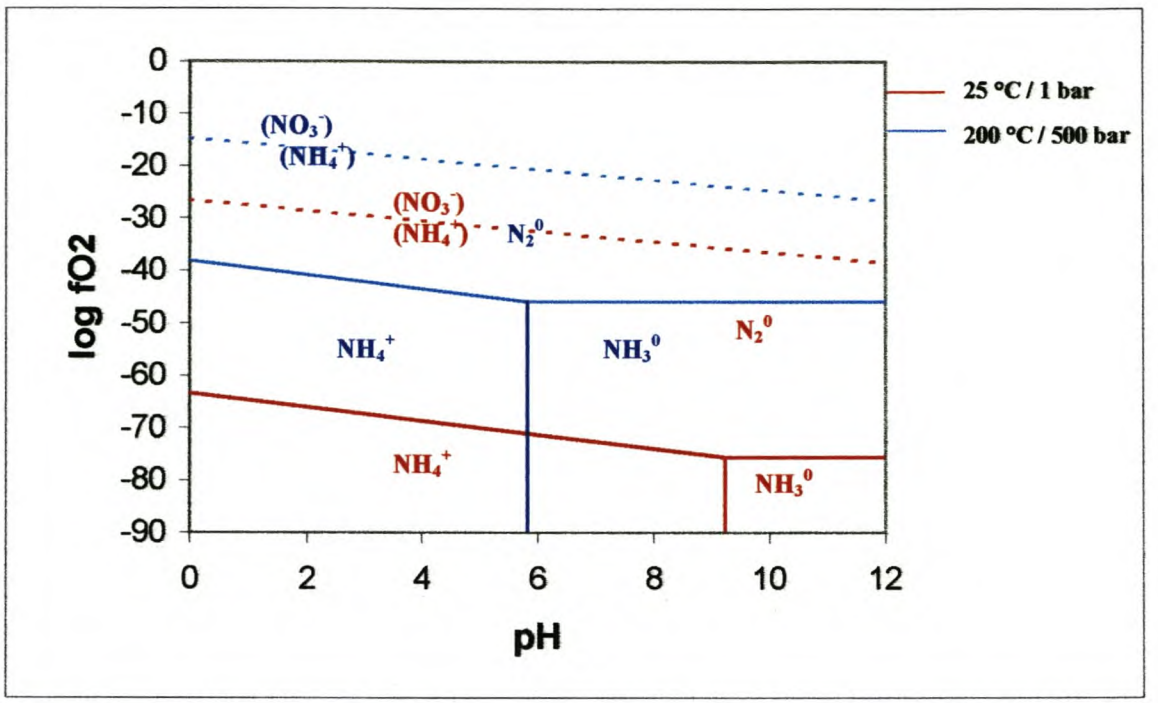

Fig. 9.10. Log f_{O_2} – pH diagram for the nitrogen system at 25 °C / 1 bar pressure and 200 °C / 500 bar pressure. The predominance boundaries at 200 °C and higher pressure are at almost the same position as those at 500 bar.

NO_3^- and NH_4^+ are the dominant ions in oxidising conditions, at analytical as well as possible entrapment conditions, with the possibility of NH_3^0 also to be present.

A detailed explanation of the above reactions for nitrogen and its substitutions at various temperatures and pressures is contained in Appendix C.

9.5 Conclusions

From microthermometry measurements and O-isotope data a possible late-magmatic origin and later metamorphic overprint is envisioned for the inclusion fluids in all the quartz veins studied. The positive correlation between all the cations and anions confirms that these fluids are late-magmatic rather than released during fractionation of the host granite, while the presence of organic acids suggest that a portion of the inclusion fluids was of sedimentary origin.

No distinctive variation in bulk fluid chemistry and salinity between inclusion fluids from the two apparent vein systems was recognised. Possible original differences might have been reset during later processes of fluid circulation that affected the whole study area, as suggested by the relatively uniform distribution of inclusion populations throughout the sample series.

High values of acetate and nitrate in samples RM 17 and 21 might be related to a specific inclusion type, namely the dark irregular ones with temperatures between 240 and 360 °C, which dominates in these samples. It has been suggested that this inclusion population represents a late phase of renewed fluid circulation from a possibly different source than the other inclusions. If this population is the source of the organic components, it most likely represents a fluid that was released from possibly Malmesbury rocks, as suggested by O-isotope data, during Cape Orogeny metamorphism.

Fluid salinity and pH determined for individual inclusions as well as bulk fluid indicate a relatively dilute, alkaline fluid, which most probably remained relatively constant for these components.

Data on fluid chemistry has proved useful in estimating fluid composition at the conditions of entrapment using the sulphate and nitrate systems, showing that different ions of these species were originally present. This information could be used in modelling the conditions of the source environment(s).

Truesdell and Fournier's Na-K-Ca geothermometer was shown to provide inaccurate results on a bulk fluid comprising various generations of fluid inclusions when compared to temperatures measured for individual inclusions by microthermometry. It might be more suitable if only one fluid population is present.

10 SCANNING ELECTRON MICROSCOPE (SEM) DATA

10.1 Introduction

SEM analysis of opened fluid inclusions can prove useful in identifying daughter crystals within inclusions. Since these daughter minerals indicate saturation of the fluid with respect to these phases at the conditions of formation, they provide useful information on fluid composition. These results are however semi-quantitative at best, since the electron beam would analyse anything around and behind the selected daughter crystal.

10.2 Results and discussion

Only a few samples were selected to illustrate the application of the SEM in fluid inclusion analysis. Six quartz pieces of 2 - 3mm were chipped off each sample rock using a modified miniature machinist's vice, e.g. as illustrated by Hallbauer (1983), and mounted onto a metal stub with the freshly broken surface facing upwards. The mounted sample was then gold coated and covered to prevent dust settling onto the sample surface.

Analyses were done at the University of Stellenbosch Physics department.

The number of inclusion generations and their shapes compare with that identified under the petrographic microscope, while daughter crystals not observed earlier were detected with the use of the SEM. In the six samples analysed these crystals were found in irregular as well as angular inclusions.

Flat, prismatic K-Al daughter crystals are present in irregular inclusions of samples RM 57 and 55 (Photos 10.1 and 10.2) as well as in an angular inclusion in RM 57 (Photo 10.3). X-ray spectra recorded for these daughter crystals are included as well. An irregular inclusion in RM 55 contains a calcite crystal (Photo 10.4). In RM 53 an Fe-Mn crystal is hosted within an angular inclusion, while Ti-needles (possibly rutile) were found in an angular-irregular inclusion in RM 54 (Photo 10.5).

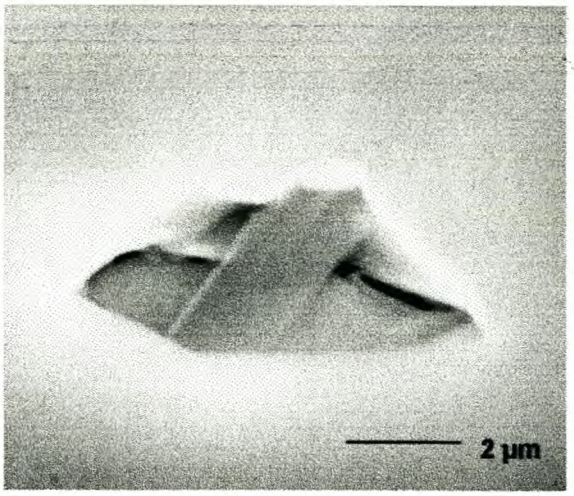

Photo 10.1. K-Al rich daughter crystal in sample RM 57.

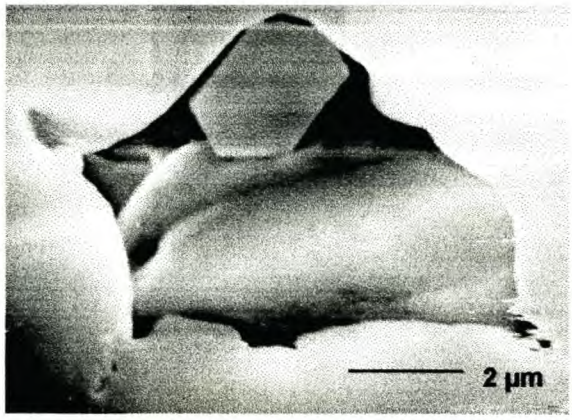

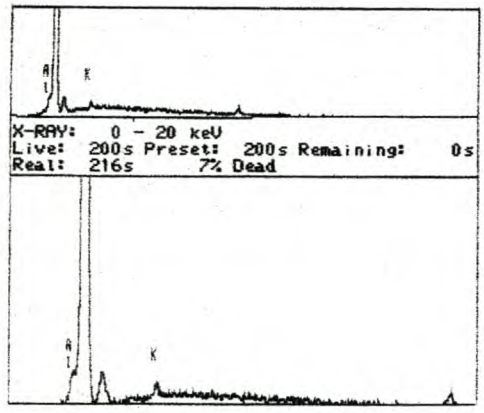

Photo 10.2. Daughter crystal in RM 55, with the same composition as in RM 57.

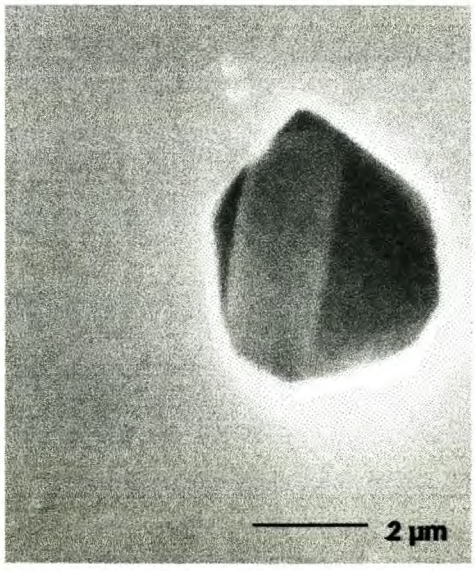

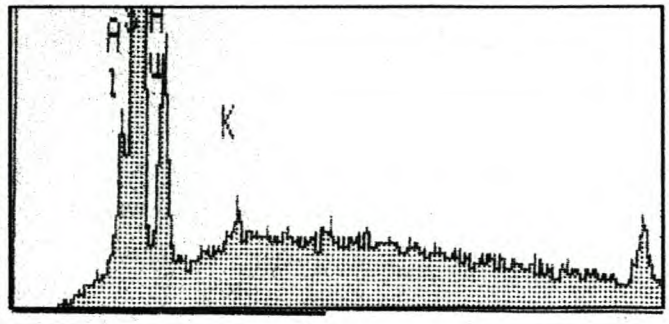

Photo 10.3. An angular inclusion in RM 57 containing a K-rich daughter crystal.

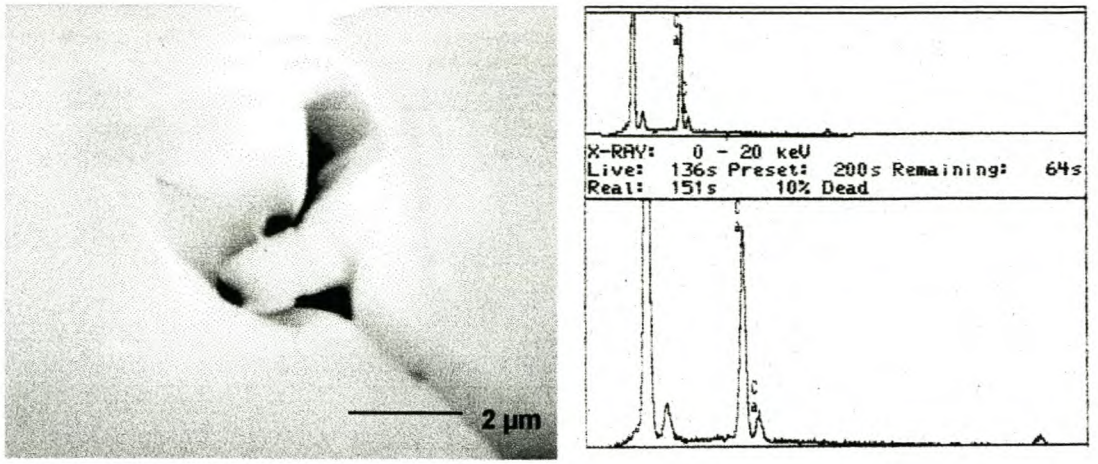

Photo 10.4. A Fe-Mn daughter crystal within an angular inclusion in RM 53.

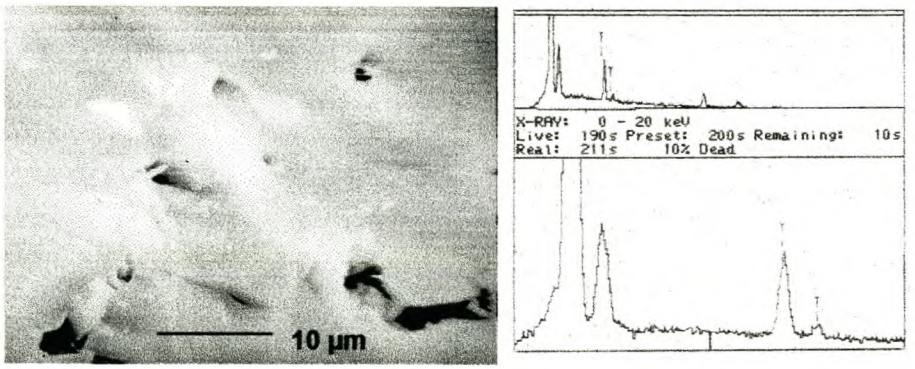

Photo 10.5. Ti-rich needles in an inclusion in RM 53.

10.3 Conclusion

The presence of daughter crystals in some inclusions contradicts the low fluid salinity determined by microthermometry. It is, however, possible that these crystals are present in the very small inclusions on which measurements could not be made. They are either present in extremely small quantities or insoluble under analytical conditions, since bulk fluid chemistry obtained by CE did not reveal a highly saline fluid.

11 FLUID FORMATION MODEL

11.1 Relationship between quartz vein systems

The plutons of the Cape Granite Suite that intruded into the Malmesbury sedimentary rocks in the Tygerberg terrane are classified as syn- to post-tectonic, peraluminous, S-type granitoids and were subdivided in Sa1, Sa2 and Sb types by Scheepers (1995). The mineralization occurring in the Tygerberg terrane, hosted by quartz veins and saddle reefs, is the result of late-magmatic fluids that permeated through the granites and into fractures extending from the granite into the surrounding sediments. Bruwer (1997) has shown that the Sn-mineralization at Kuiperskraal is the result of fractionation of the underlying Sa2 granite in the Kuilsriver pluton, producing a metal- and volatile-rich hydrothermal fluid. The fluid had a temperature ranging from 200 to 379 °C and salinity < 15 wt.% NaCl, with the high-temperature phase of the fluid (340 – 370 °C) responsible for the Sn-mineralization.

The quartz veins and saddle reefs hosting the Sn-mineralization are all NW-trending, dipping at an angle between 15 and 50° to the SE. One set of barren quartz-biotite±chlorite veins sampled in the study area also has this orientation, while a second set of these veins strike W to NW and dips at a near vertical angle, all hosted by either granite or Malmesbury sediments. Except for their orientation, no differences regarding associated minerals, inclusion characteristics or fluid chemistry indicated a difference in origin. Although no age relationships could be determined for these quartz veins, their presence in the granites and its classification as late-magmatic provides an early age of at least 510 Ma, while reactivation of the fluid system most likely occurred at various intervals until the final stages of the Cape Orogeny.

11.2 Fluid composition and origin

Bulk fluid chemistry as determined by CE suggests a relative simple fluid composition, with the major cations being $Na^+ > Ca^{2+} > K^+ > NH4^+$, and the anions $Cl^- >$ acetate $> NO_3^- > F^-$. The alkali elements, Ca^{2+}, Sr^{2+}, Mg^{2+}, Li^+, and Cl^- have been contributed from a granitic source, Mn^{2+}, NO_3^-, and the organic acids could be supplied by sedimentary rocks, while Zn^{2+} and SO_4^{2+} add a possible sulfide source for a portion of the fluids.

Microthermometry identified similar temperature populations for the samples in this study than those found in the mineralized and barren quartz veins of the Kuiperskraal Sn-deposit. The difference is that in the former the whole temperature range of inclusions occur in one sample, while at Kuiperskraal the late, low temperature quartz-calcite-actinolite veins only contain low-temperature inclusions.

The origin of the various inclusion populations is suggested as follows;

1. Remnants of a high temperature population (370 – 390 °C) found only in one sample, suggest that the first late-magmatic fluids to crystallize was of this temperature, which compares to the temperature of fluids from which cassiterite at Kuiperskraal crystallized. The absence of associated mineralization indicates that these fluids possibly originated from the less fractionated and metal rich granites. After a slight decrease in temperature the 310 – 360 °C population was trapped.

2. Later cooler fluids circulating through the fracture system, of similar origin than above, was responsible for the 230 – 300 °C population.

3. During the final cooling stages of this fluid system the 160 – 200 °C population became entrapped. It is uncertain if the fluids at this stage still had a largely magmatic composition or if fluids released during metamorphism of the surrounding sediments have already been introduced.

4. The last stage of fluid circulation is represented by the dark, irregular inclusions of elevated temperature (240 – 360 °C). The high concentration of organic acids that can be related to this fluid population characterizes it as being of a sedimentary origin, where diagenetic transformations of organic material lead to the formation of organic acids (Lundegard and Kharaka, 1994). The thermal energy required to produce these organic acid species may have been supplied during regional metamorphism of the Malmesbury sediments during the Cape Orogeny. Formation temperatures measured by microthermometry for this fluid fall in the 200 - 300 °C range estimated by Hälbich and Cornell (1983) for the above deformation period. O-isotope data also supports the theory of a largely magmatic origin for the inclusion fluids with a strong metamorphic overprint.

12 EVALUATION OF THE CE TECHNIQUE AND ITS APPLICATION TO EXPLORATION WITH REFERENCE TO HYDROTHERMAL QUARTZ

12.1 Sample selection, study and preparation

As mentioned earlier, when fluid inclusion studies are to be incorporated in the exploration process, a possible exploration target should already have been identified through association with a specific tectonic environment. The selection of samples suitable for CE is similar to that of any other analytical technique on fluid inclusions, being that the quartz vein sample and its fluid content must be large enough to be representative of the bulk of the (mineralising) fluid forming the vein system.

Before commencing with any analyses, a petrographical study is essential in establishing the number of inclusion generations present, with a single one being the ideal situation. A bulk analysis of all the inclusion generations could be obtained, while portions of thin section wafers containing a single inclusion type can be selected, since a sample amount of less than 1 gram is sufficient for extraction and analysis by CE.

Cleaning of the sample fraction to be analysed from mineral impurities is an important but time-consuming part of the sample preparation, because although only a small amount of sample is required for CE (a few gram), the sample size must be representative of all the fluids present for individual or bulk fluid analysis.

12.2 Analytical procedure

12.2.1 Crush-leach method

The largest source of ambiguity introduced by the crush-leach procedure used for CE, namely wet crushing in an "open system", results from CO_2 in its various forms. Free CO_2 from the atmosphere may be added to the leach fluid during crushing, producing contaminant H_2CO_3 with the water and excess HCO_3^- upon analysis. Blank crushes may establish the extent of CO_2

contamination, but as this value will not always be constant and would be large in comparison with the amount of CO_2 (if present) in the inclusions, this will not be an accurate parameter. Dissolution of free CO_2 to HCO_3^- will also dissolve any solid carbonate impurities and add cations and carbon to the solution.

Using a leach solution that has been purged with argon gas to remove any oxygen, although atmospheric oxygen might still influence the oxidising potential of the leach solution, may prevent oxidation of sulphide species to sulphate. Crushing in vacuum would then be ideal to limit atmospheric contamination, as well as make simultaneous analysis of the gas species possible by first measuring the released gasses and then washing the crushed fragments and sample holder walls with pure water (Roedder et al., 1963).

Loss of gasses upon opening may also precipitate solids that are relatively insoluble in pure leach water (Roedder, 1984). There is very little that can be done to avoid this, as it results from the disturbed equilibrium of the system.

12.2.2 Elimination of contamination factors during CE analytical procedure

As outlined in section 6.3.3, contamination could result from various sources and care has to be taken in establishing these factors and the amount to which they contribute. A sequential elimination procedure involving cation and anion analyses, from when the sample is crushed until analytical data is obtained, can be outlined as follows:

1. Blank analyses of MQ and MQ-TBA water in new sample vials. Contamination from the vials is unlikely, but if present could not be distinguished from that of the water.
2. MQ and MQ-TBA blanks from clean, but previously used sample vials.
3. MQ-TBA blanks of both course and fine filter paper.
4. MQ-TBA blanks of sample holders in which filtrate will be stored before analysis. The water is left for up to 7 days (the maximum time that a sample will be left between cation anad anion analyses) to determine if the sample holder would desorb any ions. Vice versa,

a solution containing various cations of low concentration levels (10-1000 ppb) should also be left for the same time to determine if any ions are lost to the surface walls by adsorption during storage. Struempler (1973) studied the adsorption of 0.5 ppb silver, 10 ppb lead, 1 ppb cadmium, and 10^{-7} g / ml solution zinc and nickel onto borosilicate glass, polyethylene and polypropylene container walls. He found that silver and lead completely adsorbed onto all container surfaces within 4 - 8 days, with polypropylene being the least desirable container for storage of low concentration cations. This loss would not have such a drastic effect for cations present in large concentrations, but it would be advisable to do cation analyses first in order to minimise any adsorption.

5. In order to determine the amount of atmospheric CO_2 absorbed by the leach fluid during crushing, as well as any ions that might be added by the corundum mortar, a "blank crush" is done. The same amount of MQ-TBA water is "crushed" for the same length of time (approximately 2 min.) as during sample crushing and the fluid analysed. No filtration of this water is necessary.
6. It would also be of value if it could be determined if the quartz structure contributed any cations or whether the TBA cation exchanger is effective in removing all the inclusion fluid cations from the quartz surface during crushing. Using so-called Brazillian quartz for this purpose might be useful, although it is not completely inclusion free.
7. When the amount of contamination (if any) from each of these factors have been determined and minimised or excluded where possible, a number of blank runs incorporating all the steps of the crush-leach procedure can be done so that a single value for contamination can be subtracted from the sample value.

12.2.3 Optimising conditions for detection of the maximum amount of dissolved species

No single cation or anion electrolyte can be used in detecting all the possible species as well as provide good peak separation. By trial and error, a set of electrolytes can be selected, each suitable for optimum detection of specific ionic species. A sample analysis could therefore

consist of a number of cation and anion runs to eliminate contamination factors and ensure a qualitative analysis of the inclusion fluid.

12.3 Other techniques to compliment CE data

The **Karl Fischer titration** has proved very useful in determining the water content of the inclusions so that fluid chemistry could be expressed as the concentration of ions per volume of inclusion fluid and not just per sample weight. Fluid salinity could also be determined in terms of TDS.

The use of **microthermometry** in calculating formation temperatures and salinity of individual inclusions has proved invaluable in establishing inclusion paragenesis as well as show that the application of Fournier and Truesdell's Na-K-Ca geothermometer (1973) to bulk inclusion fluid yields inaccurate results.

Analysis of the **gaseous components** of the inclusion fluids is important if a complete data set is to be obtained for modelling the entrapment conditions. It provides information on the pressure of formation, density of the fluid and is a necessary component in thermodynamic calculations.

Identification of daughter phases by a number of destructive and non-destructive techniques are valuable in explaining charge imbalances that might arise in fluid analysis by CE if these daughter phases do not dissolve. The **SEM**, as used in this study, is one of the methods to identify simple and complex crystals, although only providing semi-quantitative analysis. It also identified daughter minerals that was not observed under the microscope.

In a bulk analysis where there are several inclusion generations and it is not always clear if some of them are related to the same trapping process or not, identification of microdomains, resulting from different processes of quartz recrystallization, by **cathodoluminescence,** can aid in determining microcrack chronology and its relationship to fluid inclusions.

13 CONCLUSIONS

Capillary electrophoresis has been shown a useful tool in the analysis of fluid inclusions in quartz by its capacity to determine a large number of ionic species at very low levels. Fluid chemistry data of the sampled vein system identified two sources from which fluids were released during the history of the systems, namely a granitic source and metamorphosed sediments. Bulk fluid salinity and pH could also be estimated from CE data.

In conjunction with fluid formation temperatures measured by microthermometry as well as O-isotope data on the vein quartz, a model was formulated for the various fluid phases present in the quartz. The origin of the various inclusion populations is suggested as follows;

1. Remnants of a high temperature population (370 – 390 °C) found only in one sample, suggest that the first late-magmatic fluids to crystallize was of this temperature, which compares to the temperature of fluids from which cassiterite at Kuiperskraal crystallized. The absence of associated mineralization indicates that these fluids possibly originated from the less fractionated and metal rich granites. After a slight decrease in temperature the 310 – 360 °C population was trapped.

2. Later cooler fluids circulating through the fracture system, of similar origin than above, was responsible for the 230 – 300 °C population.

3. During the final cooling stages of this fluid system the 160 – 200 °C population became entrapped. It is uncertain if the fluids at this stage still had a largely magmatic composition or if fluids released during metamorphism of the surrounding sediments have already been introduced.

4. The last stage of fluid circulation is represented by the dark, irregular inclusions of elevated temperature (240 – 360 °C). The high concentration of organic acids that can be related to this fluid population characterizes it as being of a sedimentary origin, where diagenetic

transformations of organic material lead to the formation of organic acids (Lundegard and Kharaka, 1994). The thermal energy required to produce these organic acid species may have been supplied during regional metamorphism of the Malmesbury sediments during the Cape Orogeny. Formation temperatures measured by microthermometry for this fluid fall in the 200 - 300 °C range estimated by Hälbich and Cornell (1983) for the above deformation period. O-isotope data also supports the theory of a largely magmatic origin for the inclusion fluids with a strong metamorphic overprint.

All the quartz veins in the study area were classificied as late-magmatic, with an estimated early age of at least 510 Ma, while reactivation of the fluid system most likely occurred at various intervals until the final stages of the Cape Orogeny.

The observations and conclusions were in accordance with the general view on the geological and geochemical history of the study area.

Bulk fluid inclusion chemistry obtained by CE can therefore provide valuable information regarding the various fluid generations as long as inclusion populations are investigated individually to explain and correlate bulk data.

The crush-leach fluid extraction procedure used for CE analysis in this study has been optimised to eliminate contamination factors as far as possible. Extraction of the inclusion contents in vacuum, though, would not only minimise contaminating components and exclude atmospheric oxidation of some of the dissolved species, but would also make simultaneous analysis of the gas species possible by first measuring the released gasses and then washing the crushed fragments and sample holder walls with pure water.

ACKNOWLEDGEMENTS

Thanks to Dr. Chris Harris, Geology Dept. UCT, for conducting my O-isotope analysis, as well as Mr. Steenkamp at the Physics Dept., Stellenbosch, for assistance with the SEM, and Mr. Hendrikse for preparing thin sections of my samples.

Thanks to my husband, Clint, and my parents for their motivational support, also thanks to Clint for not smashing the computer when it didn't want to co-operate and we all got frustrated.

My brother in law, Barry: you saved my project (and my sanity) by removing the critters from the cables.

REFERENCES

Andrawes, F., Holzer, G. Roedder, E., Gibson, E.K. Jr., and Oro, J., 1984. Gas chromatographic analysis of volatiles in fluid and gas inclusions. *Jnl. Chromatogr.*, **302**, 181-193.

Armstrong, R., de Wit, M.J., Reid, D., York, D., Zartman, R., 1998. Cape Town's Table Mountain Group reveals rapid pan-African uplift of its basement rocks. *Jnl. Afr. Earth Sci.*, **27**, 10-11.

Banks, D.A., and Yardley, B.W.D., 1992. Crush-leach analysis of fluid inclusions in small natural and synthetic samples. *Geoch. Cosmoch. Acta*, **56**, 245-248.

Barnes, H.L., and Kullerud, G., 1961. Equilibria in sulfur-containing aqueous solutions in the system Fe-S-O, and their correlation during ore deposition. *Econ. Geol.* **56**, 648-688.

Barres, O., Burneau, A., Dubessy, J., Pagel, M., 1987. Application of micro-FT-IR spectroscopy to individual hydrocarbon fluid inclusion analysis. *Applied Spectroscopy*, **41**, 1000-10008.

Benz, N.J. and Fritz, J.S. (1994). Studies on the determination of inorganic anions by capillary electrophoresis. *Jnl. Chrom. A*, **671**, 437-443.

Bodnar, R.J., Reynolds, T.J., Kuehn, C.A., 1985. Fluid inclusion systematics in epithermal systems. *In* Berger, B.R. and Bethke, P.M. (eds.), Geology and geochemistry of epithermal systems. *Rev. Econ. Geol.* **2**, 73-97.

Bottrell, S.H., Yardley, B.W.D. and Buckley, F., 1988. A modified crush-leach method for the analysis of fluid inclusion electrolytes. *Bull. Mineral.*, **111**, 279-290.

Bruwer, L., 1997. Petrology of the Neoproterozoic, exo-granitic Kuiperskraal Sn-Zn-As deposit, Western Cape Province, South Africa. M. Sc. Thesis (unpubl.), Univ. Stellenbosch.

Burruss, R.C., Cercone, K.R., and Harris, P.M., 1985. Timing of hydrocarbon migration evidenced from fluid inclusions in calcite cements, tectonics and burial history. In (Schneidermann, N. & Harris, P.M., eds.), *Carbonate Cements Symposium*, 277-289. Soc. Econ. Paleon. & Mineral.

Campbell, A.R., and Larson, P.B., 1998. Introduction to stable isotope applications in hydrothermal systems. *In* Richards, J.P. & Larson, P.B. (Eds.), *Rev. Econ. Geol.,* **10**, 173-193. Soc. Econ. Geol., Inc., 1998.

Channer, D.M.D., and Spooner, E.T.C., 1992. Analysis of fluid inclusion leachates from quartz by ion chromatography. *Geochem. Cosmochim. Acta*, **56**, 249-259.

Chemale, J.F., Van Schmus, W.R., Scheepers, R., Gresse, P.G. In press. New age constraints on the late Neoproterozoic evolution of the Saldania Belt, South Africa. *Jnl. S. Am. Earth Sci.*

Da Silva, L.C., Gresse, P.G., Scheepers, R., McNaughton, N.J., Hartmann, L.A., Fletcher, I.R., 2000. U-Pb SHRIMP and Sm-Nd age constraints on the timing and sources of the Pan-African Cape Granite Suite, South Africa. *Jnl. Afr. Earth Sci.,* **30**, 795-815.

De Villiers, J.E., 1980. The geology of the country between Bellville and Agter-Paarl. *Trans. Geol. Soc. S.A.*, **83**, 63-67.

Dubessy, J., Audeoud, D., Wilkens, R., and Kosztolanyi, C., 1982. The use of Raman microprobe MOLE in the determination of the electrolytes dissolved in the aqueous phase of fluid inclusions. *Chem. Geol.* **37**, 137-150.

Dunlevey, J.N. 1992. Pan African crustal evolution of south-western Africa. *Jnl. Afr. Earth Sci.* **15**, 207-216.

Eberius, E. (1958). Wasserbestimmung mit Karl-Fischer-Lösung. 2nd edition, Verlag Chemie Weinheim.

Ellis, A.J., 1970. Quantitative interpretation of chemical charateristics of hydrothermal systems. In *Proc. United Nations Symp. on the development and utilization of geothermal resources, Pisa, 1970, Vol. 2, part 1. Geothermics Spec. Issue,* **2**, 516-528.

Everett, D.B., 1984. An investigation of tin occurrences at Durbanville, southwestern Cape. Hons. Proj. (unpubl.), Univ. Cape Town, 31p.

Faure, G., 1977. Principles of isotope geology. John Wiley & Sons, New York, p351-373.

Fischer, K., 1935. New method for the volumetric determination of water content in liquids and solids (in German). *Angew. Chem.*, **48**, 394-396.

Fletcher, P., 1993. Chemical thermodynamics for earth scientists. Longman Group UK Ltd., 464p.

Fournier, R.O., 1985. The behaviour of silica in hydrothermal systems. *In* Geology and geochemistry of epithermal systems. *Rev. Econ. Geol.* **2**, 45-59.

Fournier, R.O. and Truesdell, A.H., 1973. An empirical Na-K-Ca geothermometer for natural waters. *Geochem. Cosmochim. Acta*, **37**, 1255-1275.

Frimmel, H.E., & Frank, W., 1998. Neoproterozoic tectono-thermal evolution of the Gariep Belt and its basement, Namibia/South Africa. *Pecambrian Research*

Gresse, P.G., 1979. Geologie van die Kanonkop area. Unpubl., 3pp.

Gresse, P.G., Theron, J.N., Fitch, F.J., Miller, J.A., 1992. Tectonic inversion and radiometric resetting of the basin in the Cape Fold Belt. *In* De Wit, M.J. (Ed.), Inversion tectonics in the Cape Fold Belt. Balkema, Rotterdam, pp. 217-228.

Gresse, P.G. and Scheepers, R. 1993. Neoproterozoic to Cambrian (Namibian) rocks of South Africa: A geochronological and geotectonic review. *Jnl. Afr. Earth Sci.* **16**, 375-393.

Guha, J. and Gagnon, M., 1990. Gas composition of fluid inclusions using solid probe mass spectrometry and its application to the study of mineralizing processes. *Geoch. Cosmoch. Acta.* **54**, 553-558.

Hall, W.E. & Friedman, Irving, 1963. Composition of fluid inclusions, Cave-in-Rock fluorite district, Illinois, and Upper Mississippi Valley zinc-lead district. *Econ. Geol.* **58**, 886-911.

Hallbauer, D.K., 1983. Geochemistry and fluid inclusions in detrital minerals as guides to their provenance and distribution. Proc., Int'l Conf on Applied Mineralogy, Johannesburg, June 1981.

Hallbauer, D.K., 1994. Geochemical trace element analysis for ionic species by capillary electrophoresis. *Min. Mag.*, **58A** (V.M. Goldschmidt Conference Abstracts), 362-363.

Hälbich, I.W and Cornell, D.H. 1983. Metamorphic history of the Cape Fold Belt. *Spec. Publ. Geol. Soc. S. Afr.*, **12**. In: Söhnge, A.P.G. and Hälbich, I.W. (Eds.). Geodynamics of the Cape Fold Belt, 131-148.

Harris, C., Faure, K., Drummond, R.E. & Scheepers, R. 1997. Oxygen and hydrogen isotope geochemistry of S- and I-type granitoids: the Cape Granite suite, South Africa. *Chem. Geol.* **143**, 95-114.

Hartnady, C.J.H., Newton, A.R., and Theron, J.N. 1974. The stratigraphy and structure of the Malmesbury Group in the Southwestern Cape. *Bulletin Precambrian Research Unit, University Cape Town* **15**, 193-213.

Henley, R.W., Truesdell, A.H. & Barton Jr., P.B. 1984. Fluid-mineral equilibria in hydrothermal systems. Reviews in Economic Geology, Vol. 1.

Ho, S.E., 1987. Fluid inclusions: their potential as an exploration tool for Archean gold deposits. *Geol. Dept. and Univ. Ext. Univ. West. Australia Publ.*, **11**, 239-263.

Horn, E.E., and Traxel, K., 1987. Investigation of individual fluid inclusions with the Heidelberg proton microprobe. – A non-destructive analytical method. *Chem. Geol.* **61** (1/4), 29-35.

Huang, X., Gordon, M., & Zare, R.A. 1988. *Anal. Chem.* **60**, 375.

Jandik, P., Jones, W.R., Weston, A., Waters Corporation & Brown, P.R. (1991). Electrophoretic capillary ion analysis: Origins, principles, and applications. *LC•GC,* **9**, 634.

Jandik, P. & Jones, W. R. (1991). Optimization of detection sensitivity in the capillary electrophoresis of inorganic anions. *Jnl. Chromatogr.* **546**, 431-443.

Johnson, J.W., Oelkers, E.H.,and Helgeson, H.C., 1992. SUPCRT92: A software package for calculating the standard molal thermodynamic properties of minerals, gasses, aqueous species, and reactions from 1 –5000 bars and 0 – 1000 °C. *Comp. & Geosc.*, **18**, 899-947.

Jones, W.R. & Jandik, P. 1991. Controlled changes of selectivity in the separation of ions by capillary electrophoresis. *Jnl. Chromatogr.,* **546**, 445-458.

Kalinichenko, A.M., Pasal'skaya, L.F., Matyash, I.V., and Proshko, V. Ya., 1985a. Investigation of the composition of the fluid phase of inclusions by the method of PMR and gas chromatography (abstract). *Seventh All-Union Conference on thermobarometry and geochemistry of ore forming fluids, L'vov, USSR,* September 1985, **2**, 231-232 (in Russian). *19.

Kalinichenko, A.M., Pasal'skaya, L.F., Proshko, V. Ya., and Matyash, I.V., 1985b. Fluid inclusions in quartz according to PMR and gas chromatographic data. *Dopov. Akad. Nauk Ukr. RSR, Ser. B., Geol. Khim. Biol. Nauki,* no. 4, 23-26 (in Ukranian; English abstract). *18.

Kalyuzhnyi, V.A., 1982. Principles of knowledge about mineral forming fluids. "Naukova Dumka" Publ. House, Kiev (in Russian). ***15, *16, *20.**

Krige, A.V. 1921. The nature of the tin deposits near Kuilsrivier, Stellenbosch District, and their relationship to the other occurrences in the neighbourhood. *Trans. Geol. Soc. South Africa*, **24**, 53-70.

Lattanzi, Pierfranco, 1991. Applications of fluid inclusions in the study and exploration of mineral deposits. *Eur. Jnl. Miner.*, **3**, 689-701.

Lee, Y-H, and Lin, T. –I., 1994. Determination of metal cations by capillary electrophoresis – Effect of background carrier and complexing agents. *Jnl. Chrom. A*, **675**, 227-236.

Li, S.F.Y., 1992. Capillary electrophoresis. Elsevier. 555p

Lundegard, P.D., and Kharaka, Y.K., *In* Pittman, E.D. and Lewan, M.D. (Eds.), Organic acids in geological processes, Springer-Verlag, Heidelberg, Berlin, 1994, 40-69.

Mikkers, F.E.P, Everaerts, F.M., & Verheggen, T.P.M. 1979. *Jnl. Chromatogr.* **169**, 18.

Nellmapius, M.E., 1912. Note on the nature and origin of the Vredehoek tin deposits, Cape Town. *Trans. Geol. Soc. South Africa*, **15**, 1-3.

Oehrle, S.A. 1996. Analysis of anions in drinking water by capillary ion electrophoresis. *Jnl. Chromatogr. A*, **733**, 101-104.

Peters, W.C. 1978. Exploration and mining geology. John Wiley & Sons, Inc. , 696p.

Pirajno, F. & Bentley, P.N. 1985. Greisen related scheelite, gold and sulphide mineraliztion at Kirwans Hill and Bateman Creek, Reefton District, Westland, New Zealand. *New Zealand Jnl. Geology Geophysics*, **28**, 97-109.

Pirajno, F., 1992. Hydrothermal mineral deposits. Springer-Verlag Berlin Heidelberg, 709p.

Roedder, E., Ingram, B. & Hall, W.E., 1963. Studies of fluid inclusions III: Extraction and quantitative analysis of inclusions in the milligram range. *Econ. Geol.,* **58**, 353-374.

Roedder, E. Fluid inclusions as samples of ore fluid. In Barnes, H.L., ed. (1969). Geochemistry of hydrothermal ore deposits.Wiley & Sons, New York, NY, 798p.

Roedder, E., 1971. Fluid inclusion studies on the porphyry-type ore deposits at Bingham, Utah, Butte, Montana, and Climax, Colorado. *Econ. Geol.* **66**, 98-120.

Roedder, E., 1976. Fluid inclusion evidence on the genesis of ores in sedimentary and volcanic rocks. *In* Wolf, K.H (ed.), Handbook of strata-bound and strata-form ore deposits. Elsevier, Amsterdam, **2**, 67-110.

Roedder, E. 1977. Fluid inclusions as tools in mineral exploration. SEG distinguished lecture in scientific research. *Econ. Geol.*, **72**, 503-525.

Roedder, E. 1984. Fluid inclusions: Rev. in Miner., Mineralogical Society America, no. 12.

Roedder, E. 1990. Fluid inclusion analysis: Prologue and epilogue. *Geochim. Cosmochim. Acta*, **54**, 495-507.

Rozendaal, A., Gresse, P.G., Scheepers, R., De Beer, C.H., 1994. Structural setting of the Riviera W-Mo deposit, Western Cape, South Africa. *S. Afr. Jnl. Geol.*, **97**, 184-195.

Rozendaal, A. & Bruwer, L., 1995. Tourmaline nodules: indicators of hydrothermal alteration and Sn-Zn-(W) mineralization in the Cape Granite Suite, South Africa. *Jnl. Afr. Earth Sci.*, **21**, 141-155.

Rozendaal, A. & Scheepers, R. 1995. Magmatic and related mineral deposits of the Pan-African Saldania Belt in the Western Cape Province, South Africa. *Jnl. Afr. Earth Sci.*, **21**, 107-126.

Rozendaal, A., Gresse, P.G., Scheepers, R., Le Roux, J.P., 1999. Neoproterozoic to Early Cambrian evolution of the Pan-African Saldania Belt, South Africa. *Precambrian Research*, **97**, 303-323.

Sawkins, F.J. 1990. *Metal deposits in relation to plate techtonics*. 2nd Edition. 416p. Springer, Berlin, Heidelberg, New York.

Scheepers, R. and Cuney, M., 1992. Hydrothermal breccia-related Cu-Mo-Au mineralization in the Late Precambrian granites, Western Cape Province, South Africa. *Ore Geol. Rev.*, **7**, 1-23.

Scheepers, R. & Rozendaal, A., 1992. Relationship of the Riviera W-(Mo-Cu) deposit to the magmatism in the southwestern Cape Province, South Africa. Abstracts Geocongress, 1992. Geological Society of South Africa, Johannesburg.

Scheepers, R. 1995. Geology, geochemistry and petrogenesis of Late Precambrian S-, I- and A-type granitoids in the Saldania Belt, Western Cape, South Africa. *Jnl. Afr. Earth Sci.*, **21**, 35-58.

Scholtz, D.L. 1946. On the younger Precambrian granite plutons in the Cape Granites. *Trans. Geol. Soc. South Africa*, **49**, 35-82.

Seward, T.M., and Barnes, H.L., 1997. Metal transport by hydrothermal ore fluids, *in* Barnes, H.L. (ed.). Geochemistry of hydrothermal ore deposits, 3rd ed., New York, Wiley-Interscience, 435-486.

Shcherba, G.N. 1970. Greisens. *Int. Geol. Rev.*, **12**, 114-254.

Smith, D.M., Bryant, W.M., Mitchell, J. (jr.). 1939. Analytical procedures employing Karl Fischer reagent. I.: Nature of the reagent. *Jnl .Amer. Chem. Soc.* **61**, 2407-2412.

Struempler, A.W., 1973. Adsorption characteristics of silver, lead, cadmium, zinc, and nickel on borosilicate glass, polyethylene, polypropylene container surfaces. *Anal. Chem.*, **45**, 2251-2254.

Talor, H.P., Jr., 1968. The oxygen isotope geochemistry of igneous rocks. *Contr. Miner. Petr.*, **19**, 1-71.

Van den Kerkhof, A.M., 1990. Isochoric phase diagrams in the system $CO_2 - CH_4$ and $CO_2 - N_2$: application to fluid inclusions. *Geochem. Cosmochim. Acta*, **54**, 621-629.

Verhoef, J.C., Barendrecht, E. 1976. Mechanism and reaction rate of the Karl Fischer titration. Part I. Potentiometric measurements. *Jnl. Electroanal. Chem.* **71**, 305-315.

Verhoef, J.C., Barendrecht, E. 1977. Mechanism and reaction rate of the Karl Fischer titration. Part II. Rotating ring disk electrode measurements. *Jnl. Electroanal. Chem.* **75**, 705-717.

Verhoef, J.C., Barendrecht, E. 1977. Mechanism and reaction rate of the Karl Fischer titration. Part V. Analytical implications. *Anal. Chem. Acta* **94**, 395-403.

Verhoef, J.C., Cofino, W. P., 1978. Mechanism and reaction rate of the Karl Fischer titration. Part IV. First and second order catalytic currents at a rotating disk electrode. *Jnl. Electroanal. Chem.* 93, 75-80.

Villafranca, J.J. (ed.), 1990. Current research in protein chemistry. Academic Press.

Von Veh, M.W., 1983. Aspects of sedimentation, structure and tectonic evolution in the Tygerberg terrane, southwestern Cape Province. *Bull. Precambr. Res. Unit, Univ. Cape Town*, **32**, 1-88.

Voskresenskii, S.S., Kolosova, G.N., and Naumov, V.B., 1972. Thermobaric formation characteristics of vein quartz in the basin of the upper reaches of the Kolyma river and the denudational section. *Izv. Vyssh. Ucheb. Zaved., Geol. Razved,* **15**, no. 10, 42-45 (in Russian; abstract in *Fluid Incl. Res. – Proc. of COFFI*, **5**, 109, 1972)

Wagner, P.A., 1909. Notes on the tin deposits in the vicinity of Cape Town. *Trans. Geol. Soc. South Africa,* **12**, 102-111.

White, D.E., 1965. Saline waters of sedimentary rocks. *In* Fluids in subsurface environments – A symposium. *Amer. Assoc. Petr. Geol. Mem.*, **4**, 342-366.

Wieland, G., 1987. Water determination by Karl Fischer titration. GIT VERLAG GMBH, 97p.

Wojtusik, M.J. and Harrold, M.P., 1994. Factors influencing trace analysis with preconcentration by electrostacking. *Jnl. Chrom. A*, **671**, 411-417.

APPENDIX A

Measurements on inclusion melting and homogenization temperatures were made on a Linkam heating/freezing stage, done at the University of Stellenbosch.

The instruments was calibrated at 0 °C and 374 °C for heating by using a pure water-rich inclusion, while a synthetic CO_2 inclusion was used for the freezing point of CO_2 at –56 °C. Accuracy of measurements are within 0.2 °C.

Fluid inclusion data for quartz veins

RM 49				RM 14							
No.	**Phase**	**Tm**	**Th**	**No.**	**Phase**	**Tm**	**Th**	**No.**	**Phase**	**Tm**	**Th**
1	***L+V (I)***	-2	171	1	***L+V (R)***	0		50	***L+V (I)***	-1	225
2		-0.7		2		+0.1		51		-0.9	227
3		-1.5		3		+0.1		52		-0.5	215
4		-1.8		4		+0.1		53	***L+V (R)***	-1.2	215
5		-1.7		5		+0.7		54		-1	220
6		-1.5		6		+0.2		55	***L+V (I)***	-0.2	222
7		-1.5		7		+0.5		56		+0.5	
8		-1		8		-1.5		57		+0.5	
9		-1.9		9		-1.2		58		+0.3	
10		-1.9		10		+0.5		59		-0.3	244
11	***L+V (I)***		298	11		+0.6		60		-0.1	245
12	***L+V (D)***			12		-0.6		61		-0.7	230
13	L to V	0.1	322	13		-0.6		62		-1	230
14	L to V	0.2	314	14	***L+V (R)***	+0.5		63		-0.9	241
15	L to V	0.2	341	15		+0.6		64		-0.7	220
16	L to V	0.1	340	16		+0.6		65		-0.9	238
17	L to V	0.2	344	17		+0.5		66		-0.6	244
18	***L+V (I)***		295	18		+0.1		67		-0.2	240
19			292	19	***L***	0.1	341	68		+0.7	
20			302	20		0.2	349	69		+0.1	
21			282	21		0.2	352	70		-0.5	240
22			225	22		0.1	361	71		-0.6	228
				23		0.3	370	72		-0.5	248
RM 42				24	***L+V (R)***	-1	235	73		-0.7	230
No.	**Phase**	**Tm**	**Th**	25		-1.1	235	74		-0.2	229
1	***L+V (I)***	-4.7	266	26		-1.1	235	75		-0.1	245
2		-3.5	280	27		-1	235	76		+0.5	230
3		-5.6	320	28		-1	237	77		-0.5	240
4		-3.4	325	29		-0.7	232	78		-0.5	232
5		-4.3	330	30		-0.2	235	79		-0.3	245
6		-4.2	335	31				80		-0.5	227
7		-3.9		32				81			228
8		-3.1		33				82			216
9		-5.7		34				83			227
10		-4.7		35				84			235
11		-4.9		36	***L+V (D)***	+0.7	250	85			245
12		-5.1		37		+1	236	86			247
13		-4.2		38		+0.4	260	87	***L+V (R)***	+0.2	
14		-5.2		39		+0.2	257	88		+1	
15		-4.7		40		+0.4	237	89		-1	300
16		-4.7		41		+0.7	241	90		-1.4	293
17		-5.8		42		+0.1	255	91		-1	269
18	***L+V (I)***	-4.5	344	43		+0.6	239	92		-1.3	243
19		-5.2	350	44		+0.2	247	93		-0.7	235
20		-4.2	319	45		+0.3	252	94		-0.4	244
21	L to V	-5	365	46		+0.1	263	95		-0.8	
22		-3.7		47		+0.5	284	96		-0.4	
23	***L+V (D)***		348	48		+1.1		97		-0.7	
24			336	49	***L+V (I)***	-0.8	224	98		-0.2	
25	L to V		333								

Tm=melting temperature; Th=homogenization temperature;
(R) = round, (I) = irregular and (D) = dark inclusions

Fluid inclusion data for quartz veins (Cont.)

RM Z - Quartz				RM Z - Cassiterite				RM 23			
No.	**Phase**	**Tm**	**Th**	**No.**	**Phase**	**Tm**	**Th**	**No.**	**Phase**	**Tm**	**Th**
1	***L+V (R)***	+2.4	221	1	***L+V (D)***			1	***L+V (R)***	-0.8	170
2		+1.2	230	2	L to V	-1.5	337	2		-1.7	188
3		+0.1	200	3	L to V	-1.2	344	3		+3	
4		-2.5	255	4	L to V	-1.6	345	4		+1.1	
5		-1.2	260	5	L to V	-1.3	347	5		+1.9	
6		-2	210	6	L to V	-1.1	270	6		-1.8	
7		-1.4	305	7	L to V	-1.5	276	7		+0.9	
8		-2.2	280	8	L to V	-1.5	286	8		+1.6	
9		-0.7	290	9	L to V	-1.4	288	9		+2.3	
10			302	10	L to V	-1.2	292	10		+1.5	
11			205	11	L to V	-1.3	298	11		+2.5	
12			235	12	L to V	-1.3	301	12		-1.5	
13			245	13	***L+V (R)***		201	13		-1.5	
14			262					14		-0.8	
15	***L+V (D)***	+0.6	338					15		+1.5	
16	L to V	-1.8	345					16		-0.8	
17		-2.9	285					17		+0.6	
18		-3.1	295					18		+1.3	
19		-3.3	300					19		-0.7	
20		-3.4	284					20	***L (I)***		
21		-3.7	285					21	L to V	0.3	342
22		-3.1	290					22	L to V	0.3	349
23		-2.8	246					23	L to V	0.2	350
24		-2.5						24	L to V	0.1	372
25	L to V		345					25	L to V	0.3	395
26	***L+V (I)***	-1.2						26	L to V	0.2	376
27		-1.5						27	n=10 L to V	0.1	324-326
28		-2						28	***L (D)***	-1.5	227
29		-2						29	L to V	-1.3	260
30		-1.8						30	L to V	-1.5	265
31	***L+V (I)***	-2	302					31	L to V	-1.2	278
32		-1.4	285					32	L to V	-1.4	230
33		-1.6	300					33	L to V	-1.5	274
34		-1.8	285								
35		-2.4	245								
36		-2.3	295								
37	***L+V (R)***	-2.4	270								
38		-2.1	235								
39		-2.4	260								
40		-2.8									
41		-2.5									
42		-2.7									
43		-2.8									

Tm=melting temperature; Th=homogenization temperature;
(R) = round, (I) = irregular and (D) = dark inclusions

Fluid inclusion data for quartz veins (Cont.)

RM 57

No.	Phase	Tm	Th	No.	Phase	Tm	Th	No.	Phase	Tm	Th
1	*L+V (D)*	-2.4	224	51	*L+V (I)*	-2	242	101	*L+V (D)*	+0.3	300
2		-2.9	230	52		-2.3	268	102		+1.3	321
3		-3.8	236	53		-2	270	103		+0.4	334
4		-3.7	208	54		-2.4	250	104		+0.3	305
5		-3.5	228	55		-1.6	260	105		0	351
6		-0.3		56		-1.6	266	106		+0.5	337
7		-0.4		57		-1.8	230	107		+0.7	340
8		-1.8	236	58		-1.2	243	108			328
9		-2.6	238	59		-2.2	244	109			307
10		-2.6	240	60		-1.3	220	110			317
11		-2.5	224	61		-2.1	217	111	L to V	0.5	378
12		-2.5	219	62		-2.2	215	112	L to V	0.3	304
13		-2.4	210	63		-1.9	217	113	L to V	0.5	329
14		-3.5		64		-1.8	216	114	L to V	0.4	347
15		-3.1	254	65		-1.7	217	115	L to V	0.3	368
16		-2.1	206	66		-2.7	234	116	(n=10)L to V	-1.5	276
17		-1.7	220	67		-2.3	280	117	(n=10)L to V	-1.2	268
18		-1.9	208	68		-2.5	268				
19		-1.8	237	69		-2.2	262				
20		-2.6	213	70		-3	266				
21		-2.9	215	71		-2.7	235				
22		-1.1	204	72		-4.7	260				
23		-3	229	73		-4	262				
24		-2.8	204	74		-4	250				
25		-1.8	234	75		-2.6	260				
26		-1.7	224	76		-2.8	276				
27		-1.5	231	77		-3	242				
28		-0.3	280	78		-2.4	244				
29		-0.6	250	79		-2.7	240				
30		-0.4	208	80		-2	238				
31		-2	263	81		-0.3	226				
32		-1.1	244	82	*L+V (I)*	-3	235				
33		-2.7	268	83		-2.4	240				
34		-2.4	274	84		-3.4	256				
35		-2.1		85		-2.7	260				
36		-1.6		86		-0.3	217				
37	*L+V (I)*	-0.7		87		-1.6	243				
38		-0.5		88		-2.2	235				
39		0		89		-2.4	227				
40		-0.8		90		-2.1	243				
41		-1.3		91		-2.1	235				
42		-0.6		92		-1.2	290				
43		-1.2		93		-0.3	280				
44		-1		94		-2.3	284				
45		-1.1		95		-3.5	261				
46	*L/ L+V (I)*	0.2		96		-2.9					
47	(n=10)L to V	1.3	283 - 286	97		-3.5					
48	(n=10)L to V	0.3	300 - 307	98							
49		0.4		99							
50		0.4		100							

Tm=melting temperature; Th=homogenization temperature;
(R) = round, (I) = irregular and (D) = dark inclusions

Fluid inclusion data for quartz veins (Cont.)

RM 1

No.	Phase	Tm	Th	No.	Phase	Tm	Th
1	***L+V (R)***	-0.4	161	48	***L+V (I)***	-0.6	251
2		-0.3	175	49		-0.4	276
3		-0.3	179	50		-0.4	250
4		-0.3	186	51		-0.4	249
5			171	52		-0.4	276
6		-0.2	173	53		-0.5	284
7		-0.4	183	54		-0.3	261
8			163	55		-0.6	262
9			175	56		-0.5	261
10		-0.2	169	57		-0.5	292
11		-0.2	176	58		-0.4	300
12		-0.5	172	59		-0.3	225
13		-0.4	168	60		-0.3	314
14		-0.4	175	61		-0.3	302
15		-0.2	159	62		-0.4	370
16		-0.3	162	63			280
17		-0.4	157	64			314
18		-0.5	163	65	***L+V (D)***	0.4	304
19		-0.5	169	66		0.3	322
20		-0.4	162	67		0.4	297
21		-0.3	163	68		0.2	299
22			164	69		0.3	308
23		-0.4	169				
24		-0.5	288				
25			237				
26			290				
27		-0.2	289				
28		-0.4	302				
29		-0.3	270				
30		-0.4	293				
31		-0.3	263				
32			284				
33		-0.3	294				
34		-0.3	306				
35			317				
36		-0.2	299				
37			302				
	L (R)						
38	L to V		269				
39	L to V		260				
40	L to V		264				
41	***L+V (I)***	-0.5	178				
42			188				
43		-0.4	198				
44		-0.5	191				
45			197				
46		-0.4	206				
47		-0.3	214				

Tm=melting temperature; Th=homogenization temperature;
(R) = round, (I) = irregular and (D) = dark inclusions

Fluid inclusion data for quartz veins (Cont.)

RM 16a				RM 39			
No.	**Phase**	**Tm**	**Th**	**No.**	**Phase**	**Tm**	**Th**
1	***L+V (R)***	-3	202	1	***L+V (R)***		205
2			206	2			215
3		-2.8	196	3			204
4		-2.8	193	4			240
5		-2.8	194	5			255
6		-2.4	197	6			258
7		-2.5	199	7			272
8		-2.2	187	8			320
9		-2.4	182	9			235
10		-1.6	193	10			269
11		-1.6	185	11			365
12		-1.6	197	12			280
13		-1.2	259	13	***L+V (I)***		340
14		-1	270	14			311
15			215	15			326
16		-2.4	226	16			347
17		-2.5	167	17	***L+V (D)***		320
18		-2.2	292	18			325
19			267	19			310
20		-2.8	270	20			335
21			272	21	***L+V (I)***		212
22		-2.4	270	22			222
23		-1.6	260	23			252
24		-3	249	24			277
25		-2.8	271	25			278
26		-2.4	202				
27			203				
28			212				
29	L to V	-1.7	228				
30	L to V	-2.6	230				
31	L to V	-2.9	368				
32	L to V		260				
33	***L+V (I)***		208				
34			213				
35	***L (I)***						
36	L to V	-2.6	228				
37	L to V	-1.5	239				
38	L to V	-1.8	240				
39	L to V	-2.6	258				
40	***L+V (I)***	0	275				
41		-0.1	285				
42		0.1	298				
43		0.2	317				
44	L to V	0.1	309				
45	L to V	0.1	311				
46	L to V	0.1	313				
47	L to V	0.1	332				
48	L to V	0.1	348				
49	L to V	0.2	291				
50	L to V	-0.1	325				
51	L to V	0.2	328				
52	L to V	0.2	347				
53	***L (I)***						
54	L to V		336				

Tm=melting temperature; Th=homogenization temperature;
(R) = round, (I) = irregular and (D) = dark inclusions

APPENDIX B

Salinity calculations

As a result of correction factors applied to CIA and Karl Fischer data, the ionic concentrations can be expressed as weight percentages of the fluid present in the sample.

Cation and anion concentrations were added together and expressed as total dissolved solids (TDS) in mg/ml. Another correction was then made to the dilution factor of 10 used for the CIA data, now that the true amount of dilution was determined through Karl Fischer analyses. The mass of dissolved solids were deducted from the equation for concentration (C) where C (mg/ml) = mass(mg)/volume(ml), and salinity expressed as the weight percentage of this mass relative to the total mass of the inclusion (water + dissolved solids).

APPENDIX C

Thermodynamic calculations

Sulphur system

Equilibrium reactions are as follows:

$$H_2S^0 = HS^- + H^+ \quad \text{- (1)}$$

$$HSO_4^- = SO_4^{2-} + H^+ \quad \text{- (2)}$$

$$H_2S^0 + 2O_2(g) = HSO_4^- + H^+ \quad \text{- (3)}$$

$$H_2S^0 + 2O_2(g) = SO_4^{2-} + 2H^+ \quad \text{- (4)}$$

$$HS^- + 2O_2(g) = SO_4^{2-} + H^+ \quad \text{- (5)}$$

The equilibrium constants for above reactions are:

$$K_1 = \frac{a_{HS^-}\, a_{H^+}}{a_{H_2S^0}}$$

$$K_2 = \frac{a_{SO_4^{2-}}\, a_{H^+}}{a_{HSO_4^-}}$$

$$K_3 = \frac{a_{HSO_4^-}\, a_{H^+}}{a_{H_2S^0}\, f^2_{O_2}}$$

$$K_4 = \frac{a_{SO_4^{2-}}\, a^2_{H^+}}{a_{H_2S^0}\, f^2_{O_2}}$$

$$K_5 = \frac{a_{SO_4^{2-}}\, a_{H^+}}{a_{HS^-}\, f^2_{O_2}}$$

Taking the log value on each side, we get:

$$\log K_1 = \log \frac{a_{HS^-}}{a_{H_2S^0}} + \log a_{H^+}$$

$$\log K_2 = \log \frac{a_{SO_4^{2-}}}{a_{HSO_4^-}} + \log a_{H^+}$$

$$\log K_3 = \log \frac{a_{HSO_4^-}}{a_{H_2S^0}} + \log a_{H^+} - 2\log f_{O_2}$$

$$\log K_4 = \log \frac{a_{SO_4^{2-}}}{a_{H_2S^0}} + 2\log a_{H^+} - 2\log f_{O_2}$$

$$\log K_5 = \log \frac{a_{SO_4^{2-}}}{a_{HS^-}} + \log a_{H^+} - 2\log f_{O_2}$$

Substituting $\log a_{H^+}$ = -pH, and setting the activities of two sulphur species at their isoactivity boundaries equal so that the log value of this term is zero, the above equations for the predominance boundaries simplify to:

H_2S^0 – HS^- boundary: $\quad pH = -\log K_1$

HSO_4^- - SO_4^{2-} boundary: $\quad pH = -K_2$

H_2S^0 – HSO_4^- boundary: $\quad \log f_{O_2} = -0.5pH - 0.5\log K_3$

H_2S^0 – SO_4^{2-} boundary: $\quad \log f_{O_2} = -pH - 0.5\log K_4$

HS^- – SO_4^{2-} boundary: $\quad \log f_{O_2} = -0.5pH - 0.5\log K_5$

From Table 9.4 in the text, boundaries can be calculated for higher temperatures by substituting the corresponding log K values.

Nitrogen system

Equilibrium reactions for the nitrogen predominance diagram are as follows:

$$NH_3^0 + H^+ = NH_4^+ \qquad \text{- (1)}$$

$$N_2^0 + 3H_2O(l) = 2NH_3^0 + 1.5O_2(g) \qquad \text{- (2)}$$

$$N_2^0 + 3H_2O(l) + 2H^+ = 2NH_4^+ + 1.5O_2(g) \qquad \text{- (3)}$$

$$NO_3^- + 2H^+ + H_2O(l) = NH_4^+ + 2O_2(g) \qquad \text{- (4)}$$

The equilibrium constants for above reactions are:

$$K_1 = \frac{a_{NH_4^+}}{a_{NH_3^0}\, a_{H^+}}$$

$$K_2 = \frac{a^2_{NH_3^0}\, f^{3/2}_{O_2}}{a_{N_2^0}}$$

$$K_3 = \frac{a^2_{NH_4^+}\, f^{3/2}_{O_2}}{a_{N_2^0}\, a^2_{H^+}}$$

$$K_4 = \frac{a_{NH_4^+}\, f^2_{O_2}}{a_{NO_3^-}\, a^2_{H^+}}$$

pH and log K are substituted in the same way as for the sulphur system , and activities are set equal. For the NH_3^0/N_2^0 and the NH_4^+/N_2^0 boundaries a value need to be assigned to the total activity of dissolved nitrogen because all the nitrogen species do not cancel out. A value of 0.001 is chosen. Taking log values on both sides of the equation and solving log (0.001), the equations resolve to:

NH_3^0 - NH_4^+ boundary: $pH = -\log K_1$

NH_3^0 - N_2^0 boundary: $\log f_{O_2} = 2/3(\log K_2 + 3)$

NH_4^+ - N_2^0 boundary: $\log f_{O_2} = 2/3(\log K_3 + 3) - 4/3pH$

NO_3^- - NH_4^+ boundary: $\log f_{O_2} = 0.5\log K_4 - pH$

From Table 9.5 in the text, boundaries can be calculated for higher temperatures by substituting the corresponding log K values.